AD-A081 711 MASSACHUSETTS INST OF TECH LEXINGTON LINCOLN LAB F/G 9/5
FACTORS AFFECTING THE PERFORMANCE OF ADAPTIVE ANTENNA SYSTEMS A--ETC(U)
AUG 79 J T MAYHAN, F W FLOYD F19628-78-C-0002
UNCLASSIFIED TN-1979-14 ESD-TR-79-197 NL

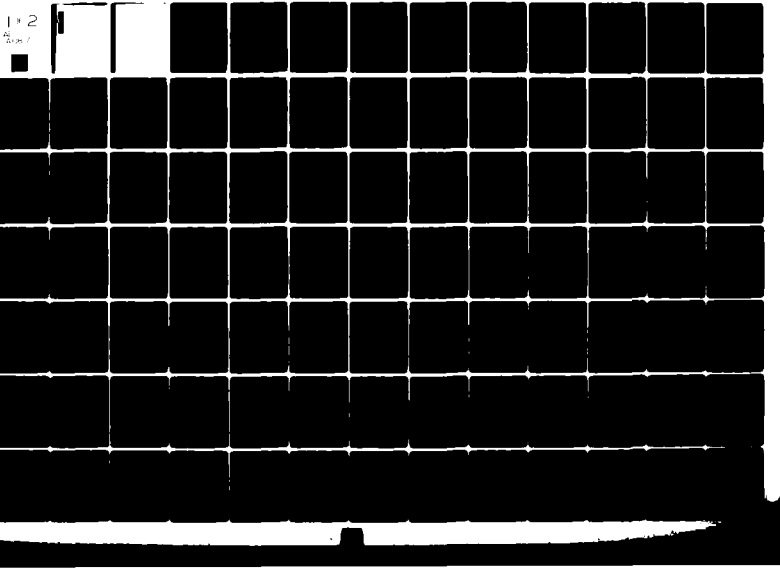

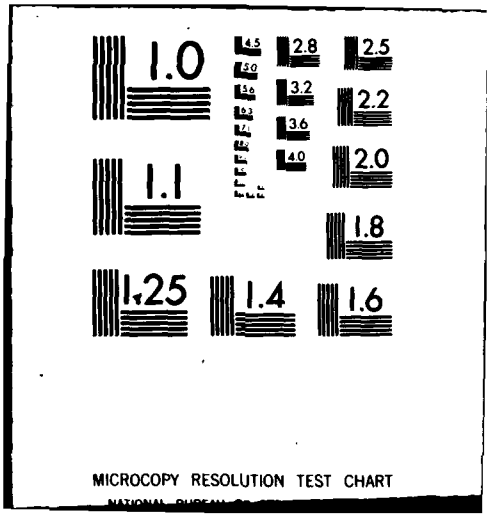
1.0
1.1
1.25
1.4
1.6
1.8
2.0
2.2
2.5
2.8
3.2
3.6
4.0
4.5
5.0
5.6
6.3
7.1
MICROCOPY RESOLUTION TEST CHART

MASSACHUSETTS INSTITUTE OF TECHNOLOGY

LINCOLN LABORATORY

FACTORS AFFECTING THE PERFORMANCE OF ADAPTIVE ANTENNA SYSTEMS AND SOME EVALUATION TECHNIQUES

J. T. MAYHAN

Group 61

F. W. FLOYD

Group 68

TECHNICAL NOTE 1979-14

9 AUGUST 1979

LEXINGTON MASSACHUSETTS

ABSTRACT

The basic performance of an adaptive antenna system is influenced somewhat independently by two sub-systems: the antenna and the adaptive processor. Choice of the antenna type (multiple beam antenna or phased array) and the design of the adaptive processor (which is used to control the weighting at each antenna feed port) depends strongly on the specific requirement of a particular system. To date, much has been published on the ideal performance characteristics of adaptive nulling antenna systems. However, little has been published on the effects of hardware component imperfections on system performance. To characterize these effects is the purpose of this note. We present methods for categorizing, analyzing and measuring the effects of a few of the key components which are common to the majority of adaptive systems implemented to date. Some examples we will discuss are those effects due to antenna type, antenna tolerance errors, channel tracking errors, weighting circuits, hard-limiters, correlators and base-band components. We analyze these from the viewpoint of the degree of cancellation achievable by the adaptive processor and also their impact on loop dynamics (where appropriate). In order to illustrate the various effects, measured performance results obtained using an experimental Applebaum-Howell type adaptive processor will be presented.

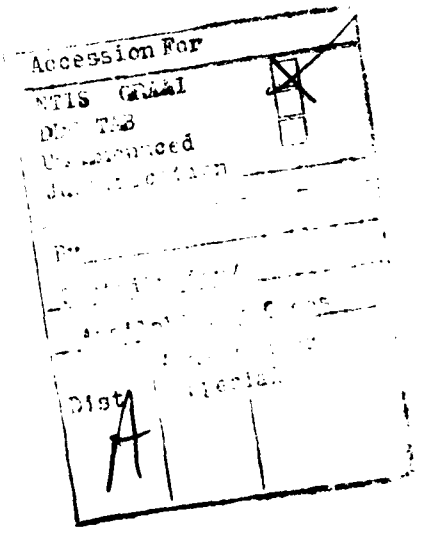

CONTENTS

I. INTRODUCTION

Adaptive antennas are capable of autonomously changing their radiation pattern characteristics in response to the signals incident on the aperture. This is generally accomplished by applying amplitude and phase control (weighting) at the output of each of several feed-ports designed into the antenna system, where the weighting is adjusted according to some specified control algorithm. For communications systems where the antenna field of view (FOV) may contain both interference and signal sources, adaptive antennas can be utilized to improve the signal-to-interference ratio. This is done by autonomously changing the pattern so that relative pattern maxima are directed toward the desired user locations and pattern minima (nulls) are directed toward the interference locations.

The basic performance of such an adaptive antenna system is influenced somewhat independently by two sub-systems: the antenna and the adaptive processor. Choice of the antenna type (multiple beam antenna (MBA) or phased array (PA)) and configuration (number of beams or array element positions) is usually determined by such considerations as signal interference proximity (i.e., resolution), number of interference sources, nulling bandwidth, number of simultaneous users and their locations over the FOV, the specific FOV over which the antenna must be designed to operate, etc. Similarly, the design of the adaptive processor, which is used to control the weighting at each antenna feed-port, depends strongly on such factors as how the user signals are to be distinguished from interference signals, the time required for the processor to "adapt" to a steady behavior, the bandwidth of operation, etc. For these reasons, the specific characteristics of existing adaptive nulling systems are as different as there are applications for adaptive nulling techniques.

To date, much has been published on the ideal performance characteristics of adaptive nulling antenna systems. However, little has been published on the effects of hardware component imperfections on system performance. To characterize these effects is the purpose of this note. We present methods for categorizing, analyzing and measuring the effects of a few of the key

components which are common to the majority of adaptive systems implemented to date. Some examples we will discuss are those effects due to antenna type, antenna tolerance errors, channel tracking errors, weighting circuits, hard-limiters, correlators and base-band components. We analyze these from the viewpoint of the degree of cancellation achievable by the adaptive processor and also their impact on loop dynamics (where appropriate). We will also identify several techniques we have found useful in evaluating these component effects. One such technique has already been published in Lincoln Laboratory Technical Note 1978-1[1] and we will utilize this material where appropriate. Others will be developed in the forthcoming sections.

The characterization of the performance of the antenna sub-system has been discussed in some detail in Ref. 1; hence, the major thrust of this note will be to concentrate on those factors associated with the adaptive processor sub-system. However, a brief summary of antenna dispersion (i.e., frequency variations introduced by the antenna) and some updated estimates on the effect of antenna type (MBA vs PA) on cancellation will be included here. In order to illustrate the various component effects, measured performance results obtained from an experimental Applebaum-Howell type adaptive processor will be presented.

II. BACKGROUND

In this section we present a brief summary of the basic equations characterizing the performance of a wideband Applebaum-Howells type adaptive nulling processor. A simplified diagram of the processor is illustrated in Fig. 1. The narrowband analysis pertaining to this type of processor has been discussed in some detail in a review article by Gabriel[2]. In our model, we include the frequency response of the various components (e.g., the antenna, RF front-ends, IF filters, etc.) in order that a wideband characterization of the processor can be obtained. We also include in our analysis the effects of a frequency-dependent feedthrough component inherent in the weight circuitry. We adopt the following notation:

$n(t)$ = complex envelope of a single interference noise waveform incident on the aperture.

$S_n(\omega)$ = power spectral density of the noise, $n(t)$.

$A_k(\omega)$ = frequency response function of the k^{th} antenna element (including time delay in the case of a Phased Array).

$H_k(\omega)$ = channel frequency response function characterizing the kth channel RF/IF mixer, amplifiers, and filters, over the nulling bandwidth.

$E_k(\omega)$ = overall frequency response of kth channel. $E_k(\omega) = A_k(\omega) \cdot H_k(\omega)$.

$v_k(t)$ = complex envelope of signal voltage at the input to the kth weight circuit.

$w_k^*(t)$ = complex, frequency independent weight, where "*" denotes complex conjugate.

$\gamma_k^*(\omega)$ = frequency-dependent feedthrough path present in the weight circuitry.

$v_o(t)$ = complex envelope of the processor output voltage.

$X_k(t)$ = complex envelope of the correlator mixer output.

τ_o = time constant of first order filter following the correlation mixer.

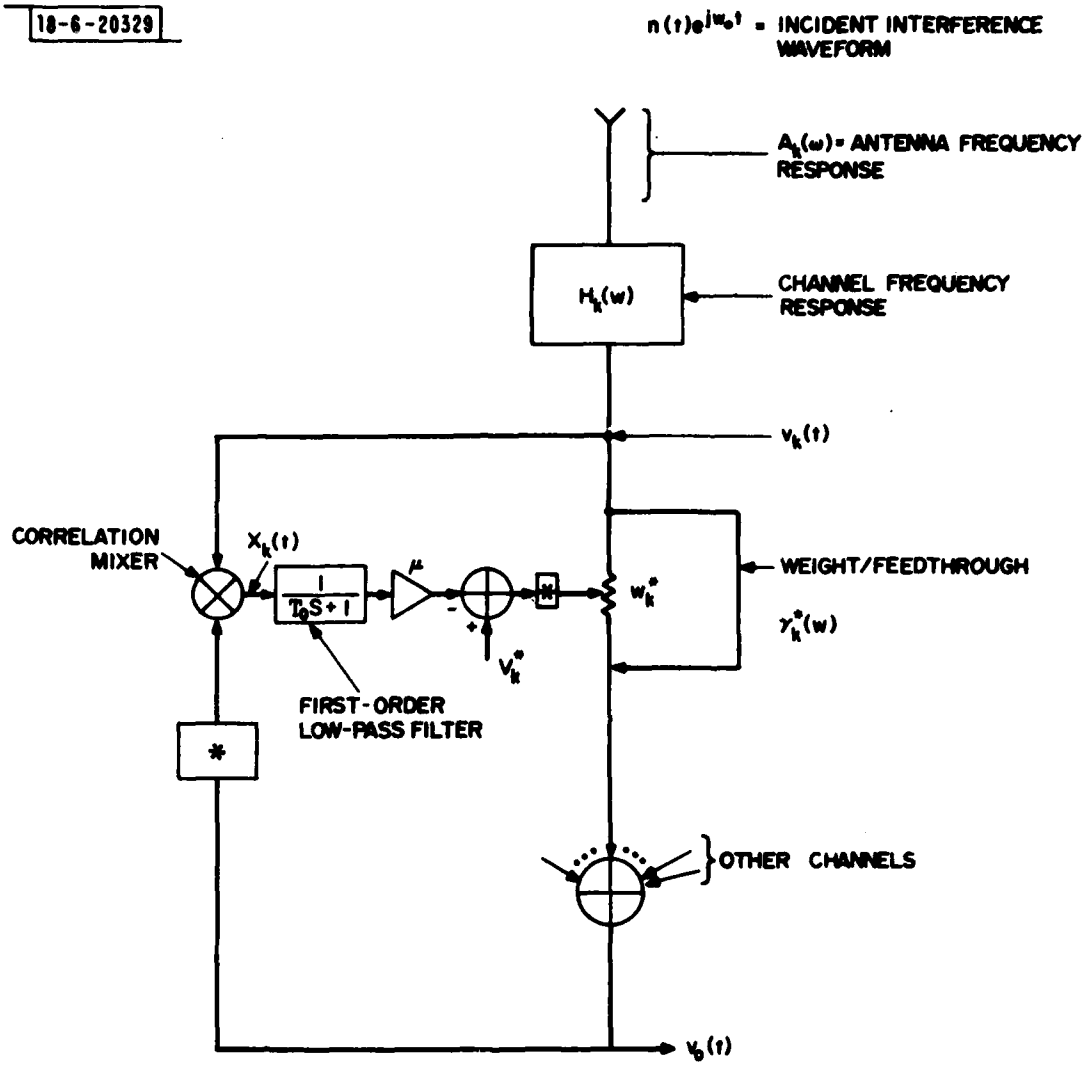

Fig. 1. k^{th} channel of an N-channel, wideband Applebaum-Howells type adaptive nulling processor.

μ = feedback loop gain.

V_k^* = complex beam steering voltage specifying the quiescent (no interference sources) weight setting and thereby the quiescent radiation pattern.

$R_{k,q}(\tau)$ = cross correlation between $v_k(t)$ and $v_q(t)$.

$S_{k,q}(\omega)$ = cross power spectral density of $v_k(t)$ and $v_q(t)$.

ω_o = carrier radian frequency of input waveform.

BW_c = closed-loop bandwidth in hertz.

BW = nulling bandwidth (as determined by $H_k(\omega)$) in hertz.

R_j = total power of n(t) in the nulling bandwidth

$$R_j = \frac{1}{2\pi} \int_{-\infty}^{\infty} S_n(\omega)\, d\omega \quad .$$

C = cancellation: $C = (I/N)_a/(I/N)_b$.

$(I/N)_{b,a}$ = ratio of interference noise level to thermal noise power before adaption (b) or after adaption (a).

Complex notation is used because most commonly employed weighting techniques use the inphase (I) and quadrature (Q) outputs of the correlation mixer to drive separate I and Q weight circuits in each channel. These are modelled as a single, complex weight circuit with a frequency response which is given by

$$\omega_k^* + \gamma_k^*(\omega) = \alpha_k - j\beta_k + (\gamma_{k1}(\omega) - j\gamma_{k2}(\omega)) \qquad (1)$$

where α_k and β_k denote the I and Q frequency independent weights and $\gamma_{k1}(\omega)$ and $\gamma_{k2}(\omega)$ denote the I and Q frequency dependent weight feedthrough paths respectively. α_k and β_k are assumed directly controllable over the range -1 to +1 by means of drive voltages derived from the I and Q outputs of the correlator circuitry.

Using the above notation, the processor output, $v_o(t)$ can be expressed as a weighted sum of the N waveforms, $v_k(t)$, k = 1, ..., N:

$$v_o(t) = \sum_{q=1}^{N} w_q^* v_q(t) + \sum_{q=1}^{N} \int_{-\infty}^{\infty} \Gamma_q^*(-\tau)\, v_q(t-\tau)\, d\tau \qquad (2)$$

where we have defined the impulse response of $\gamma(\omega)$ to be $\gamma(\omega) \leftrightarrow \Gamma(t)$, where the arrow "$\leftrightarrow$" denotes a Fourier transform pair. Note that $\gamma(\omega) \leftrightarrow \Gamma(t)$ implies that $\gamma^*(\omega) \leftrightarrow \Gamma^*(-t)$, leading to the presence of $\Gamma_q^*(-\tau)$ in the convolution integral in Eq. (2). By considering the basic feedback relations defined at the sum junction in the baseband branch of the loop, it can be shown[2] that each complex weight, w_k satisfies the first-order differential equation,

$$\tau_o \dot{w}_k + w_k + \mu X_k = V_k \quad , \quad k = 1, \ldots, N \qquad (3)$$

where $X_k(t)$ is the output of the kth complex correlation mixer and the dot notation indicates a time derivative. The complex correlation mixer consists of separate I and Q mixers followed by low pass filters to select the lower side band. In complex notation the mixer output is given by $X_k(t) = v_k(t)\, v_o^*(t)$. Note that $X_k(t)$ is a stochastic waveform. It is conventional to design the feedback loops so that the closed loop bandwidth is considerably less than the bandwidth of n(t) after filtering by the bandpass filters in the RF/IF front end. In this case, Eq. (3) acts to yield an averaging or integrating effect on $X_k(t)$. If the input process is stationary over the loop adaption time, then the "short time average" of $w_k(t)$ (averaged over the time scale, $1/BW_c$, where BW_c is the closed-loop bandwidth in hertz) can be estimated by averaging Eq. (3) over the ensemble of sample functions of n(t). We obtain

$$\tau_o \dot{w}_k + w_k + \mu E\{X_k\} = V_k \quad , \quad k = 1, \ldots, N \qquad (4)$$

where, for convenience, we now denote $E\{w_k\}$ by the same variable, w_k. It remains to determine $E\{X_k\}$. Using Eq. (2) we obtain

$$E\{X_k\} = \sum_{q=1}^{N} w_q \, E\{v_k(t) v_q^*(t)\}$$

$$+ \sum_{q=1}^{N} \int_{-\infty}^{\infty} \Gamma_q(-\tau) \, E\{v_k(t) v_q^*(t-\tau)\} \, d\tau \qquad (5)$$

Consider the case where a single interference source is incident on the antenna. The expected value in Eq. (5) is readily expressed in terms of the power spectral density, $S_n(\omega)$ of the interference source input process, n(t). First, define $R_{k,q}(\tau)$ to be the cross-correlation function between $v_k(t)$ and $v_q(t)$[3], and denote the cross power spectral density to be $S_{k,q}(\omega) \leftrightarrow R_{k,q}(\tau)$. Then Eq. (5) can be written as

$$E\{X_k\} = \sum_{q=1}^{N} w_q \, R_{k,q}(o) + \sum_{q=1}^{N} \int_{-\infty}^{\infty} \Gamma_q^*(-\tau) \, R_{k,q}(\tau) \, d\tau \qquad (6)$$

The integral in (6) can be expressed in terms of $S_{k,q}(\omega)$ by replacing $\Gamma_q^*(-\tau)$ and $R_{k,q}(\tau)$ by their Fourier transforms.

$$\int_{-\infty}^{\infty} \Gamma_q^*(-\tau) \, R_{k,q}(\tau) \, d\tau = \frac{1}{2\pi} \int_{-\infty}^{\infty} \gamma_q(\omega) \, S_{k,q}(\omega) \, d\omega \qquad (7)$$

Using Eq. (7), Eq. (6) can be rewritten in the form

$$E\{X_k\} = \sum_{q=1}^{N} \frac{1}{2\pi} \int_{-\infty}^{\infty} (w_q + \gamma_q(\omega)) \, S_{k,q}(\omega) \, d\omega \qquad (8)$$

The cross-spectral density $S_{k,q}(\omega)$ is readily expressed in terms of $S_n(\omega)$ using the results of Ref. 3 (Chapter 9):

$$S_{k,q}(\omega) = A_k(\omega) \, A_q^*(\omega) \, H_k(\omega) \, H_q^*(\omega) \, S_n(\omega) \qquad (9)$$

Finally, we assume that $S_n(\omega)$ is white over the nulling band and define $S_n(\omega) = R_j/BW$ where we assume each $H_k(\omega)$ has a nominal bandwidth of BW Hertz, and R_j denotes the average power of the incident noise process over the

nulling band arising from a single interference source. In this case Eq. (8) can be written in the simplified form

$$E\{X_k\} = R_j \sum_{q=1}^{N} \langle (w_q + \gamma_q(\omega))\ A_k(\omega)\ A_q^*(\omega)\ H_k(\omega)\ H_q^*(\omega) \rangle \tag{10}$$

where the bracket notation $\langle \cdot \rangle$ denotes an average over the nulling bandwidth

$$\langle \cdot \rangle \equiv \frac{1}{2\pi BW} \int_{\omega_o - \pi BW}^{\omega_o + \pi BW} (\cdot)\ d\omega \tag{11}$$

Using Eq. (10) in Eq. (4), the time evolution of the N weights $w_1(t), \ldots, w_N(t)$ can be expressed in vector form as

$$\tau_o \dot{\underline{w}} + \underline{w} + \mu \langle R_j\ \underline{E}\ \underline{E}^\dagger \cdot (\underline{w} + \underline{\gamma}) \rangle = \underline{V} \tag{12}$$

where the notation "†" denotes the complex conjugate transpose operation, the underbar denotes a column vector of the N appropriate scalar variables, and $E_k(\omega) \equiv H_k(\omega)\ A_k(\omega)$ is the overall channel frequency response.

Equation (12) governs the time-evolution of the complex weight $\underline{w}$ for a white noise process as an input to the processor resulting from a single interference source, and with frequency dependent channel characteristics embodied in $\underline{E}(\omega)$. For ideal weight circuits, $\underline{\gamma}(\omega) = 0$ and Eq. (12) reduces to

$$\tau_o \dot{\underline{w}} + \underline{w} + \mu \underline{\underline{R}} \cdot \underline{w} = \underline{V} \tag{13}$$

where the matrix $\underline{\underline{R}} = R_j \langle \underline{E}\ \underline{E}^\dagger \rangle$ as defined above.* Equation (13) is the conventional form of the equations characterizing the time-evolution of $\underline{w}$ that is discussed in Ref. 2 for narrow-band channels and in Ref. 1 for wide-band channels. The effect of $\underline{\gamma}$ on the performance of the processor is one of the component error effects to be considered in the following sections.

---

*A more general definition of R is

$$R = E\{\underline{v}(t)\ \underline{v}(t)^\dagger\} \tag{14}$$

The definition used in Eq. (13) is a special case which is particularly useful in testing or characterizing nulling performance in the frequency domain.

We conclude this section by defining some parameters that are useful for characterizing the performance of a processor. The expected value of power output of the processor is given by

$$P_o = E\{|v_o(t)|^2\} \tag{15}$$

Strictly speaking, this is an ensemble average defined over the ensemble of sample functions of the input noise process, n(t). Practically speaking, it is essentially the same as a time average of the power as long as the average is taken over an interval of time greater than the inverse nulling bandwidth (in hertz). Using the same procedure used above, P_o can be expressed as a frequency average

$$P_o = \langle (\underline{w} + \underline{\gamma}(\omega))^\dagger \cdot R_j \, \underline{E}(\omega) \, \underline{E}^\dagger(\omega) \cdot (\underline{w} + \underline{\gamma}(\omega)) \rangle \tag{16}$$

$\underline{w}$ in Eq. (16) is frequency independent. If $\underline{E}(\omega)$ and $\underline{\gamma}(\omega)$ vary significantly over the nulling bandwidth, the average output power will necessarily be greater than the case where $\underline{\gamma}$ and $\underline{E}$ are frequency independent. To assess these effects, it is convenient to define the cancellation, C, by

$$C = (I/N)_a / (I/N)_b \tag{17}$$

where (I/N) denotes the ratio of average interference output power (i.e., that contribution of P_o due to n(t)) to the average thermal noise output power. The subscripts "a" and "b" denote "after adaption" and "before adaption," respectively. $(I/N)_b$ is a function of the steering vector, $\underline{V}$, which is the weight setting in the absence of interference (or quiescent weight setting). Following Ref. 2, it is conventional to normalize the incident interference power, R_j, to receiver thermal noise power. When this is done, the cross-spectral density, $S_{k,q}(\omega)$ of the thermal noise is an identity matrix. This assumes the noise in each channel to be uncorrelated with the other channels and of the same power level as the other channels. Then, using Eq. (16), the expression for $(I/N)_{a \text{ or } b}$ reduces to

$$(I/N)_{a \text{ or } b} = \frac{\langle (\underline{w} + \underline{\gamma})^{\dagger} \cdot R_j \, \underline{E}\,\underline{E}^{\dagger} \cdot (\underline{w} + \underline{\gamma}) \rangle}{\langle (\underline{w} + \underline{\gamma})^{\dagger} \cdot (\underline{w} + \underline{\gamma}) \rangle} \tag{18}$$

where we get the "after adaption" or "before adaption" value by inserting the appropriate weight vectors. When $\underline{\gamma} = 0$ this reduces to the more familiar form,

$$(I/N)\Big|_{\gamma=0} = \frac{\underline{w}^{\dagger} \cdot \underline{\underline{R}} \cdot \underline{w}}{\underline{w}^{\dagger} \cdot \underline{w}} \tag{19}$$

where, as before, $\underline{\underline{R}} = R_j \langle \underline{E}\,\underline{E}^{\dagger} \rangle$.

The above definitions are the basis for a systematic approach to classifying and quantizing the effects of component imperfections on the overall performance of an adaptive antenna system. For example, antenna dispersion is accounted for by $A_k(\omega)$. Channel tracking errors, or the mismatches in the channel frequency responses, can be incorporated in the $H_k(\omega)$ and so on. In the following sections, these error effects are quantified in terms of their impact on the achievable cancellation, C. Cancellation is not entirely satisfactory for use as a figure of merit because it depends not only on the error effects, but also on the choice of steering vector, $\underline{V}$, power level, and processor threshold level. Quoting a cancellation number alone can therefore be misleading unless one specifies the other conditions for which it is applicable. We have generally used one of two standard choices of beam steering vectors in the following discussions. Unless otherwise stated, we have used an "earth coverage" quiescent radiation pattern, which is a uniform gain beam 18° wide. The corresponding $\underline{V}$ for a PA is $\underline{V}$ = col(1, 0, 0, ...). The other standard choice is a $\underline{V}$ that points a maximum gain beam in some specified direction.

Finally, before proceeding to a discussion of the results summarized in Section III, some basic assumptions inherent in these results should be discussed. First, we assume weight circuits whose phase and amplitude are ideally frequency independent. This precludes the use of tapped delay line

or other frequency dependent weight designs. Second, we constrain the processor to allocate only a single degree of freedom per interference source. When a single interference source is incident on an adaptive antenna, the adaptive processor will generally allocate as many degrees of freedom as are needed to form a null over the total nulling bandwidth. However, this situation is undesirable for several reasons, perhaps the most important of which is that using more than a single degree of freedom to form a wideband null on the source leads to a spatially broad null. (Note: for an array, the phase at each element varies as $\omega \sin\theta$ -- or simply, as $\omega\theta$ for small θ. Hence, the processor output is a function of $\omega\theta$, so that fixing θ and varying ω gives the same result as fixing ω and varying θ.) Hence, if one allocates several processor degrees of freedom to null a single source over, say, a 20% frequency band, the angular width of the resulting spatial null will be 20% of the interference source off-axis angle. This significantly limits the off-axis angular resolution achievable with the antenna. Another reason for constraining the processor to one degree of freedom per source is simply that the systems we have considered have a limited number of degrees of freedom and we want to maximize the number of sources they are capable of nulling.

III. CLASSIFICATION OF COMPONENT ERROR CHARACTERISTICS AND THEIR EFFECTS

A block diagram illustrating the basic sections of an adaptive antenna feedback nulling system is shown in Fig. 2. We use a feedback nulling processor to develop the effects of the various components on performance. Most results, however, are readily applicable to other types of processors such as open-loop and feed-forward processors. The feedback mechanism, however, does compensate for certain frequency independent errors which would affect the cancellation performance of open-loop systems. Parameters characterizing each sub-section of the processor are listed in each block. The effects of parameters associated with each sub-section on the cancellation achievable from the processor will be developed in detail in Sec. IV. For convenience these results are summarized in Table 1. A brief discussion of Table 1 will

TABLE 1

FACTORS AFFECTING CANCELLATION

EFFECT	CANCELLATION DEPENDENCE
1. Antenna Dispersion	
a) N-Element Array	$C = K_1\left(\frac{D}{\lambda} \sin \theta \cdot FBW\right)^2$
b) MBA - Time Delayed Beams	$C = K_2(FBW)^2$
2. Correlated Channel Tracking Errors (Δ = RMS Path Length Mismatch consisting of Antenna Placement Errors Normal to the Plane Containing the Array or Cable/ Channel Path Length Mismatch)	$C \lesssim \frac{1}{3}\left(\frac{\pi BW}{v_p}\right)^2 \Delta^2$
3. Uncorrelated Channel Tracking Error (σ^2)	
a) Earth Coverage	$C \leq \sigma_{MAX}^2$
b) Beam to User	$C \leq \sigma_{MAX}^2/N$
4. Weight Circuits	
a) Feedthrough (Isolation $\lvert\gamma_o\rvert^2$)	
Uncorrelated Feedthrough (σ^2)	$C \leq N\lvert\gamma_o\rvert^2 \sigma^2$
Correlated Feedthrough (delay τ)	$C \leq N^2\lvert\gamma_o\rvert^2 \frac{(\pi BW\tau)^2}{3}$
b) Weight Quantization (σ^2)	$C \leq \sigma^2$
c) I/Q Imbalance (Frequency Independent)	No effect.
5. Errors in Feedback Paths	
a) Frequency Independent	Equivalent to Beam Steering Vector Error (Loop Stability may be affected)
b) Frequency Dependent	Weak Dependence
c) Weight Noise	Spectrum Modulation of Communications Signals
6. Hard-Limiting in Feedback Loops	Small Eigenvalue Suppression Relative to Non-Limited System $s_2 \rightarrow s_2/\sqrt{\mu s_1}$

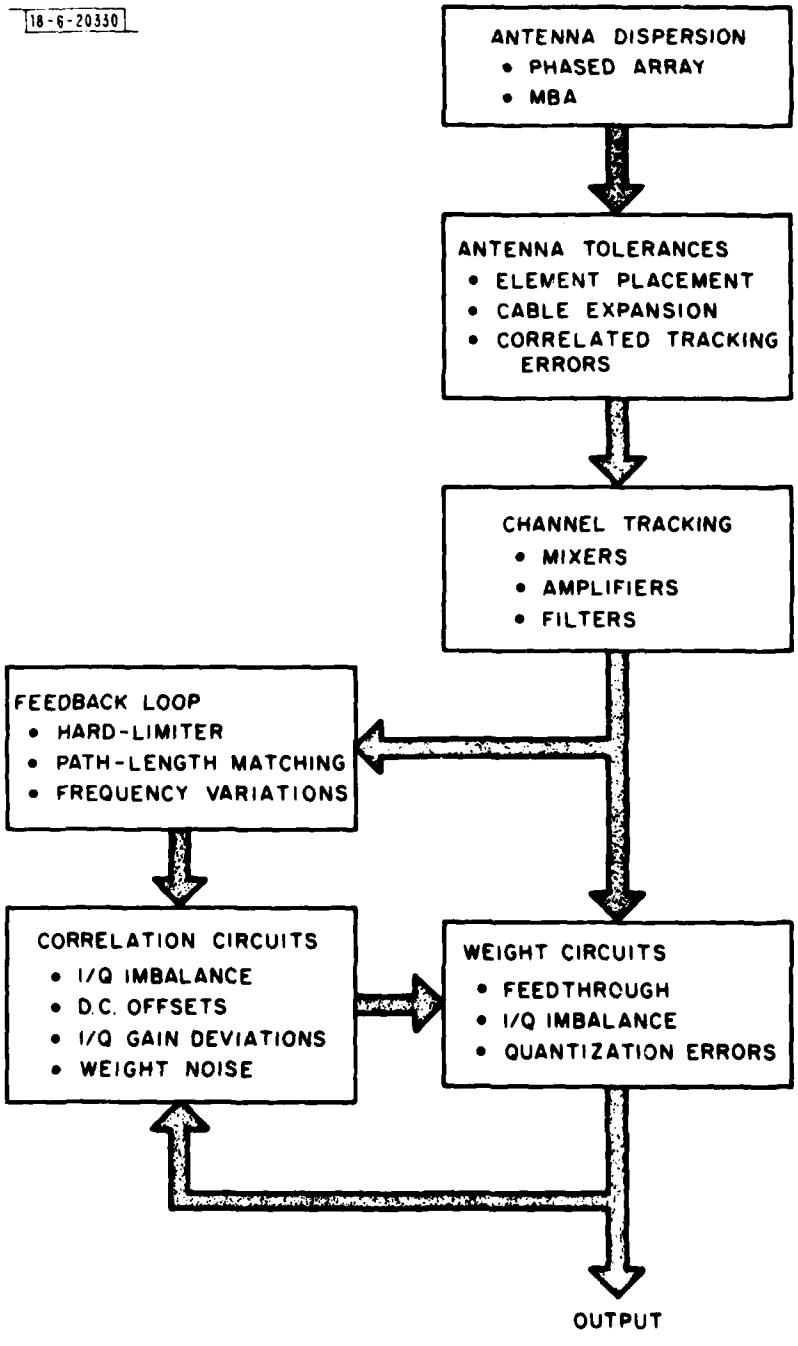

Fig. 2. Component effects characterizing a closed-loop adaptive nulling processor.

be presented in the remainder of this section; the reader not interested in the development of Section IV leading up to these results may readily skip to Section V.

Recognizing that the results of Table I apply with the assumptions mentioned above and in Section II, the cancellation dependence on each sub-section of the processor can now be considered.

1. Antenna Dispersion

The effects of antenna frequency dependence (i.e., antenna dispersion) on the cancellation achievable with a particular antenna type have been studied in some detail in Ref. 1. Basically, antenna dispersion results from the differing frequency responses of each element of the adaptive antenna. Generally each antenna output port has a frequency response function that depends on the interference source location. The nature of this frequency dependence is fundamentally different for an array antenna when compared to a multiple beam antenna employing time delayed beams, and this difference clearly shows up in the dependence of cancellation on aperture size. Although the cancellation is a function of fractional bandwidth (FBW = BW/f_o, f_o = center frequency, BW = bandwidth in Hertz) and degrades according to $(FBW)^2$ for both antenna types, the cancellation of an MBA becomes independent of its diameter for very large apertures whereas the performance for the PA degrades as $(D/\lambda)^2$. Therefore, MBA's become inherently more broad band at higher frequencies when larger apertures might be used. A theoretical development with computer simulations verifying this result will be presented in Sec. IV.

2. Correlated Tracking Errors

Assembly of the antenna system usually results in errors in positioning the antenna elements and matching the cable lengths. Generally, for a satellite at geosynchronous orbit, only the placement errors that are perpendicular to the plane containing the array are important. These can be described statistically as an rms error, Δ, in the overall path length of each channel. The important conclusion from the result of Table I is that

matching of these path lengths is dependent only on the bandwidth and not the RF or IF frequencies. The cancellation deteriorates approximately as $\frac{1}{3}(\pi BW\Delta/v_p)^2$ where v_p is the phase velocity in the propagation medium. These tolerances on path length matching must be maintained following the antenna through each channel down to the sum junction, although v_p will vary dependent on the propagation medium.

3. Uncorrelated Channel Tracking Errors

Implementation of the N-channels of an adaptive processor usually results in differences in the frequency response functions (i.e., tracking errors) of each channel. These tracking errors can usually be characterized by an rms amplitude and phase error, $\sigma^2 = \sigma_A^2 + \sigma_\phi^2$, which tends to be uncorrelated from channel to channel. The tracking errors are generally dominated by the filters in each channel which set the processor nulling bandwidth and by the mixers which may be used to convert each channel to an IF frequency for weighting. The effects of such uncorrelated tracking errors have been discussed in some detail in Ref. 1, and the cancellation limits for two particular modes of operation listed in Table I are developed in that reference. The most notable of those results is that in the case of an earth coverage quiescent pattern obtained from a PA antenna, best cancellation results are obtained by selecting the "best" channel (i.e., the one with the lowest measured rms tracking error) as the reference channel.

4. Weight Circuits

The usual approach to adaptive processing is to implement frequency independent weights -- i.e., ones for which amplitude and phase hold the same values over the entire nulling band. In reality such a weight is achievable only within certain limits. We have found that a good model applicable to many realistic weight circuit designs is an ideal, frequency-independent weight shunted by a non-weighted feedthrough path (see Fig. 1). The amount of feedthrough is characterized by an isolation parameter, $|\gamma_o|^2$, and a time delay, τ, relative to the weighted path.

This model can accommodate two basically different types of feedthrough -- correlated and uncorrelated. In the latter case the k^{th} channel feedthrough path is characterized as a random function of frequency, $\gamma_k(\omega)$, with mean, γ_{ok}, and standard deviation, σ_k. The $\gamma_k(\omega)$ are assumed to be uncorrelated from channel-to-channel in the sense that

$$\int_{-\infty}^{\infty} \langle (\gamma_k(\omega) - \gamma_{ok})\ (\gamma_j(\omega) - \gamma_{oj})^* \rangle\ 0 \ = \ 0 \tag{20}$$

For uncorrelated feedthrough we assume τ_k to be 0.

To model correlated feedthrough we have a frequency-independent isolation parameter, γ_{ok}, in series with a time delay in which case the frequency response of the k^{th} feedthrough path is

$$\gamma_k^*(\omega) \ = \ \gamma_{ok}\ e^{-j\omega\tau_k} \tag{21}$$

The $\gamma_k(\omega)$ are obviously correlated from channel to channel with the case of equal time delays yielding maximum correlation. The correlated feedthrough model is applicable to several real weight circuit designs and is considered to be a more useful model than uncorrelated feedthrough.

Notice from Table I that the cancellation effects of feedthrough are functionally similar to the effects of channel tracking errors except that cancellation performance degrades as N^2 where N is the number of channels. When the processor is assembled, two-channel measurements are the simplest to make; this is usually the manner in which the performance is specified. If the two-channel measurement yields a measured cancellation, C_2, then the system performance will degrade by $(N/2)^2$ relative to C_2 in an N-channel system. This corresponds to a 12-dB degradation for an 8-channel processor. A more thorough examination of feedthrough, and techniques for measuring this effect, is presented in Sections IV and V.

Other types of errors which might occur in the weighting circuits are I/Q imbalance and weight-quantization, if digital control of the weights is used. I/Q imbalance results from an I/Q-type weight where the phases of the

I and Q sections of the weight are not in true quadrature (for example, an imperfect hybrid is used). Normally the deviation from quadrature is on the order of 1-5°, depending on the IF frequency. However, most hybrids are broadband devices so that this deviation from quadrature is generally constant over the nulling band. In this case, it can be shown that a closed-loop feedback algorithm compensates for this error so that it imposes no limitations on cancellation. If the I/Q phase difference should vary with frequency, its effect on cancellation will be the same as for a weighted channel-tracking error.

Weight quantization usually results in a weight setting that is slightly different from optimum. If $\underline{w}$ is the optimum weight, then $\underline{w}_q = \underline{w} + \Delta\underline{w}$ is the applied weight as a result of quantization. The quantization error, $\Delta\underline{w}$, is similar mathematically to an rms mismatch between channels when averaged over all possible weight settings. The cancellation is then limited by σ^2, which we defined as the rms quantization error (see Eq. (65)).

5. Feedback Path Errors

The basic function of the feedback loops in an adaptive processor is to sense the N × N correlation matrix of the N signal channels. Denote this correlation matrix by $\underline{\underline{R}}$. The array output power is then given by (without feedthrough)

$$P_o = \underline{w}^{\dagger} \cdot \underline{\underline{R}} \cdot \underline{w} \tag{22}$$

where $\underline{w}$ is a column vector of the weights and "†" denotes the complex conjugate transpose operation. For an ideal system, then, the steady-state adapted weights are given by (see Eq. (13), with $\tau_o \dot{\underline{w}} = 0$)

$$\underline{w} = [I + \mu\underline{\underline{R}}]^{-1} \cdot \underline{V} \tag{23}$$

where μ is the effective processor gain and $\underline{V}$ the quiescent beam steering vector. It is readily shown that using Eq. (23) in (22) results in a minimum in the radiation pattern in the direction of all interference sources while

yielding the best rms fit to the quiescent pattern defined by $\underline{V}$.[4] However, in a realistic system, due to the inherent errors present in the feedback loops, a slightly erroneous correlation matrix, $\underline{\underline{R}}'$, is actually sensed. Two basic questions then arise. How do the errors in $\underline{\underline{R}}'$ affect the achievable cancellation and how do these errors affect loop stability (i.e., the transient response during adaption)? A stability analysis for first-order control loops is presented in Sec. IV. The effects on cancellation are summarized in Table I.

The effect of errors in $\underline{\underline{R}}'$ can be conveniently separated into frequency independent errors and frequency dependent errors. Examples of the former include errors in quadrature hybrids, mixer imbalance, dc offsets, and differences in loop gains, whereas examples of the latter would include loop path length mismatches, and loop amplifier and filter tracking errors. Frequency independent errors have no effect on the capability of the processor to null the interference. Their main effects are to modify the equivalent beam steering voltages and to modify the stability margin of the loops. Frequency dependent errors in the feedback loop can degrade the ability of the processor to null the interference, but such effects are only second order relative to channel tracking errors. In fact, we show in Section IV that if the signal channels track perfectly, then frequency dependent errors in the feedback loops are totally compensated for by the feedback mechanism.

A third source of error can be attributed to the feedback circuitry weight noise, either generated independently in each loop or by the modulation induced on the weights as a result of the interference.[5] The main effect of this "weight jitter" is to modulate the signal waveforms passing through the weight circuits making the processor behave as a time varying multi-path communications channel. This can affect the signal detectability and induce cross talk between signals closely spaced in frequency. For example, when a c-w signal is incident on the antenna, weight noise generated internal to the baseband circuits modulates this signal so that the power spectrum of the output broadens, resulting in a higher total power level at the output. This effect can be used as a diagnostic tool to measure weight noise arising within the feedback loops.

6. Hard Limiting in the Feedback Loop

Previous analysis[6] on the effects of hard-limiting in adaptive feedback loops has led to the conclusion that such limiting relaxes circuit dynamic range requirements, while having little effect on the system cancellation performance. For a certain class of feedback loop designs, we have found this result to be valid for a single interference source, but not when multiple interference sources are present. A detailed analysis of the effects of hard-limited nulling processors can be found in Ref. 7. The effect of hard-limiting on cancellation performance (relative to a non-limited system designed for the same threshold power) is summarized in Table I for the case of two sources, P_1 and P_2, which generate two eigenvalues, s_1 and s_2, of the correlation matrix. Hard-limiting in the feedback loops has the effect of increasing the sensitivity threshold (or equivalently decreasing the feedback loop gain) applied to the smaller eigenvalue. For example, if the larger eigenvalue is 40 dB above the design threshold, the effective threshold for the smaller eigenvalue is raised by 20 dB and the smaller eigenvalue will not be sensed or nulled by the processor unless it is 20 dB or more above the design threshold. The result is a reduced sensitivity to the weaker sources, and reduced suppression of these sources relative to a non-hard-limited system.

IV. ANALYSIS OF COMPONENT IMPERFECTIONS ON CANCELLATION AND LOOP DYNAMICS

The previous section summarized some estimates of component limitations on system cancellation capabilities. In this section we develop these estimates in detail and also consider the effects of loop component errors on loop stability. Uncorrelated channel-tracking errors and hard-limiting effects are considered elsewhere[1,7] and will not be discussed further in this note. The remaining component effects will be developed in this Section.

A. Antenna Dispersion Effects

In this Section we assume the antenna and processor to be "ideal" (in the sense that no errors or imperfections are present) and consider the fundamental limitations on cancellation imposed by the antenna itself.

The achievable cancellation for a given size aperture depends strongly on the operating frequency, fractional nulling bandwidth and field-of-view. Furthermore, cancellation depends strongly on the choice of the steering vector that governs the quiescent radiation pattern (e.g., earth coverage or directed-beam-to-user). A rule of thumb for geosynchronous satellite antennas is that ideal antenna dispersion will limit achievable cancellation to about 40 dB over a 3% bandwidth with a D/λ of 10[4], for interference sources within 8° of boresight using one degree of freedom per interference source. An aperture diameter of 10λ is a lower limit for what would be required on a satellite-borne antenna operating at UHF. Since aperture sizes much larger than 10λ will be desired at higher frequencies and since fractional bandwidths larger than 3% might be employed in spread-spectrum communications systems, it is desirable to extrapolate this rule of thumb to larger D/λ's and to larger bandwidths. Since the cancellation performance of multiple beam antennas and phased arrays is different, we consider them separately. We shall show that the MBA has considerably greater bandwidth potential than the PA as D/λ increases.

1. Phased Array

The dependence of cancellation on bandwidth and aperture size can be determined directly from the eigenvalues of the expected value of the correlation matrix of the signals at the antenna output ports. Denote this matrix by $\underline{\underline{R}}$, the corresponding eigenvalues by $s_1, s_2, \ldots, s_n$ and the eigenvectors as $\underline{e}_1, \underline{e}_2, \ldots, \underline{e}_N$. Then the cancellation, C, is generally given by[1]

$$C = K\, s_2/s_1 \tag{24}$$

where K is a constant depending on the steering vector $\underline{V}$ and array configuration and we assume that $\underline{e}_2^{\dagger} \cdot \underline{V} \neq 0$ (the case $\underline{e}_2^{\dagger} \cdot \underline{V} = 0$ would correspond to a special case unique to a particular choice of $\underline{V}$ -- in this case $C \alpha s_3/s_1$). It remains now to estimate s_1 and s_2 as functions of D/λ and bandwidth. In Appendix I we show that for the phased array,

$$C = K\, (D/\lambda \sin\theta * FBW)^2 \tag{25}$$

where K is a constant and θ is the scan angle relative to array broadside. This is the functional dependence shown in Table I. For example, since C increases as $(D/\lambda)^2$, increasing D from 10λ to 100λ for a fixed antenna geometry degrades the achievable nulling performance by 20 dB! For $D/\lambda = 10$, $\theta = 8°$ and FBW = .032, a typical number for C is 10^{-4} and we can express (25) in the form

$$C = 5.2 \times 10^{-2}\, (D/\lambda \sin\theta * FBW)^2 \tag{26}$$

Of course, better cancellation levels might be obtained by using up more than one degree of freedom per interference source, but this results in a broader angular null and therefore less gain for users in close proximity to the interference source. It also limits the maximum number of interference sources which can be nulled by the array. Equation (26) indicates that for a fractional bandwidth of 2%, null depths on the order of 25 dB are realizable for an aperture diameter of 100λ, using a single degree of freedom per interference source. A wider fractional bandwidth of 5% would reduce the cancellation performance to less than -20 dB for the same size aperture.

As an example to illustrate the validity of the approximations leading up to Eq. (25), consider the 13-element thinned array illustrated in Fig. 3 having the normalized coordinates for each element indicated in the Figure. A signal source is positioned at angular coordinates $\theta_s = 7.7°$, $\phi_s = 0°$ and an interference source 0.3° away at $\theta_i = 8.0°$, $\phi_i = 0°$, which is equivalent to an elevation angle to the satellite of 20°. This spacing of 0.3° between user and interference corresponds to a half-power beamwidth/2 for $D/\lambda \approx 100$. Figure 4 illustrates the behavior of the first four eigenvalues of the correlation matrix of interference signals as functions of D/λ assuming a fixed fractional bandwidth of .046 and white noise interference spectrum over this band. s_1 corresponds to the array output power realized with a maximum gain beam pointed to the interference source. Therefore, we expect s_1 to be very nearly equal to $R_j NG_e$ (where G_e is the element gain) and to be independent of D/λ. Observe from the figure that

$$s_1 \sim \text{constant} \tag{27a}$$

$$s_2 \sim (D/\lambda \sin\theta * FBW)^2 \tag{27b}$$

$$s_3 \sim (D/\lambda \sin\theta * FBW)^4 \tag{27c}$$

$$s_4 \sim (D/\lambda \sin\theta * FBW)^6 \tag{27d}$$

The behavior of s_2 is clearly consistent with the results of Appendix I. To check the validity of Eq. (26) for cancellation, we compute from our example the cancellation and user gain loss assuming that the interference power is 30 dB above the processor threshold. This threshold level of the processor is indicated in Fig. 4. Since the processor does not respond to the eigenvalues below threshold, only eigenvalues above threshold are sensed and nulled. The number of eigenvalues above threshold is the number of degrees of freedom used by the processor to form the null. The loss in user gain and cancellation are shown in Fig. 5 as a function of D/λ. We have assumed a steering vector that directs a maximum gain beam to the user in the unadapted case. The user power is negligible in its impact on processor performance.

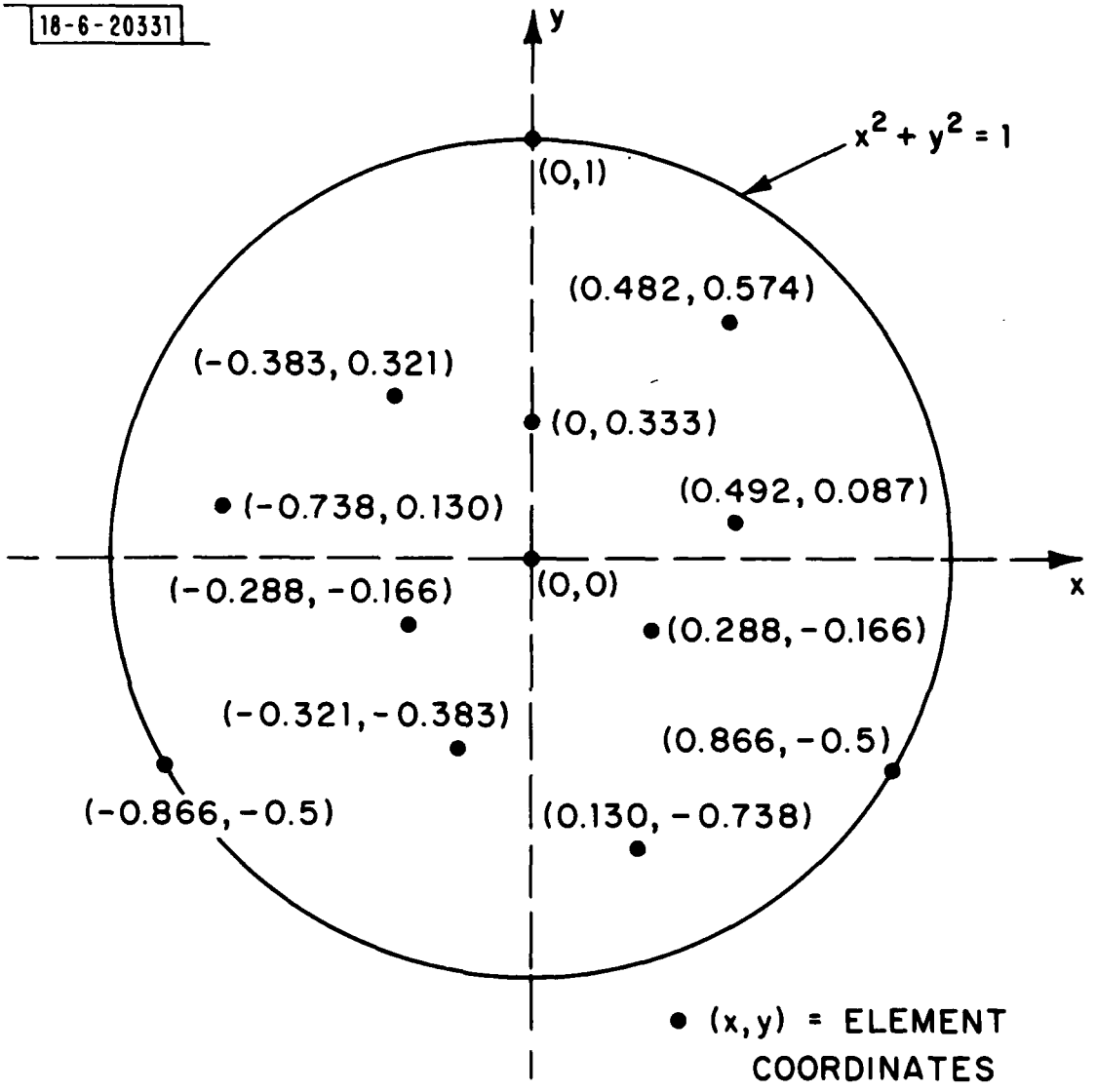

Fig. 3. 13-element thinned planar array geometry used for the simulations of Figs. 4 and 5.

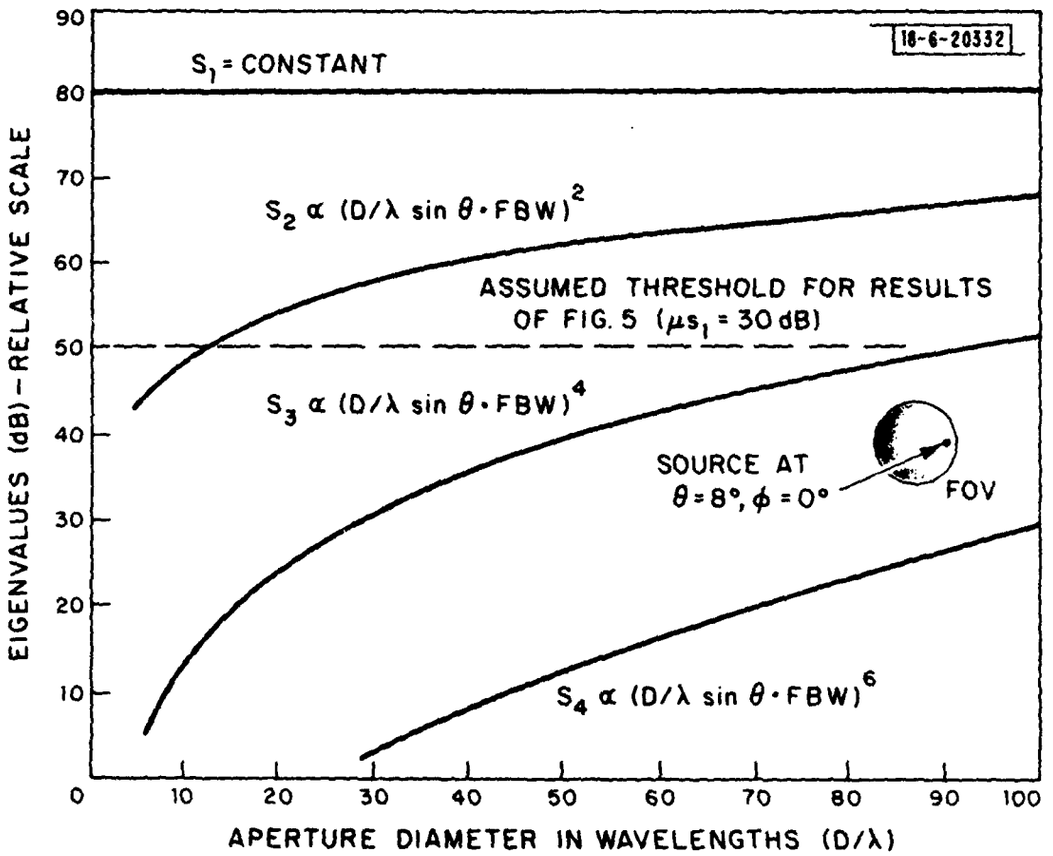

Fig. 4. Eigenvalues s_1, s_2, s_3 and s_4 vs. aperture diameter, D/λ for the 13-element planar array of Fig. 3. The interference source is positioned at $\theta_i = 8^o$, $\phi_i = 0^o$. FBW = .0455.

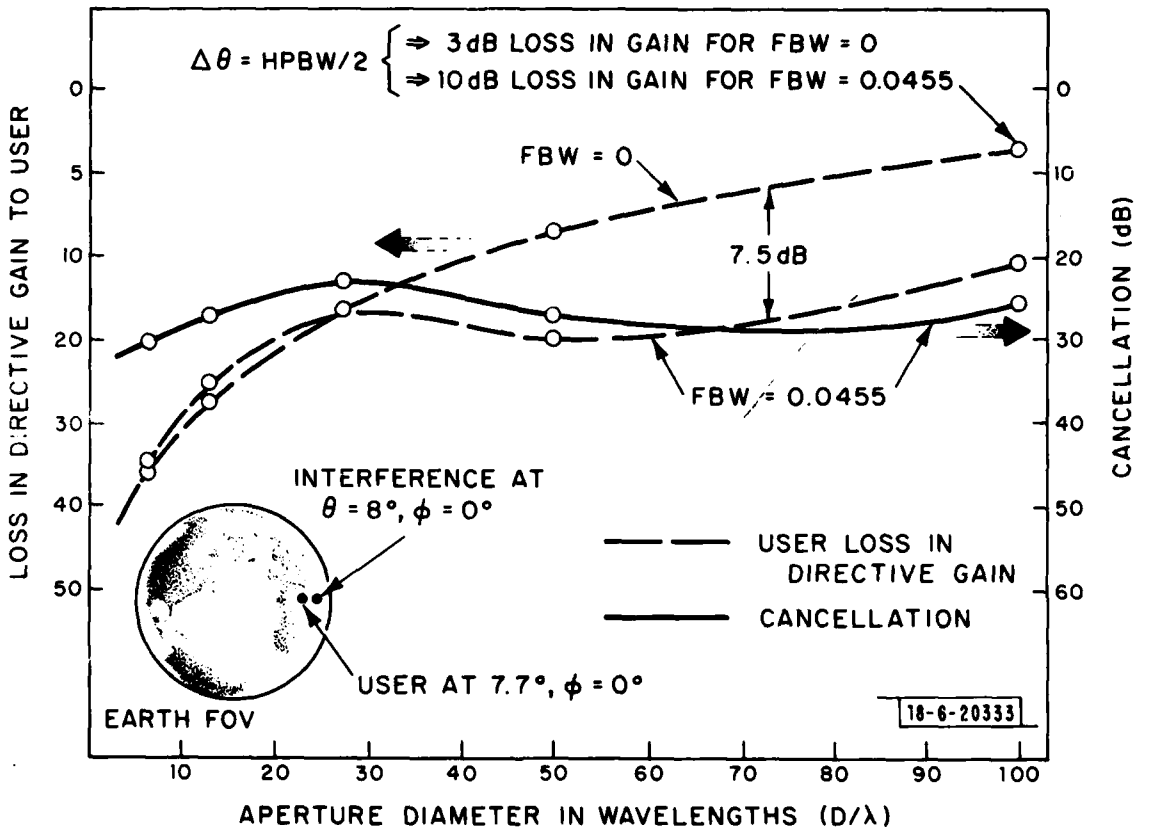

Fig. 5. Cancellation and user loss in directive gain vs. D/λ when a user source is positioned 0.3^{o} from the interference source location of Fig. 4 for the 13-element planar array of Fig. 3. $\Delta\theta = 0.3^{o}$ corresponds to a quarter half-power beamwidth (HPBW) for $D/\lambda \approx 100$.

Observe that for $D/\lambda \lesssim 15$, the processor senses only the first eigenvalue, therefore only one degree of freedom is used to null the interference. The resulting cancellation is about -30 dB. For $D/\lambda \approx 25$, the second eigenvalue is sensed so that two degrees of freedom are used to form a wide-band null. The resulting cancellation is about -25 dB, 4 dB worse than predicted by Eq. (26) (which assumes only a single eigenvalue sensed). As D/λ increases still further, the cancellation remains fairly constant at about -28 dB, even though the processor is now using more degrees of freedom to form a null. However, the user gain degrades rapidly as a consequence of the loss in resolution due to the wide-band null. To illustrate this, the loss in gain to the user which would be obtained for FBW = 0 is also plotted in the figure. Up to 7.5 dB loss in directive gain in the direction of the user occurs as a consequence of using additional degrees of freedom to wide-band the null. Therefore, the achievable S/J (signal-to-interference power ratio) improvement averaged over the band is only about 16 dB for $D/\lambda = 100$!

These results show that Eq. (26) is valid as long as a single eigenvalue per source is sensed. They also illustrate that using more than one degree of freedom may improve the cancellation, but it may not improve the S/J performance because the user gain may suffer. These results also show that the phased array becomes relatively narrow-band near the edge of the FOV. The cancellation versus bandwidth achievable with an MBA is much better than for a PA. We now consider this antenna configuration.

2. Multiple Beam Antennas

The general characteristics of multiple beam antennas for use in satellite-earth coverage applications are discussed in Ref. (8). The salient features of MBA's used for this application briefly be summarized.

A multiple-beam antenna located on a geosynchronous satellite illuminates the earth with a fixed position set of beams, the composite of which cover the earth FOV. For earth coverage illumination (i.e., a circular FOV), the beams are generally positioned hexagonally and usually are chosen to number 7, 19, 37, 61, ... in order to fully illuminate the circular FOV. To each beam-set

covering the earth, there corresponds a given size aperture consistent with this number of beams. When a lens or reflector antenna system is used, physical realization of the beam-set is obtained by offsetting an array of feeds from the focal point of the lens or reflector, transverse to the focal axis. Consequently, each beam has a beam-width and sidelobe levels consistent with full aperture illumination. As the number of beams increases to cover a fixed FOV, the aperture size, D/λ, must increase correspondingly. Hence, for a large number of beams, there is significant coupling only between adjacent beams. This leads to a correlation matrix $\underline{\underline{R}}$, defined at the feed port outputs, which is diagonally dominant. Furthermore, an interference source positioned at a specific location on the earth is characterized only by that set beams in close proximity to the source. Consequently, the eigenvalues of the feed-port correlation matrix resulting from this source are dominated by the sub-matrix generated by the beams surrounding the interference. Otherwise said, adding more beams to the antenna configuration far away from this source should not affect the eigenvalues of $\underline{\underline{R}}$. However, as discussed above, adding more beams corresponds to increasing D/λ for a fixed FOV. Consequently, we anticipate that the cancellation dependence of the MBA operating over a fixed FOV becomes independent of D/λ (or number of beams) as D/λ becomes large. Thus, the cancellation achievable with an MBA tends to be dependent on the position of an interference source within the surrounding beam set, and this positioning is predominantly aperture independent. The resulting simulations will, indeed, verify this conjecture.

Because the frequency transfer function, $A_k(\omega)$, characterizing the N beams of the MBA is much more complicated than for the phased array, it is difficult to obtain analytical results predicting the dependence of cancellation vs. $D/\lambda \sin\theta$ and FBW for the MBA similar to those of Appendix I for the phased array. Consequently we resort to computer simulations. In order to generate a simulation for the MBA paralleling the analysis of the phased array, we again separate the jammer and user positions by 0.3°. The MBA performance curves corresponding to Figs. 4 and 5 for the phased array are illustrated in Figs. 6 and 7. For $D/\lambda = 10$, 7 beams cover the FOV and were

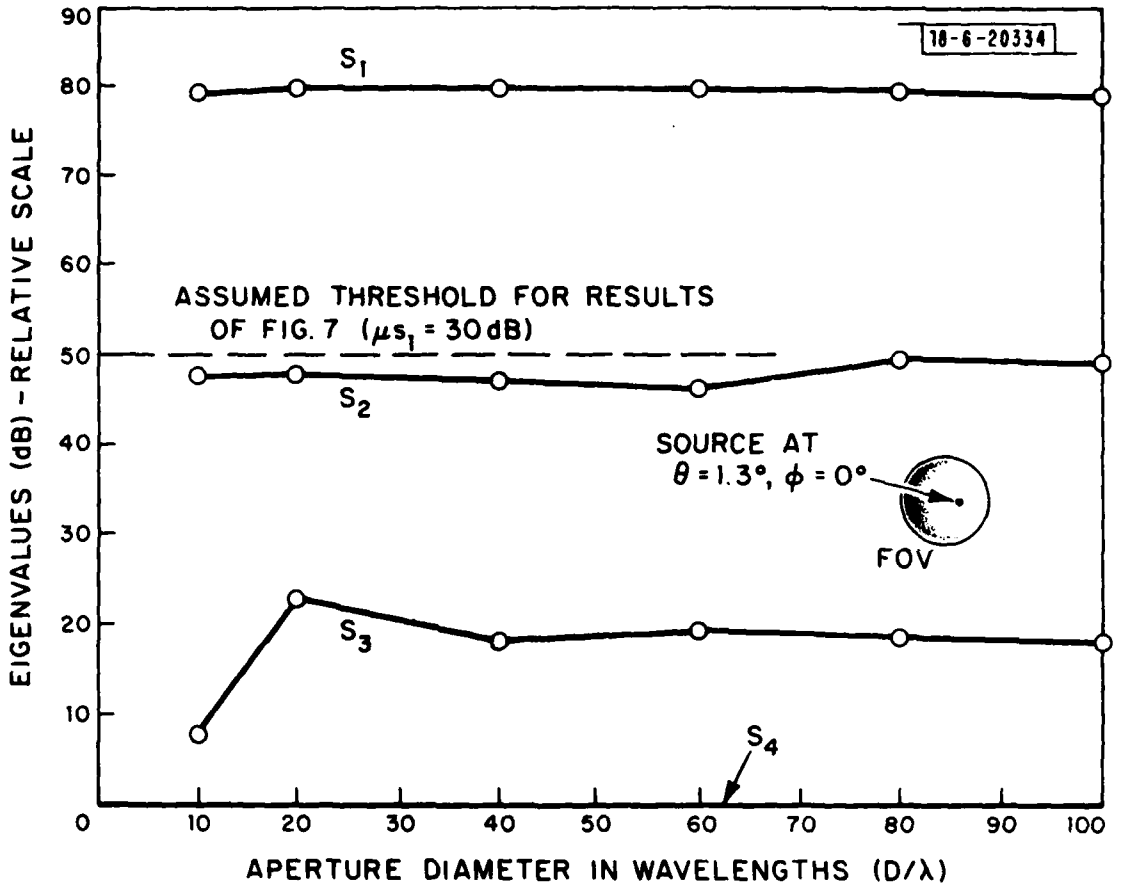

Fig. 6. Eigenvalues s_1, s_2, s_3 and s_4 vs. aperture diameter, D/λ, for a 19-beam Multiple Beam Antenna D/λ = 10 uses only 7 beans to cover FOV). Interference source is positioned at $\theta = 8^o$, $\phi = 0^o$. FBW = .0455.

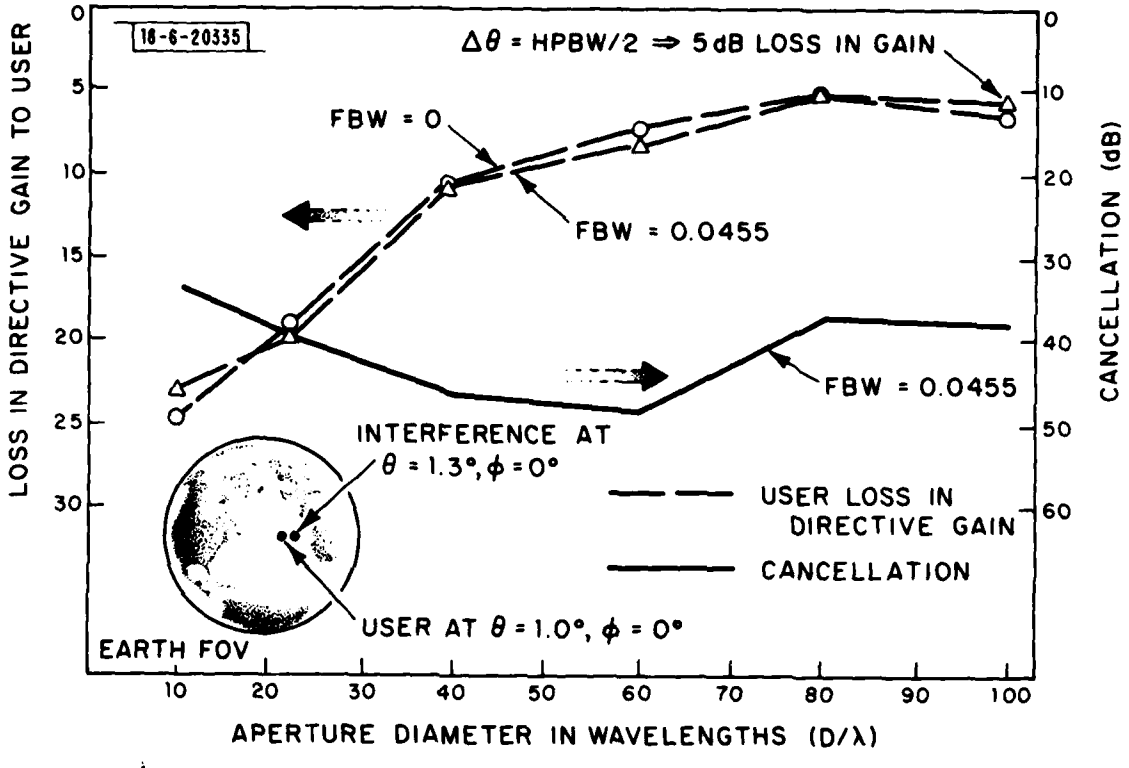

Fig. 7. Cancellation and user loss in directive gain vs. D/λ for an MBA employing time-delayed beams when a user source is positioned 0.3^{o} from the interference source location of Fig. 6. $\Delta\theta = 0.3^{o}$ corresponds to (HPBW)/2 for $D/\lambda \approx 100$.

used in the simulation. For $D/\lambda \lesssim 20$, the simulation employed only the 19 beams at the center of the FOV so that existing computer programs limited to a small number of beams could be used. The user and interference source were placed at $\theta_s = 1°$, $\phi_s = 0$ and $\phi_i = 1.3°$, $\phi_i = 0$ respectively. Since the MBA is scan angle dependent only relative to the position of the interference source amongst a triad of adjacent beams, this positioning relatively close to array broadside does not compromise the simulation results concerning bandwidth. Inclusion of the outer beams to cover the FOV completely would not affect the results appreciably. Observe in Fig. 6 that all the eigenvalues are relatively independent of aperture size. Generally, for fixed input power, s_1 should increase as $(D/\lambda)^2$, since s_1 represents the maximum power received with a maximum directivity beam pointed to the source, and this maximum gain increases as $(D/\lambda)^2$. However, in order that the nulling processor used in the simulation might see the same input power for each D/λ, we have adjusted the input power for each D/λ so that s_1 remains constant, independent of D/λ. The processor gain, μ, is then chosen for each case so that $\mu s_1 = 30$ dB. The simulations confirm that s_2 is also independent of D/λ. Then to first order, the cancellation, C, is also independent of D/λ because $C \propto s_2/s_1$ (Eq. (24)). Furthermore, we note that s_1 is relatively independent of FBW (s_1 corresponds to the output power when a maximum directivity beam is pointed to the interference). This beam is independent of frequency for the small percentage bandwidths ($\lesssim 5\%$) of interest here) whereas s_2 increases as $(FBW)^2$. Hence,

$$C = K\, s_2/s_1 = K\,(FBW)^2 \tag{28}$$

For an MBA, therefore, C is predominantly a function only of FBW. This is the result referred to in Table I. The MBA cancellation is illustrated in Fig. 7, and is considerably better than that for the PA, averaging about 40 dB over the range of D/λ considered. Furthermore, the cancellation is achieved using only a single degree of freedom. This is evidenced by examining the directive gain in the direction of the user assuming both FBW = 0 and FBW = 4.55%, which yields similar results for each FBW. For $D/\lambda = 100$, the loss in user gain at one-half power beamwidth from the interference source is 5 dB rather than the predicted 3 dB for a phased array when FBW = 0. This is because the resolution

of the MBA is poorer when the user is not positioned at a beam center. A maximum gain beam synthesized from a dyad or triad of beams has a broader beamwidth at the edge of the 19-beam FOV. Clearly, however, the overall S/J improvement is good compared to the phased array. For example, for $D/\lambda = 100$, the S/J improvement is 33 dB for the MBA compared to only 16 dB for the phased array. We should mention again that the results of the simulation are steering vector dependent, so that deeper cancellation levels might be obtained for other steering vectors.

One final note which should be mentioned regarding the MBA is that for employing an MBA with aperture sizes $D/\lambda = 100$, and, with adjacent beams spaced one HPBW apart, approximately 721 feeds are required for full earth coverage. Clearly, employing full adaptive control on each feed is impractical. One technique for simplifying the hardware would be to employ a smaller feed cluster which could be scanned to cover particular areas within the FOV. Another technique might employ a switch network to utilize only those beams containing signals in an adaptive processor with a smaller number of channels.

B. Element Positioning and Cable Length Mismatch

An array antenna in space may experience variations in its element positions or electrical path lengths as a result of the extreme temperature variations to which the outer surface of a satellite is subjected. The effect of such variations on cancellation will be analyzed in this section. If Δ is the rms differential displacement of the elements (expressed in feet), then for the cancellation to be a level C over a bandwidth BW (in MHz), the tolerance on Δ will be shown to be

$$\Delta[\text{feet}] < 542.6\ \sqrt{C}/BW \tag{29}$$

Some values of Δ for selected bandwidths and cancellation levels are tabulated in Table 2. It should be emphasized that these tolerances on Δ assure that the antenna element position errors will not degrade cancellation below the value shown. However, they do not assure that cancellation to these levels

will actually be achieved because, for some scenarios, the inherent dispersion of the antenna due to the wavefront angle of arrival dominates the cancellation performance so that in those cases position errors are not important.

TABLE 2

REQUIRED TOLERANCES ON RMS DIFFERENTIAL ELEMENT DISPLACEMENT
Δ VS. BANDWIDTH AND CANCELLATION LEVEL

BW(MHz)	C(dB)	Δ(ft)	Δ(in)
1	-30	17.2	
1	-40	5.4	
1	-50	1.7	
10	-30	1.7	
10	-40		6.5
10	-50		2.1
100	-30		2.1
100	-40		0.65
100	-50		0.21
1000	-30		0.21
1000	-40		0.07
1000	-50		0.02

Development

Let $(x_k y_k, 0)$ be the desired x,y,z coordinates of the kth element normalized to D/2, where D is the smallest diameter enclosing the array. Let the matched cable length extending from the processor of each element be ℓ. When the element is displaced, and the cable expands, the new values of these variables are $(x_k + \Delta x_k, y_k + \Delta y_k, \Delta z_k)$ and $\ell + \Delta\ell_k$, respectively. Denote the output signal at the kth port with perfect positioning by E_k^o. Then, for a wavefront of amplitude E_o incident from angle (θ,ϕ) with respect to the array reference frame, E_k^o is given by

$$E_k^{o}(\omega) = E_o\, e^{j\, k_o \frac{D}{2} W(x_k \sin\theta \cos\phi + y_k \sin\theta \sin\phi)}\, e^{-jk_o \ell W} \qquad (30)$$

where, as before, ω is the actual angular frequency, ω_o is the angular frequency at band center, $k_o = \omega_o/c$, and $W = \omega/\omega_o$. When the elements are displaced and the cables expanded, then the output $E_k(\omega)$ becomes

$$E_k(\omega) = E_k^{o}(\omega)\, e^{-jk_o \Delta\ell_k W}\, e^{+jk_o \frac{D}{2} W[\Delta x_k \sin\theta \cos\phi + \Delta y_k \sin\theta \sin\phi + \Delta z_k \cos\theta]} \qquad (31)$$

Note that errors Δx_k, Δy_k are reduced in magnitude by $\sin\theta$ ($\sin\theta < .15$ within the 8.7° FOV) so that the co-planar positioning of the elements is less critical than out of plane position or cable length. Furthermore, for some angles of arrival, the dispersion inherent in $E_k^{o}(\omega)$ will dominate all positioning errors, particularly for large antennas. However, if we wish to specify the antenna tolerances so that their effect on cancellation is negligible for all angles of arrival, then the case of $\sin\theta = 0$ (broadside incidence) is a worst-case condition.

Define $M_{k,q}(\omega) \equiv E_k(\omega)\, E_q^{*}(\omega)$. Then $\underline{\underline{M}}$ takes the form

$$\underline{\underline{M}}_{k,q}(\omega) = \underline{\underline{M}}^{o}_{k,q}(\omega)\, e^{-jk_o(\Delta\ell_k - \Delta\ell_q) W}\, e^{+jk_o \frac{D}{2}(\Delta z_k - \Delta z_w) W} \qquad (32)$$

where we have used the small angle approximation $\cos\theta = 1$ and defined $\underline{\underline{M}}^{o}_{k,q}(\omega) = E_k^{o}(\omega)\, E_q^{o*}(\omega)$. Equation (32) indicates that the dominant errors are cable expansion and deviations in out-of-plane element positioning. Define the <u>net</u> position error for the k^{th} element to be

$$\Delta_k \equiv \Delta\ell_k - \Delta z_k D/2 \qquad (33)$$

Then, assuming broadside incidence $\left(\underline{\underline{M}}^{o}_{k,q}(\omega) = |E_o|^2\right)$, we obtain

$$\underline{\underline{M}}_{k,q}(\omega) = |E_o|^2\, e^{-jk_o W(\Delta_k - \Delta_q)} \qquad (34)$$

In order to compute the effect on the cancellation level, we average $\underline{\underline{M}}(\omega)$ over the frequency band. Define $\underline{\underline{R}} = \langle \underline{\underline{M}}(\omega) \rangle$, where $\langle \cdot \rangle$ denotes a frequency average over the bandwidth of interest. Now expand $\underline{\underline{R}}$ in the form

$$\underline{\underline{R}} = \underline{\underline{R}}_o + \Delta\underline{\underline{R}} \tag{35}$$

where $\underline{\underline{R}}_o \equiv \langle \underline{\underline{M}}_o(\omega) \rangle$ and ΔR denotes a perturbation of $\underline{\underline{R}}_o$ due to the net position errors of each element. For a single interference source incident on the array, it can be shown[1] that the cancellation C for an earth coverage beam-steering vector is bounded by

$$C \leq N(s_2/s_1) \tag{36}$$

where N is the number of elements and s_1 and s_2 are the two largest eigenvalues of $\underline{\underline{R}}$. (Normally $s_1 >> s_2$ and s_2 is determined by the channel tracking errors or differences in frequency response among channels, which in this case result from the net positioning errors.) To determine s_1 and s_2, we average Eq. (34) over FBW and obtain

$$\underline{\underline{R}} = |E_o|^2 \, e^{jk_o(\Delta_k - \Delta_q)} \left[\frac{\sin\left(\frac{k_o FBW}{2}(\Delta_k - \Delta_q)\right)}{\left(k_o \frac{FBW}{2}(\Delta_k - \Delta_q)\right)} \right] \tag{37}$$

To express (37) in the form of Eq. (35), assume that $k_o|\Delta_k - \Delta_q| << 1$ and also that $\frac{k_o FBW}{2} |\Delta_k - \Delta_q| = \frac{\pi BW}{c} |\Delta_k - \Delta_q| << 1$, where BW is the nulling bandwidth in hertz. Then (37) can be written in the form

$$\underline{\underline{R}} = |E_o|^2 \left\{ 1 - \frac{1}{6}\left(\frac{\pi BW}{c}\right)^2 (\Delta_k - \Delta_q)^2 + jk_o(\Delta_k - \Delta_q) \right\} \tag{38}$$

It is reasonable to assume that each Δk is an independent random variable with zero mean. Let Δ be the standard deviation of the distribution of position errors, then

$$E\left\{ (\Delta_k - \Delta_q)^2 \right\} = \begin{cases} 0 \text{ for } k=q \\ 2\Delta^2 \text{ for } k \neq q \end{cases} \tag{39}$$

where $E\{\cdot\}$ denotes the expected value taken over the distribution of position errors. The expected value of $\underline{\underline{R}}$, denoted by $\overline{\underline{\underline{R}}}$, is therefore given by

$$\overline{\underline{\underline{R}}}_{k,q} = |E_o|^2 \left\{1 - \frac{1}{3}\left(\frac{\pi BW}{c}\right)^2 \Delta^2(1-\delta_{k,q})\right\} \tag{40}$$

where $\delta_{k,q}$ is the Kronceker delta function. Equation (40) can be expressed in the form

$$\overline{\underline{\underline{R}}} = |E_o{}^2| \left\{(1-\varepsilon)\ \hat{1}\ \hat{1}^\dagger + \varepsilon \underline{\underline{I}}\right\} \tag{41}$$

where we have defined $\hat{1} = \text{col}[1,1,\ldots,1]$, $\varepsilon \equiv \frac{1}{3}\left(\frac{\pi BW}{c}\right)^2 \Delta^2$, "†" is the complex conjugate transpose, and $\underline{\underline{I}}$ is the identity matrix. The eigenvalues s_1 and s_2 of $\overline{\underline{\underline{R}}}$ can readily be determined to be

$$\begin{aligned} s_1 &\simeq |E_o|^2(1-\varepsilon)\ N \\ s_2 &\simeq |E_o|^2\varepsilon \end{aligned} \tag{42}$$

so that, using Eq. (36) bounding the cancellation C, we obtain

$$C \leq \frac{\varepsilon}{1-\varepsilon} \simeq \frac{1}{3}\left(\frac{\pi BW}{c}\right)^2 \Delta^2 \tag{43}$$

Expressing BW in MHz and Δ in feet then leads to Eq. (29) specifying the allowable tolerances on Δ as a function of the desired cancellation and bandwidth. Recall that (43) is based on a statistical average. There will be some variation in the actual cancellation achieved.

C. Weighting Circuits

There are several methods for implementing amplitude and phase control in each channel of an adaptive processor. Perhaps the simplest technique is an attenuator and phase shifter in series as illustrated in Fig. 8a. This topology can be quite useful for certain applications. Its limitations lie in its inability to turn off completely, due to the finite dynamic range of real attenuators, but perhaps more significantly, it is difficult to couple this type of weight to the output of an analog adaptive processor. As shown

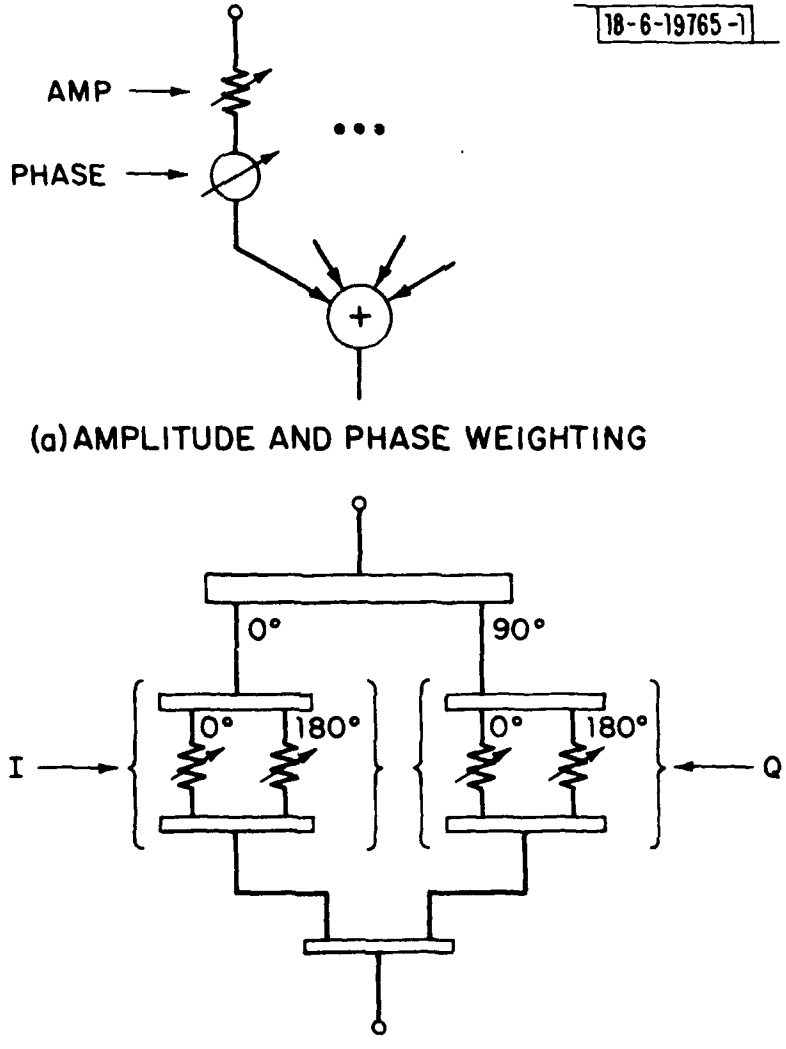

Fig. 8. Two common techniques used to obtain amplitude and phase control at the output of each antenna port: (a) Attenuator in series with phase-shift, (b) Inphase (I) and quadrature (Q) weighting.

in Section III, the weight control output of the processor is usually available as "inphase" (I) and "quadrature" (Q) voltage for each weight. This output must be converted to an amplitude and phase form to drive the attenuator and phase shifter, thus complicating the circuitry. To avoid this, the weighting is usually accomplished in terms of the I and Q components directly, as illustrated in Fig. 8b. In this case, the I and Q components are separated by a quadrature hybrid. The I and Q branches can then be driven directly by the I and Q components of the correlator output. When implemented as in Fig. 8b, each complex weight circuit, depending on the weight setting, can have as much as 12 to 14 dB of insertion loss from the splitting and combining losses of the hybrids. A lower insertion loss topology for I and Q weighting is illustrated in Fig. 9. In this scheme, both attenuation and phase reversal are accomplished with two fewer hybrids than in Fig. 8b, resulting in a 6 dB improvement in insertion loss. The drive voltage, V_d, which is derived from the Q control voltage, controls the pin-diode resistance, which varies the reflection coefficients Γ_1 and Γ_2 (which are nominally equal) over the range -1 to +1. This allows both attenuation and phase reversal. A direct consequence of this technique, however, is the presence of a "feedthrough" component which is independent of control voltage. In this case it arises in the hybrid parasitic coupling. In practice, a small component of feedthrough is usually present in any weighting circuit. It has an important effect on performance and it is of interest to analyze its effect on cancellation.

Development

The basic equations characterizing the effects of weight feedthrough on the adapted output power have been developed in Section II. The composite weight, including feedthrough, is modeled as a single, complex weight circuit with a frequency response which is given by Eq. (1). That part of the weight which is directly controllable, denoted by $\underline{w}$, via the I and Q correlator outputs is governed by Eq. (12). The corresponding output power accounting for the presence of feedthrough is given by Eq. (15). These equations are generally difficult to solve unless one resorts to numerical simulations. However, if

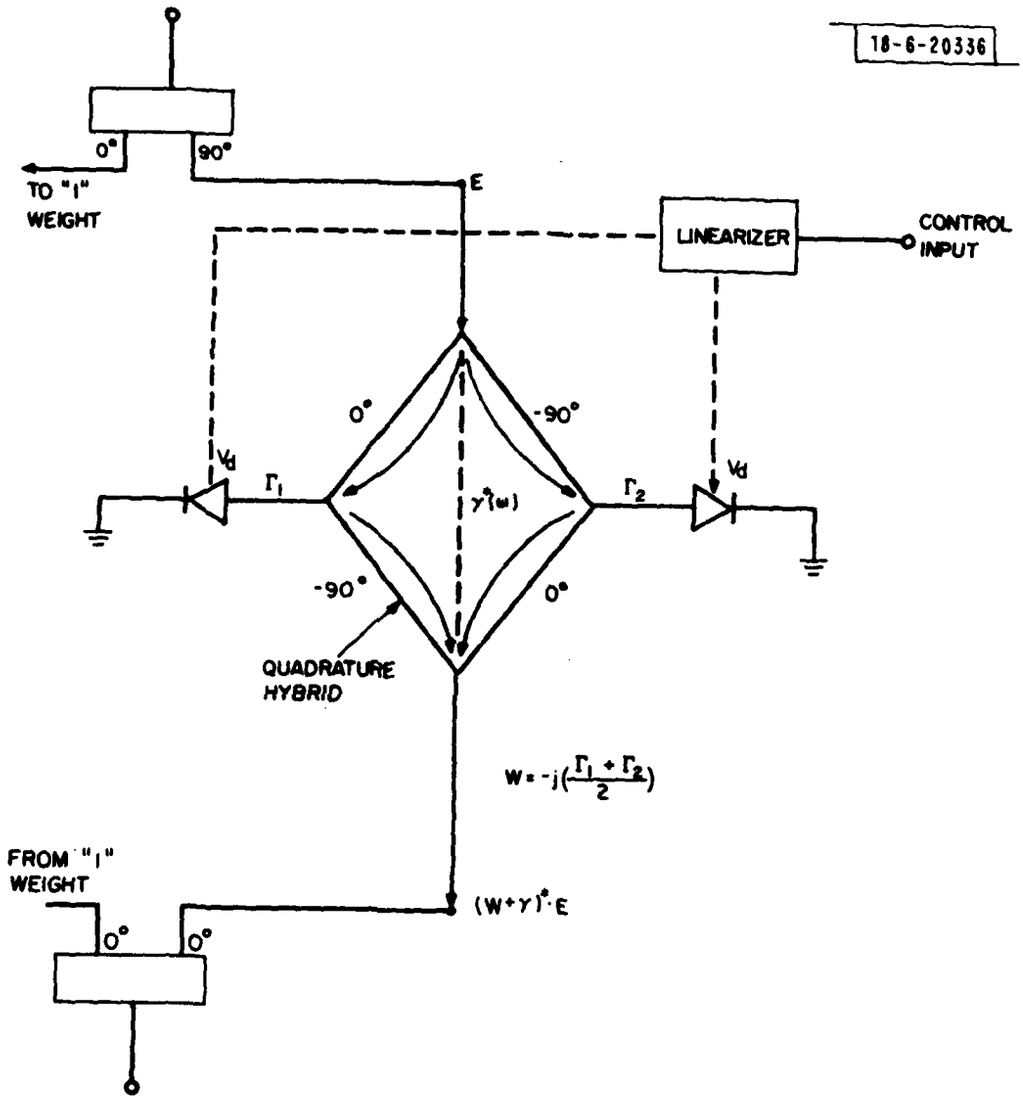

Fig. 9. Low insertion loss weight topology for obtaining amplitude and phase control.

we assume an array antenna geometry, and broadside incidence for the interference source, then the questions simplify to a tractable form. With these assumptions, $\underline{E}\,\underline{E}^{\dagger}$ is independent of frequency and Eqs. (12) and (15) reduce to the simpler form

$$\tau_o \dot{\underline{w}} + [\underline{\underline{I}} + \mu \underline{\underline{R}}] \cdot (\underline{w} + \langle \underline{\gamma} \rangle) = \underline{V} + \langle \underline{\gamma} \rangle \tag{44}$$

and

$$P_o = \left\langle (\underline{w} + \langle \underline{\gamma} \rangle + \Delta \underline{\gamma})^{\dagger} \cdot \underline{\underline{R}} \cdot (\underline{w} + \langle \underline{\gamma} \rangle + \Delta \underline{\gamma}) \right\rangle \tag{45}$$

where, as before, we have defined $\underline{\underline{R}} = R_j \, \underline{E}\,\underline{E}^{\dagger}$ and

$$\gamma(\omega) = \langle \gamma(\omega) \rangle + \Delta \underline{\gamma}(\omega) \tag{46}$$

Note, by definition, $\langle \Delta \underline{\gamma} \rangle = 0$. In the steady state, solutions to Eq. (44) take the form

$$\underline{w} + \langle \underline{\gamma} \rangle = [\underline{\underline{I}} + \mu \underline{\underline{R}}]^{-1} \cdot \underline{V} \tag{47}$$

Equation (47) points out that the control loops only compensate for the <u>average</u> of $\underline{\gamma}(\omega)$ over the nulling band. This occurs because feedthrough is not sensed in the covariance matrix, $\underline{\underline{R}}$, as are, for example, weighted channel frequency variations (e.g., those occurring in the front end filters). Using (45) and (47), and noting $\langle \Delta \underline{\gamma} \rangle = 0$, then the adapted output power, P_o, is given by

$$P_o = \underline{V}^{\dagger} \cdot [\underline{\underline{I}} + \mu \underline{\underline{R}}]^{-1} \cdot \underline{\underline{R}} \cdot [\underline{\underline{I}} + \mu \underline{\underline{R}}]^{-1} \cdot \underline{V} + \left\langle \Delta \underline{\gamma}^{\dagger} \cdot \underline{\underline{R}} \cdot \Delta \underline{\gamma} \right\rangle \tag{48}$$

The first term in (48) is the output of an <u>ideal</u> processor (i.e., one with no feedthrough). The second term is a residual component of power due to the frequency variation in the feedthrough. This residual power is <u>weight independent</u>, and cannot be compensated for by the adaption process!

The above limitations are quite significant and have considerable impact on system performance. To illustrate this impact, let us rewrite Eq. (48) in the form

$$P_o = P_a(\text{without feedthrough}) + k \, P_{in} \tag{49}$$

That is, the actual output of the nulling processor consists of the theoretical adapted output, assuming perfect weights, plus a residual term proportional to the input power. Figure 10 illustrates the effect of this latter term on system performance. In Fig. 10, we plot the input-output power relationship for the nulling processor either in the quiescent (unadapted) state or the adapted state. The difference between the two curves is indicative of the cancellation realized by the processor. Clearly the constant k, dependent on $\underline{\Delta\gamma}$, limits the achievable cancellation. In the general case (i.e., non-broadside incidence), the constant k is dependent on the feedthrough parameters (i.e., isolation, time delay, etc.), interference-source angle of arrival, and quiescent steering vector. For weight circuits designed to be as identical as possible, k would be near maximum for broadside incidence. Consequently, it is for this case which we estimate quantitatively the cancellation dependence on feedthrough in the following paragraphs.

To obtain an estimate of the constant k, consider the second term in Eq. (48). We have

$$(P_o)_{\text{feedthrough}} = \langle \underline{\Delta\gamma}^{\dagger} \cdot \underline{\underline{R}} \cdot \underline{\Delta\gamma} \rangle = R_j \, \underline{E}^{\dagger} \cdot \langle \underline{\Delta\gamma} \underline{\Delta\gamma}^{\dagger} \rangle \cdot \underline{E} \tag{50}$$

The cancellation C is defined in Eq. (16). Assuming the feedthrough term dominates the adapted output power, then $(I/N)_a$ is given by

$$(I/N)_a = \frac{R_j \, \underline{E}^{\dagger} \cdot \langle \underline{\Delta\gamma} \, \underline{\Delta\gamma}^{\dagger} \rangle \cdot \underline{E}}{(\underline{w} + \langle \underline{\gamma} \rangle)^{\dagger} \cdot (\underline{w} + \langle \underline{\gamma} \rangle)} \tag{51}$$

In order to simplify Eq. (51), note that, for broadside incidence, $\underline{E}$ is proportional to the first eigenvector, $\underline{e}_1$, of $\underline{\underline{R}}$. Furthermore, assuming an earth coverage quiescent steering vector, it can be shown that Eq. (47) reduces to

$$\underline{w} + \langle \underline{\gamma} \rangle = \text{col}\left[1 - \frac{1}{N}, -\frac{1}{N}, \ldots, -\frac{1}{N}\right] \tag{52}$$

valid for broadside incidence. Hence

$$(\underline{w} + \langle \underline{\gamma} \rangle)^{\dagger} \cdot (\underline{w} + \langle \underline{\gamma} \rangle) = 1 - \frac{1}{N} \tag{53}$$

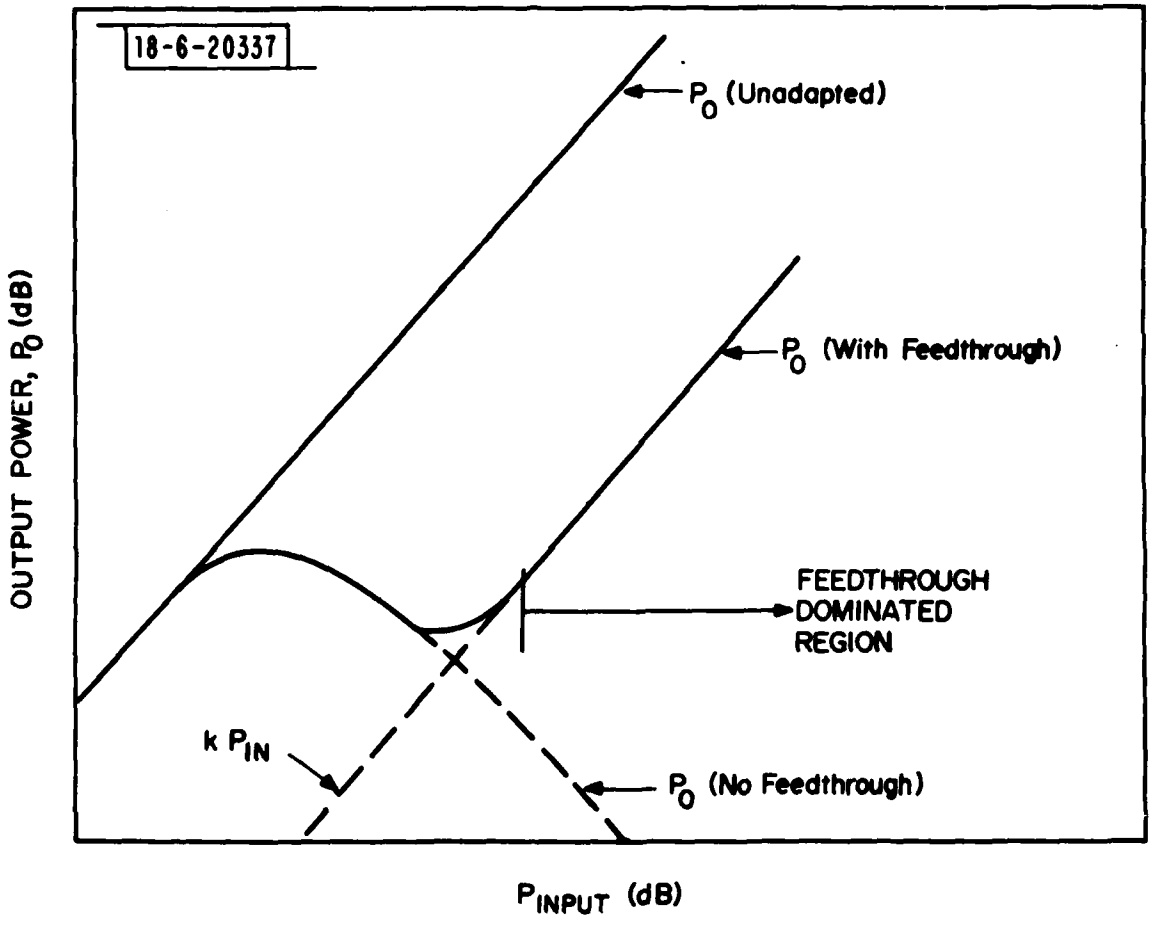

Fig. 10. Output power vs. input power for a nulling processor illustrating the effect of weight feedthrough on the cancellation performance.

Consequently, the expression for $(I/N)_a$ becomes

$$(I/N)_a = R_j(\underline{E}^\dagger \cdot \underline{E}) \frac{\underline{e}_1^\dagger \cdot \langle \Delta\gamma\ \Delta\gamma^\dagger \rangle \cdot \underline{e}_1}{1 - 1/N} \tag{54}$$

Now $R_j \underline{E}^\dagger \cdot \underline{E} = R_j \sum_{k=1}^{N} |E_k|^2 = \text{Trace}(\underline{\underline{R}}) \approx s_1 = \text{maximum eigenvalue of } \underline{\underline{R}}$. Hence,

$$(I/N)_a = \frac{N}{N-1} s_1\, \underline{e}_1^\dagger \cdot \langle \underline{\Delta\gamma}\ \underline{\Delta\gamma}^\dagger \rangle \cdot \underline{e}_1 \tag{55}$$

To compute $(I/N)_b$ for the same earth coverage quiescent constraint, we note

$$(I/N)_b = \frac{\underline{V}^\dagger \cdot \underline{\underline{R}} \cdot \underline{V}}{\underline{V}^\dagger \cdot \underline{V}} = s_1/N \tag{56}$$

so the cancellation C is given by (see Eq. (16))

$$C = N\underline{e}_1^\dagger \cdot \langle \underline{\Delta\gamma}\ \underline{\Delta\gamma}^\dagger \rangle \cdot \underline{e}_1 \tag{57}$$

Clearly, the cancellation is directly dependent on the frequency variation of the feedthrough. Equation (57) can be estimated for two characteristically different types of feedthrough -- correlated and uncorrelated.

(a) Uncorrelated Feedthrough -- One example of uncorrelated feedthrough which might occur is when the feedthrough path length from weight input-output is the same as the weighted path length from input-output, but the isolation $\langle \underline{\Delta\gamma}\ \underline{\Delta\gamma}^\dagger \rangle$ takes the form of a diagonal matrix

$$\langle \underline{\Delta\gamma}\ \underline{\Delta\gamma}^\dagger \rangle = |\gamma_o|^2 \begin{bmatrix} \sigma^2 & & 0 \\ & \sigma^2 & \\ & \ddots & \\ 0 & & \sigma^2 \end{bmatrix} \tag{58}$$

where σ^2 is the isolation tracking error, and $|\gamma_o|^2$ the isolation level of the feedthrough path relative to the weighted path. Then (57) reduces to

$$C \sim N|\gamma_o|^2 \sigma^2 \tag{59}$$

which is the result tabulated in Table 1. Equation (59) assumes an earth coverage steering vector. Since $(I/N)_b$ is dependent on steering vector, whereas $(I/N)_a$ is an absolute level independent of steering vector, Eq. (57) specifying C would change dependent on $\underline{V}$. Otherwise said, referring to Fig. 10, the unadapted curve in Fig. 10 moves up or down dependent on $\underline{V}$, whereas the nulled output in the feedthrough limited region remains independent of $\underline{V}$.

(b) Correlated Feedthrough -- Correlated feedthrough errors occur when a time delay difference exists between the weighted and feedthrough paths. Effects on cancellation due to this type of error can be estimated assuming identical time delay mismatches, defined by τ, for each weighting circuit. Then $\underline{\gamma}(\omega)$ takes the form

$$\underline{\gamma}(\omega) = \underline{\gamma}_o \, e^{jW(\omega_o T)} \tag{60}$$

It is a straightforward procedure to evaluate $\langle \underline{\Delta\gamma} \, \underline{\Delta\gamma}^\dagger \rangle$. We obtain

$$\langle \underline{\Delta\gamma} \, \underline{\Delta\gamma}^\dagger \rangle = \underline{\gamma}_o \, \underline{\gamma}_o^\dagger \left\langle \left| e^{j\Delta W \omega_o T} - \frac{\sin \pi \, BW T}{\pi BW \cdot T} \right|^2 \right\rangle \tag{61}$$

where BW = bandwidth (Hertz), and $\Delta W = W-1$. For $BW \cdot T << 1$, we obtain

$$\langle \underline{\Delta\gamma} \, \underline{\Delta\gamma}^\dagger \rangle = \underline{\gamma}_o \, \underline{\gamma}_o^\dagger \, \frac{(\pi \cdot BW \cdot T)^2}{3} \tag{62}$$

Substituting Eq. (62) into (57), and noting that $\underline{e}_1^\dagger = \frac{1}{\sqrt{N}} [1,1, \ldots, 1]$, we obtain

$$C \lesssim N^2 \, |\gamma_o|^2 \, \frac{(\pi \cdot BW \cdot T)^2}{3} \tag{63}$$

Equation (63) is the result cited in Table 1.

Finally, although not related to the feedthrough effect developed above, it remains to evaluate the effects of using quantized weights, as alluded to in Table 1. It is interesting to note that analyzing this effect is similar mathematically to that for the feedthrough analysis. To see this, we express the error in weight setting in the form

$$\underline{w} = \overline{\underline{w}} + \Delta\underline{w} \tag{64}$$

where $\bar{\underline{w}}$ is the precise (desired) weight and $\Delta\underline{w}$ is the error due to quantization. Define the rms quantization error according to

$$\sigma^2 \equiv E\left\{\left|1 - \frac{w_k}{\bar{w}_k}\right|^2\right\} = \frac{1}{\bar{w}_k^2} E\{\Delta w_k^2\} \tag{65}$$

where the expected value is statistically a function of all possible weight settings. The adapted interference to thermal noise ratio is given by

$$(I/N)_a = \frac{E\{\underline{w}^\dagger \cdot \underline{\underline{R}} \cdot \underline{w}\}}{E\{\underline{w}^\dagger \cdot \underline{w}\}} \simeq \frac{E\{\Delta\underline{w}^\dagger \cdot \underline{\underline{R}} \cdot \Delta w\}}{\bar{\underline{w}}^\dagger \cdot \bar{\underline{w}}} \tag{66}$$

We can express Eq. (65) in the same form as (51), i.e.,

$$(I/N)_a = \frac{\underline{E}^\dagger \cdot E\{\Delta\underline{w}\ \Delta\underline{w}^\dagger\} \cdot \underline{E}}{\bar{\underline{w}}^\dagger \cdot \bar{\underline{w}}} \cdot R_j \tag{67}$$

Assuming uncorrelated errors between channels, and using Eq. (65)

$$E\{\Delta\underline{w}\ \Delta\underline{w}^\dagger\} = \begin{bmatrix} \bar{w}_1^2 & & 0 \\ & \bar{w}_2^2 & \\ & & \ddots \\ 0 & & \bar{w}_N^2 \end{bmatrix} \sigma^2 \tag{68}$$

Assuming an earth coverage steering vector constraint, we have $\bar{w}_1 = 1\text{-}1/N$, $\bar{w}_2 = \ldots = \bar{w}_N = 0\text{-}1/N$ so that (68) reduces to

$$E\{\Delta\underline{w}\ \Delta\underline{w}^\dagger\} = \sigma^2 \begin{bmatrix} (1\text{-}1/N)^2 & & 0 \\ & 1/N^2 & \\ & & \ddots \\ 0 & & 1/N^2 \end{bmatrix} \tag{69}$$

Using Eq. (69) in (67), we obtain

$$(I/N)_a = \frac{s_1\sigma^2}{N} \frac{(1 - \frac{1}{N})^2}{1 - \frac{1}{N}} = s_1\sigma^2/N \tag{70}$$

Since $(I/N)_b = s_1/N$, it follows that

$$C = \sigma^2 \tag{71}$$

which is the result referred to in Table 1.

Another class of errors alluded to in Table 1 which occurs in the weighting circuits is I/Q imbalance from true quadrature separation. Because of the inherent compensation of these errors by the action of a feedback processor, discussion of this error type is deferred to the next section.

D. Effects of Component Imperfections in the Feedback Loops

The function of an adaptive processor is to provide control of the weights following the antenna port outputs. Many techniques for adaptive control of the weights have been developed and used in practice. Each has its own peculiar properties. Since the feedback type of processor employing either analog or digital processing is most commonly used, we direct our attention to it.

As discussed in Section III, one of the basic functions of the feedback loops is to "sense" the correlation matrix of the N signal channels. In practice, the correlation matrix sensed by the control loops includes imperfections in both the signal channels and feedback channels. If these imperfections are frequency independent, then there exists a unique set of weights that minimizes the output power, therefore compensating for the errors. It is not surprising that a feedback type processor can adapt to this unique set of weights because the inherent nature of the feedback mechanism is to drive the output toward zero. Consequently, we anticipate that the main effect of frequency independent errors is their impact on loop dynamics. Otherwise said, as long as the feedback loops remain stable, the feedback processor is considerably tolerant of frequency-independent imperfections.

To demonstrate the above conjecture, and to develop a quantitative assessment of component error effects on loop dynamics, we consider the model of the analog feedback processor illustrated in Fig. 11. The following error types will be considered:

1. Pre-weighting channel tracking errors: $H_k(\omega)$
2. Post-weighting tracking errors: $C_k(\omega)$
3. Feedback loop tracking errors: $F_k(\omega)$
4. I/Q mixer imbalance errors: ε_{1k} and ε_{2k}
5. I/Q weight imbalance errors: ψ_k
6. Loop gain imbalance: μ_{1k}/μ_{2k}
7. Mixer dc offsets: V_{1k}^{dc} and V_{2k}^{dc}

As before, $A_k(\omega)$ denotes the antenna frequency response for the k^{th} channel. We assume a single pole filter ($F(s) = 1/(\tau_o s+1)$) in each feedback loop. For an N-channel system with component errors, the equations characterizing the dynamic system response must be formulated as a 2N dimensional problem. In the following, we first develop the general set of 2N equations governing the system response and then consider separately the effects of frequency independent and frequency dependent errors.

Denote the weights for the I and Q channels as α_k and β_k, respectively, where k = 1, ..., N. In a statistical formulation, α_k and β_k are characterized as random processes which are dependent on the interference noise process incident on the antenna and the time-evolution of the expectations $E\{\alpha_k\}$ and $E\{\beta_k\}$ (denoted hereafter as α_k, β_k, for simplicity) is governed by 2N differential equations. Statistical variations relative to the expected values of the weights are called "weight noise" and are treated separately in Section IV-E. From Fig. 11, we find that the 2N equations for α_k and β_k are:

$$\tau_o\dot{\alpha}_k + [\alpha_k + E\{I_k\}] = V_{1k}$$

$$\tau_o\dot{\beta}_k\, V + [\beta_k + E\{Q_k\}] = V_{2k} \qquad k = 1, \ldots, n \qquad (72)$$

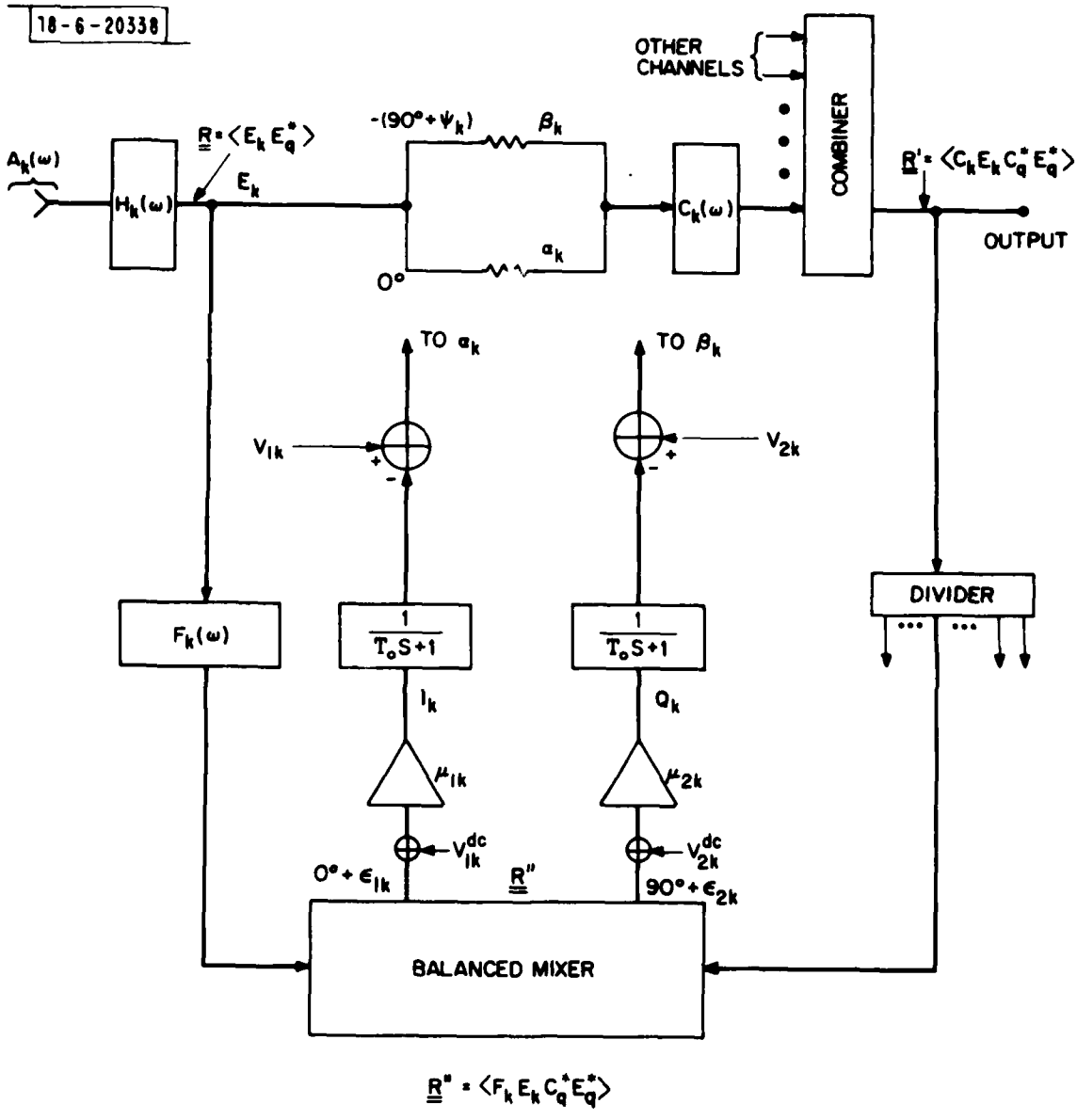

Fig. 11. Model of a wideband, analog feedback nulling processor including the effects of various component imperfections.

where the complex steering vector $\underline{V}_k = \underline{V}_{1k} + j\underline{V}_{2k}$ and we assume $\underline{\gamma}(\omega) = 0$ (i.e., no weight feedthrough) V. It can be shown that (e.g., see the analysis leading up to Eq. (13))

$$E\{I_k\} = \mu_{1k}\, \mathrm{Re}\left\{e^{+j\varepsilon_{1k}}\, (\underline{\underline{R}}'' \cdot \underline{w})_k\right\} + \mu_{1k}\, V_{1k}^{dc}$$

$$E\{Q_k\} = \mu_{2k}\, \mathrm{Im}\left\{e^{j\varepsilon_{2k}}\, (\underline{\underline{R}}'' \cdot \underline{w})_k\right\} + \mu_{2k}\, V_{2k}^{dc} \tag{73}$$

In (73), V_{1k} and V_{2k} are the I/Q channel beam steering voltages and $\underline{\underline{R}}''$ is the $N \times N$ covariance matrix sensed by the correlation mixers (Fig. 11), and is given by

$$\underline{\underline{R}}''_{k,q} = \langle F_k\, E_k\, C_q^*\, E_q^* \rangle \tag{74}$$

where $E_k(\omega) \equiv H_k(\omega)\, A_k(\omega)$. Also in (73), we have introduced the equivalent weight $\underline{w}$, defined by

$$\underline{w}_k = \alpha_k + j\beta_k\, e^{j\psi_k} \tag{75}$$

The factor $e^{j\psi_k}$ characterizing weight imbalance errors, accounts for the deviations from true quadrature. Any absolute phase error in the weight transfer function is included in the definition of $C_k(\omega)$.

Equation (72) defines 2N real equations specifying the time evolution of α_k and β_k. This evolution is dominated by the properties of $\underline{\underline{R}}''$ defined in (74). Observe that $\underline{\underline{R}}''$ is <u>non-hermetian</u>, indicating that the eigenvalues of $\underline{\underline{R}}''$ will in general be complex, leading to oscillatory solutions for α_k and β_k. Once the α_k and β_k adapt to steady state (assuming that stable solutions to (72) exist), then the adapted output power, P_o, can be computed. Define the $N \times N$ <u>signal</u> channel covariance matrix (including signal channel imperfections), $\underline{\underline{R}}'$, to be

$$\underline{\underline{R}}'_{kq} = \langle C_k\, E_k\, C_q^*\, E_q^* \rangle \tag{76}$$

The output power is then given by

$$P_o = \underline{w}^{\dagger} \cdot \underline{\underline{R}}' \cdot \underline{w} \tag{77}$$

Equation (77), when $\underline{w}$ is obtained from Eqs. (72) and (73), specifies the dependence of adapted output power on loop component errors. To determine $\underline{w}$ in the steady state, substitute Eq. (73) into (72) and set $\dot{\alpha}_k = \dot{\beta}_k = 0$. The resulting expressions, expressed in the vector, form are:

$$\begin{aligned} \underline{\alpha} + \mathrm{Re}\left\{\underline{\underline{M}}_1 \cdot \underline{\underline{R}}'' \cdot \underline{w}\right\} &= \underline{V}_1 - \underline{V}_1^{dc} \\ \underline{\beta} + \mathrm{Im}\left\{\underline{\underline{M}}_2 \cdot \underline{\underline{R}}'' \cdot \underline{w}\right\} &= \underline{V}_2 - \underline{V}_2^{dc} \end{aligned} \tag{78}$$

where we have defined the diagonal matrices

$$(\underline{\underline{M}}_1)_{k,q} = \mu_{1k} e^{+j\epsilon_{1k}} \delta_{k,q} \quad , \quad (\underline{\underline{M}}_2)_{k,q} = \mu_{2k} e^{-j\epsilon_{2k}} \delta_{k,q} \ , \tag{79}$$

$\delta_{k,q}$ is the Kronecker delta function and $(\underline{V}_1^{dc})_k \equiv \mu_{1k} V_{1k}^{dc}$, $(\underline{V}_2^{dc})_k \equiv \mu_{2k} V_{2k}^{dc}$. Observe that the effect of the mixer dc offset voltages is to modify the beam steering voltage. This does not affect the ability of the processor to null, but does affect the adapted radiation pattern away from the null. This could be a serious consideration for the mode of operation of steering a maximum gain beam to a user close to an interference source, but in the earth-coverage mode it is not a significant effect. In either case, digital calibration techniques can be used to compensate for this effect. Consequently, in the following analysis we assume $\underline{V}_1^{dc}$ and $\underline{V}_2^{dc}$ to be zero.

Closed form solutions to Eq. (78) are in general difficult to obtain. The task can be simplified considerably by assuming that the interference sources are large relative to loop threshold. That is, if $s_1, \ldots, s_N$ denote the N eigenvalues of $\underline{\underline{R}}''$, we assume that $\mu|s_j| >> 1$ for each interference source. In this case, the $\underline{\alpha}$ and $\underline{\beta}$ terms on the lefthand side of Eq. (78) are negligible. Equation (78) can then be rewritten as 2N real equations for the solution of the vector $\underline{X}$ where

$$\underline{X} = \underline{\underline{R}}'' \cdot \underline{w} \tag{80}$$

Solving (78) for $\underline{X}$, $\underline{w}$ can then be determined by inverting (80).

$$\underline{w} = \underline{\underline{R}}''^{-1} \cdot \underline{X} \tag{81}$$

Substituting (81) into (77) yields the general dependence of output power on loop component errors.

It is convenient to classify the effects of component errors into two categories: "frequency dependent" and "frequency independent." Consider first the latter category.

1. Frequency Independent Component Error Effects on Cancellation

On substituting the adapted solution, Eq. (81) into (77), P_o takes the form

$$P_o = \underline{X}^{\dagger} \cdot (\underline{\underline{R}}''^{-1})^{\dagger} \cdot \underline{\underline{R}}' \cdot \underline{\underline{R}}''^{-1} \cdot \underline{X} \tag{82}$$

If we assume all errors to be frequency independent, then (82) reduces to a simpler form. For this case, let $C_k(\omega) = e^{+j\zeta_k}$ to represent the net phase error of the kth channel and let $F_k(\omega) = e^{j\delta_k}$. Then (74) for $\underline{\underline{R}}''_{k,q}$ can be expressed in the form

$$\underline{\underline{R}}''_{k,q} = \left\langle \frac{F_k}{C_k} \cdot C_k E_k E_q^* C_q^* \right\rangle = \frac{F_k}{C_k} \underline{\underline{R}}'_{k,q} \tag{83}$$

so that $\underline{\underline{R}}'$ and $\underline{\underline{R}}''$ are related by a diagonal matrix, i.e.,

$$\underline{\underline{R}}'' = \underline{\underline{D}} \cdot \underline{\underline{R}}' \tag{84}$$

where $D_{kk} = F_k/C_k$ and $D_{k\ell} = 0$ for $\ell \neq k$. R' and R (where $\underline{\underline{R}}$ is defined at the output ports prior to weighting) are also related by a diagonal matrix. From (76),

$$R'_{k,q} = e^{j\xi_k} R_{k,q} e^{-j\xi_q} \tag{85}$$

where $R_{k,q} = \langle E_k E_q^* \rangle$, which can be written as

$$\underline{\underline{R}}' = \underline{\underline{C}} \cdot \underline{\underline{R}} \cdot \underline{\underline{C}}^{\dagger} \tag{86}$$

where $C_{kk} = e^{j\xi_k}$ and $C_{k\ell} = 0$ for $k \neq \ell$. It can be easily shown that the eigenvalues of R' are the same as those of R. Using Eq. (86) in (82), we obtain

$$P_o = [\underline{X}^{\dagger} \cdot (\underline{\underline{D}}^{-1})^{\dagger}] \cdot \underline{\underline{R}}'^{-1} \cdot [\underline{\underline{D}}^{-1} \cdot \underline{X}] \tag{87}$$

which takes the same form as the error-free solution having equivalent beam steering vector $\underline{V}_{eq} = \underline{\underline{D}}^{-1} \cdot X$. Since the $\underline{\underline{R}}'$ has the same eigenvalues as $\underline{\underline{R}}$, P_o can assume as low a value in this case as for the error free case. Consequently, we conclude that frequency independent errors, assuming the loops remain stable, do not affect the nulling capability of the feedback processor They do, however, affect the adapted radiation pattern away from the nulls. This is the result referred to in Table 1. These results have been verified by numerous computer simulations.

2. *Frequency Dependent Errors*

A general analysis of the effects of frequency dependent loop component errors is difficult to carry out. It is clear that in this case $\underline{\underline{R}}''$ and $\underline{\underline{R}}'$ are no longer simply related by Eq. (83); therefore the achievable cancellation is affected by frequency dependent errors. Setting $F_k(\omega) = 1$ and $C_k(\omega) = 1$ leads to the analysis channel tracking errors (mismatches in the $H_k(\omega)$) presented in Ref. 1. Consequently, the major thrust of this Section is to include the effects of $F_k(\omega)$ and $C_k(\omega)$ on achievable cancellation.

To accomplish this, we resort to the simple two-channel model illustrated in Fig. 12, assuming broadside incidence ($A_1 = A_2$). For this model, assume that the interference source is large relative to threshold ($\mu s_1 >> 1$). The expression for the output frequency spectrum, $V_o(\omega)$, can be shown to be

$$\begin{aligned} V_o(\omega) \propto\ & V_1^* \left[\langle F_2^* C_2 \rangle C_1(\omega) - \langle F_2^* C_1 \rangle C_2(\omega) \right] \\ & + V_2^* \left[\langle F_1^* C_1 \rangle C_2(\omega) - \langle F_1^* C_2 \rangle C_1(\omega) \right] \end{aligned} \tag{88}$$

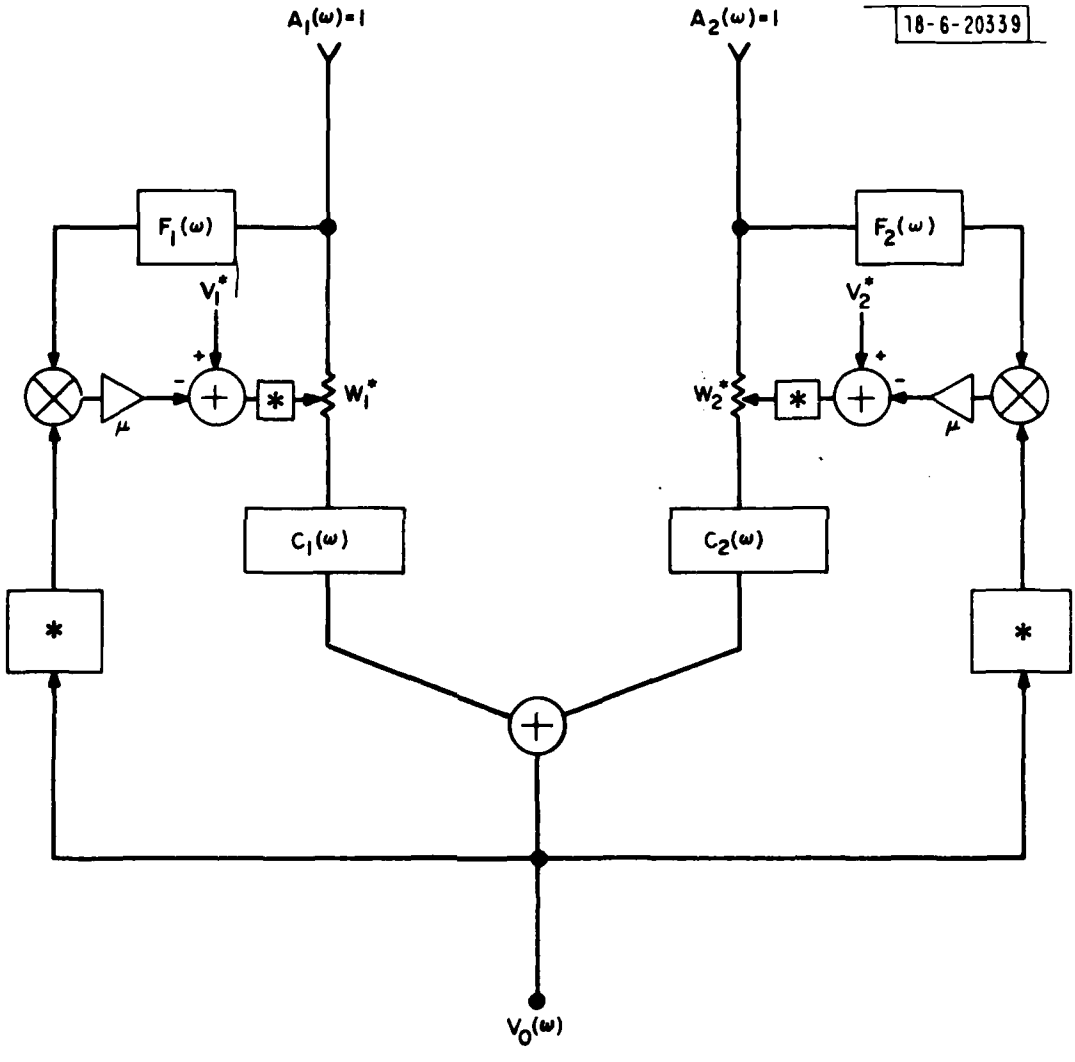

Fig. 12. Two-channel model used for frequency-dependent loop component error analysis. "*" indicates "complex-conjugate" operation.

We define the frequency response errors, $\Delta F(\omega)$ and $\Delta C(\omega)$, to be:

$$\Delta F(\omega) = F_2(\omega) - F_1(\omega)$$

$$\Delta C(\omega) = C_2(\omega) - C_1(\omega) \tag{89}$$

Using Eq. (88), we can show that the effects of ΔF on cancellation are of secondary importance relative to ΔC. That is, differences between the feedback loop frequency response functions have only a weak effect on the achievable cancellation level compared to differences in the response functions of the signal paths. To see this, substitute Eq. (89) into (88). We obtain

$$\begin{aligned} V_o(\omega) = {} & V_1^* \left[\langle F_1^* \, \Delta C \rangle \, C_1(\omega) - \langle F_1^* \, C_1 \rangle \, \Delta C(\omega) \right. \\ & + \langle \Delta F^* \, \Delta C \rangle C_1(\omega) - \langle \Delta F^* \, C_1 \rangle \, \Delta C(\omega) \left. \right] \\ & + V_2^* \left[\langle F_1^* \, C_1 \rangle \Delta C(\omega) - \langle F_1^* \, \Delta C \rangle \, C_1(\omega) \right] \end{aligned} \tag{90}$$

Equation (90) characterizes the output frequency spectrum of the output signal voltages. For an ideal system, $V_o(\omega)$ would be zero. The fact that it is not is attributable to the tracking errors, $\Delta C(\omega)$ and $\Delta F(\omega)$. Note that all terms involving ΔF are of order $\Delta F \cdot \Delta C$, indicating only a weak dependence of cancellation on ΔF relative to its dependence on ΔC. Note that if $\Delta C = 0$, $V_o(\omega) = 0$ independent of ΔF. Consequently, we conclude that the dominant effect on cancellation is due to those frequency dependent tracking errors in the signal channel for which the results of Ref. 1 apply directly.

3. Effects on Loop Stability

Consider now the stability requirements imposed by the set of 2N differential equations, (72) and (73). It is convenient to recast these equations into the form of a single 2N × 2N matrix equation:

$$T_o \begin{bmatrix} \dot{\underline{\alpha}} \\ \dot{\underline{\beta}} \end{bmatrix} + \begin{bmatrix} \underline{\underline{I}} + \underline{\underline{A}}_1 & \underline{\underline{A}}_2 \\ \underline{\underline{B}}_1 & \underline{\underline{I}} + \underline{\underline{B}}_2 \end{bmatrix} \begin{bmatrix} \underline{\alpha} \\ \underline{\beta} \end{bmatrix} = \begin{bmatrix} \underline{V}_1 \\ \underline{V}_2 \end{bmatrix} \tag{91}$$

where

$$(\underline{\underline{A}}_1)_{k,q} = \mu_{1k}\, \mathrm{Re}\left\{\underline{\underline{R}}''_{k,q}\, e^{+j\varepsilon_{1k}}\right\}$$

$$(\underline{\underline{A}}_2)_{k,q} = \mu_{1k}\, \mathrm{Re}\left\{j\underline{\underline{R}}''_{k,q}\, e^{j(\psi_q+\varepsilon_{1k})}\right\}$$

and

$$(\underline{\underline{B}}_1)_{k,q} = \mu_{2k}\, \mathrm{Im}\left\{\underline{\underline{R}}''_{k,q}\, e^{j\varepsilon_{2k}}\right\} \qquad (92)$$

$$(\underline{\underline{B}}_2)_{k,q} = \mu_{2k}\, \mathrm{Im}\left\{j\underline{\underline{R}}''_{k,q}\, e^{j(\psi_q+\varepsilon_{2k})}\right\}$$

We consider only the narrowband (FBW << 1) case in which path length errors in the various parts of the loops can be approximated as fixed phase errors, Recall that $\underline{\underline{R}}''$ implicitly includes a frequency independent tracking error $C_q(\omega) = e^{-j\xi_q}$ due either to weight circuit hybrid mismatches or to signal channel path length errors. If we define the 2N × 2N stability matrix $\underline{\underline{S}}$ as

$$\underline{\underline{S}} = \begin{bmatrix} \underline{\underline{I}}+\underline{\underline{A}}_1 & \underline{\underline{A}}_2 \\ \underline{\underline{B}}_1 & \underline{\underline{I}}+\underline{\underline{B}}_2 \end{bmatrix} \qquad (93)$$

where $\underline{\underline{S}}$ is a real matrix, then the eigenvalues of $\underline{\underline{S}}$ determine the stability of the coupled set of 2N loops. In particular, if we denote the eigenvalues of $\underline{\underline{S}}$ by $\lambda_\ell (\ell=1 \ldots, 2N)$, then stable operation requires that

$$\mathrm{Re}(\lambda_\ell) > 0 \qquad (94)$$

for $\ell = 1, \ldots, 2N$. In general, $\underline{\underline{S}}$ is not a symmetric matrix and the λ_ℓ are in complex, admitting oscillatory or unstable solutions for α_k and β_k.

Example: A Single Loop

A general study of the stability criterion defined by Eq. (94) is complicated and requires numerical solutions for the eigenvalues of Eq. (93). However, the analysis for a single loop is analytically tractable and it is

instructive to examine this example to obtain insight into the dependence of stability on the various component errors. A single loop is shown in Fig. 13. If it is stable, it will simply tend to turn weight "off" when a signal is applied to the input.

For the case of a single loop, we adopt the following notations

(1) R_o = input power to loop relative to thermal noise

(2) $\mu_{11} = \mu$, $\mu_{21} = \eta\mu$, where η = gain mismatch between I and Q channels

(3) $\varepsilon_{11} = \varepsilon_1$, $\varepsilon_{21} = \varepsilon_2$, $\psi_1 = \psi$

(4) $C(\omega) = e^{-j\xi} F(\omega) = e^{-j(\Delta_2 - \Delta_1)} \equiv e^{-j\Delta}$

With these definitions, the stability matrix $\underline{\underline{S}}$ takes the form

$$\underline{\underline{S}} = \begin{bmatrix} 1 + \mu R_o \cos \varepsilon'_1 & -\mu R_o \sin(\psi+\varepsilon'_1) \\ \eta\mu R_o \sin \varepsilon'_2 & 1 + \eta\mu R_o \cos(\psi+\varepsilon'_2) \end{bmatrix} \tag{95}$$

where $\varepsilon'_1 = \varepsilon_1 - (\Delta-\xi)$, $\varepsilon'_2 = \varepsilon_2 - (\Delta-\xi)$. The two eigenvalues of $\underline{\underline{S}}$ can be computed directly, and are:

$$\begin{aligned} \lambda_{1,2} = {} & \left[1 + \frac{1}{2}\mu R_1(\cos \varepsilon'_1 + \eta \cos(\psi + \varepsilon'_2))\right] \\ & \mp \mu R_o \left\{\frac{1}{4}\cos^2 \varepsilon'_1 - \frac{1}{2}\eta \cos \varepsilon'_1 \cos(\psi + \varepsilon'_2) \right. \\ & \left. + \frac{\eta^2}{4}\cos^2(\psi + \varepsilon'_2) - \eta \sin\varepsilon'_2 \sin(\psi + \varepsilon'_1)\right\}^{1/2} \end{aligned} \tag{96}$$

Applying the stability criterion of Eq. (94), Eq. (96) leads to the stability diagram illustrated in Fig. 14. In this diagram, the errors η, ψ and $(\xi-\Delta)$ are treated as parameters, and stability is plotted as a function of correlator

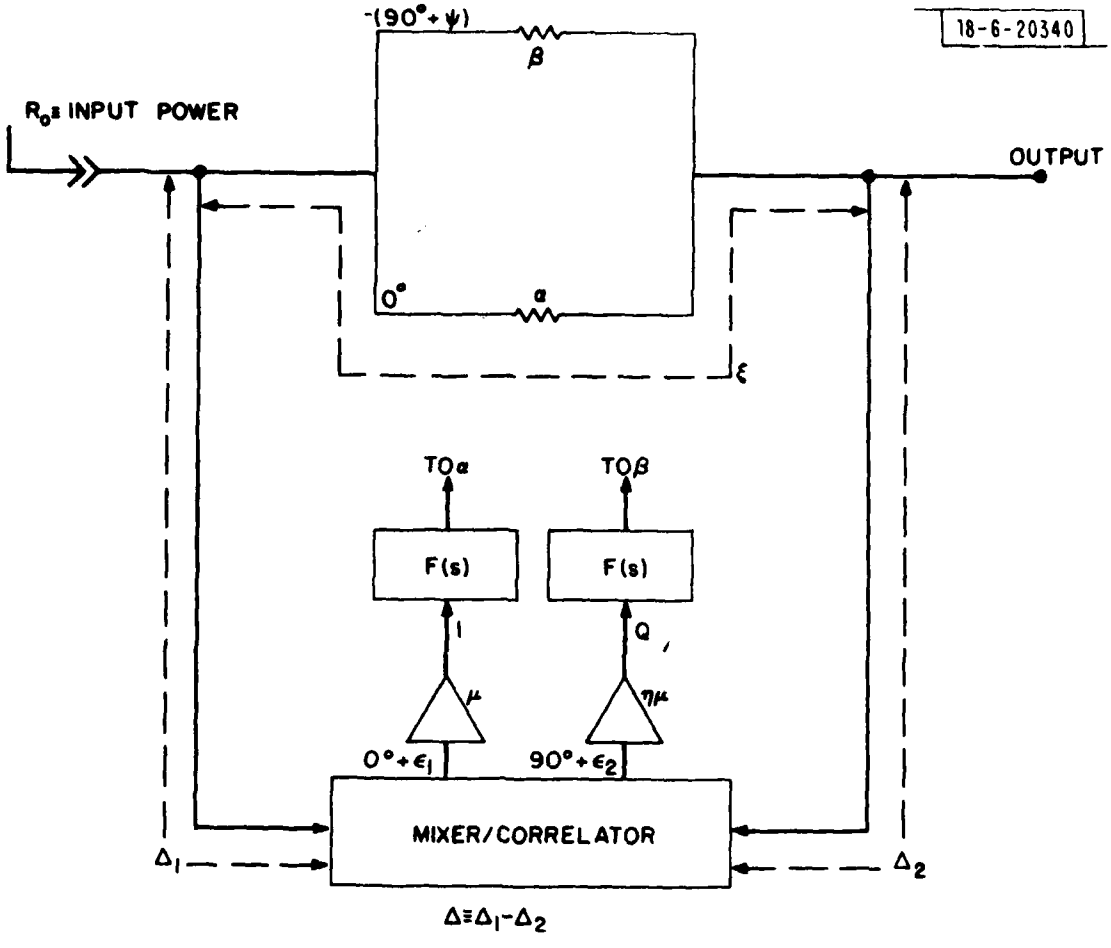

$$\epsilon_1' \equiv \epsilon_1 + (\Delta - \xi)$$

$$\epsilon_2' \equiv \epsilon_2 + (\Delta - \xi)$$

Fig. 13. Loop parameters used for the single loop stability analysis leading to the stability diagram of Fig. 14.

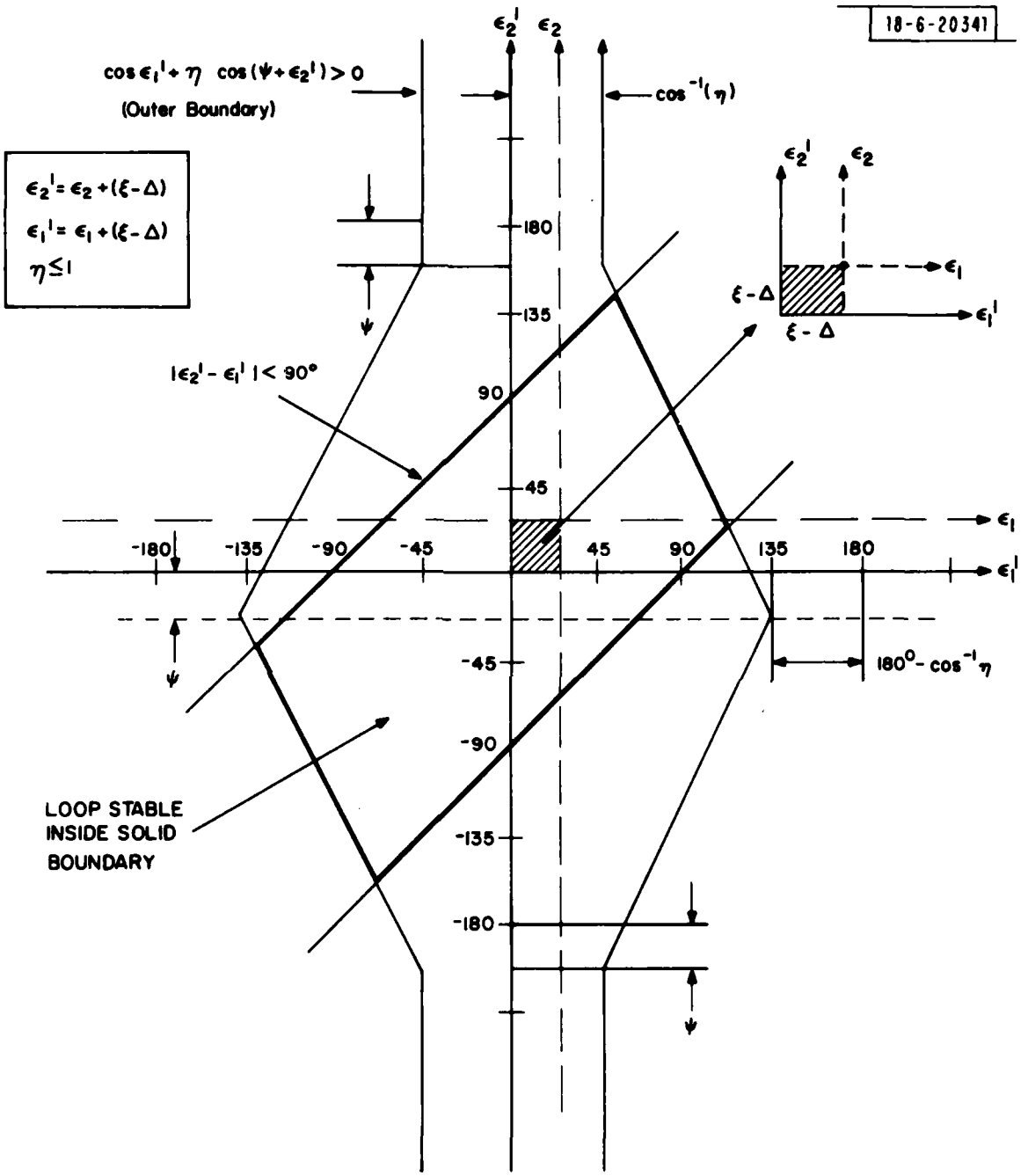

Fig. 14. Stability diagram for a single, first-order, Applebaum-Howells type control loop.

output phase errors ε_1 and ε_2. The loop is stable if ε_1, ε_2 lie inside the solid boundary indicated in the Figure. The boundary is determined from the two conditions.

$$\cos \varepsilon'_1 + \eta \cos(\psi + \varepsilon'_2) > 0 \tag{97}$$

$$|\varepsilon'_2 - \varepsilon'_1| < 90° \tag{98}$$

which follow directly from (94) and (96), assuming $\mu R_o >> 1$. In (97) and (98) we have defined

$$\varepsilon'_1 = \varepsilon_1 + (\zeta - \Delta) \tag{99}$$

$$\varepsilon'_2 = \varepsilon_2 + (\zeta - \Delta) \tag{100}$$

indicating that differential phase errors in the feedback paths are equivalent to identical correlator phase offsets in the I and Q channels. Generally speaking there is a biased region of stability about $\varepsilon'_1 = \varepsilon'_2 = 0$.

To obtain a physical feel for how the loops become unstable, consider a simple unstable condition and track through the feedback process. Basically, stability (or instability) is a consequence of the negative (or positive) feedback condition existing at the output of the correlator, where errors in the mixer generate a drive voltage in the quadrature channel. Once the quadrature channel is turned on, the output now has a component shifted 90°. Hence, should the correlator differential error between I/Q channels exceed 90°, this 90° shift combines with the quadrature weight 90° shift resulting in a 180° phase reversal at the sum junction -- i.e., the feedback in the quadrature channel is now positive feedback, resulting in an increasingly large growth in signal level driving the weight, and the loop becomes unstable. Thus, the stability boundary as a function of ε'_1, ε'_2 intersects ± 90° on all axes of the diagram. When $\varepsilon_1 = -\varepsilon_2$, a 45° error in both I and Q yields a 90° differential output error in the correlator and an unstable condition, as can be seen on the stability diagram. Errors in the hybrid (ψ) or differential path length (ζ-Δ) result in a more complicated

I/Q coupling, but essentially lead to some type of positive feedback when the loops become unstable.

Some N-Loop Examples

The above results indicate that the stability characteristics of a single loop are quite tolerant to most reasonable values of component errors. Practically speaking, one would anticipate that ε'_1 and ε'_2 would be 5 to 10° at most and that weight hybrid errors, ψ_k, would be less than 1 to 2°. Loop gains might differ by as much as 2 or 3 dB. Consequently, it appears to be relatively easy to design a single stable loop. The question then arises, "How does the processor stability depend on the number of loops and number of interference sources?"

It is useful to consider a simple special case in order to obtain a feel for the dependence on the number of loops. Consider the N-loop problem having equal I and Q mixer imbalance errors in each loop. Denote this error by ε. Then we have

$$\begin{aligned} \tau_o \dot{\underline{\alpha}} + \underline{\alpha} + \mu\, \mathrm{Re}[e^{j\varepsilon}\, \underline{\underline{R}}' \cdot \underline{w}] &= \underline{V}_1 \\ \tau_o \dot{\underline{\beta}} + \underline{\beta} + \mu\, \mathrm{Im}[e^{j\varepsilon}\, \underline{\underline{R}}' \cdot \underline{w}] &= \underline{V}_2 \end{aligned} \tag{101}$$

Equation (101) can be rewritten in complex notation as

$$\tau_o \dot{\underline{w}} + \underline{w} + \mu e^{j\varepsilon}\, \underline{\underline{R}}' \cdot \underline{w} = \underline{V}_1 + j\underline{V}_2 \tag{102}$$

where now $\underline{w} = \alpha + j\beta$ since we assume $\psi_k = 0$. Denote the eigenvalues of $\underline{\underline{R}}'$ by s_k. Then the stability of (102) is governed by the eigenvalues $\lambda_k = 1 + \mu s_k\, e^{j\varepsilon}$. Clearly, if $\mathrm{Re}(\lambda_k) \lesssim 0$, we must require that $\varepsilon < 90°$. This is the same stability requirement as for a single loop. Consequently, we anticipate that increasing the number of loops should not adversely affect the stability of the processor.

In practice, the various component errors will be statistically distributed, with some channels having little error and others, perhaps, a larger error. The above result then is a worst-case condition for this more realistic case and we anticipate the stability of the processor will improve as the number of loops increases. To examine this, we resort to a numerical simulation of Eq. (93) including all types of component errors. Each component error will be assumed to be uniformly distributed over a range within a maximum error bound. Each simulation trial uses a set of errors randomly selected from each distribution. The stability criterion for each sample set of errors can be checked by computing the eigenvalues of $\underline{\underline{S}}$ and applying the condition $\mathrm{Re}(\lambda_\ell) > 0$, $\ell=1, \ldots, 2N$. This process is repeated for a number of trials with a specified error bound for each component. The percentage of cases for which the processor is unstable is tabulated. In this manner, the probability of achieving stability can be studied as a function of the error bounds for a particular component. The result can then be used in designing the processor to a fixed set of specifications.

This procedure can be utilized to examine processor stability as a function of antenna type, number of loops and number of interference sources. Consider the results of Fig. 15, where we show processor stability as a function of the number of loops for a single interference source. For example purposes, we use the 7-element hexagonal array antenna geometry illustrated in the figure, and examine the percent of unstable eigenvalues vs error bound as the number of control loops increases from 1 to 7. For simplicity, we consider only I/Q mixer imbalance errors to illustrate the dependence on N. Observe that for a single loop, no value of mixer imbalance errors leads to an unstable loop until the ϵ_{max} exceeds 45°. This critical value allows the case $\epsilon_1 \sim -\epsilon_2$ to occur for some set of random errors. As mentioned previously, this results in an unstable loop. More importantly, observe in Fig. 15 that as the number of loops increases, the loop stability becomes tolerant of a larger error bound, as predicted above. Clearly, for 7 loops, the tolerances on I/Q mixer imbalance errors would be very easy to satisfy.

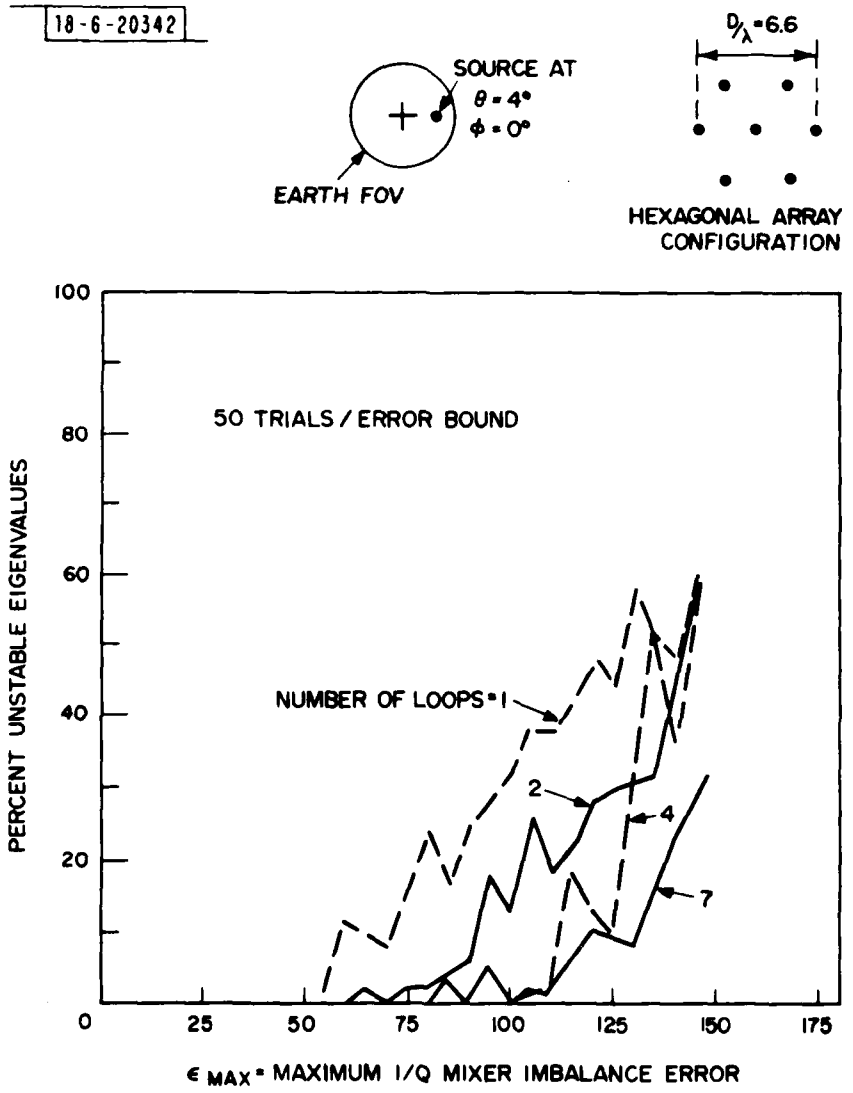

Fig. 15. Stability dependence as a function of I/Q mixer imbalance errors for 1, 2, 4 and 7 control loops. Antenna geometry used was 7-element hexagonal array haveing $D/\lambda = 6.6$ with a single interference source positioned at $\theta = 4^{o}$, $\phi = 0^{o}$. FBW = 0.

We now fix the number of loops, and vary the number of interference sources. Consider the same 7-element hexagonal array with 6 sources located on the FOV as shown in Table 3 below.

TABLE 3

RANDOM LOCATIONS OF SIX INTERFERENCE SOURCES

j	θ_j	ϕ_j
1	1°	- 10°
2	4°	30°
3	8°	80°
4	5°	135°
5	7°	205°
6	6°	280°

The probability of achieving stability as a function of the error bound on mixer imbalance errors is indicated in Fig. 16 for J=1, 4 and 6. Clearly, the sensitivity to component tolerance errors is most severe for the case of six sources incident on the 7-element array. In this case the processor has used all its degrees-of-freedom to null sources. Note, however, as suggested by our simple example above, the allowable component tolerances never become more severe than those for a single loop.

Finally, consider a 7-element array with a double triangle configuration (Fig. 17). Again, we use the 6 interference sources of Table 3. All the errors (ε_{1k}, ε_{2k}, ψ_k, ξ_k and Δ_k) are allowed to vary statistically as in the previous simulations. In this case, we tabulate the statistics of the trial cases in the following manner: We treat η (gain mismatch) as a parameter and generate a set ψ_k, ξ_k and Δ_k, k=1, ..., 7. Then for this random set of component errors, we generate a subset of ε_{1k} and ε_{2k}, k=1, ..., 7 bounded by ε_{max}. We consider twenty sample cases for ε_{1k} and ε_{2k} for each set ψ_k, ξ_k and Δ_k. We then store the percent of unstable values as a function of

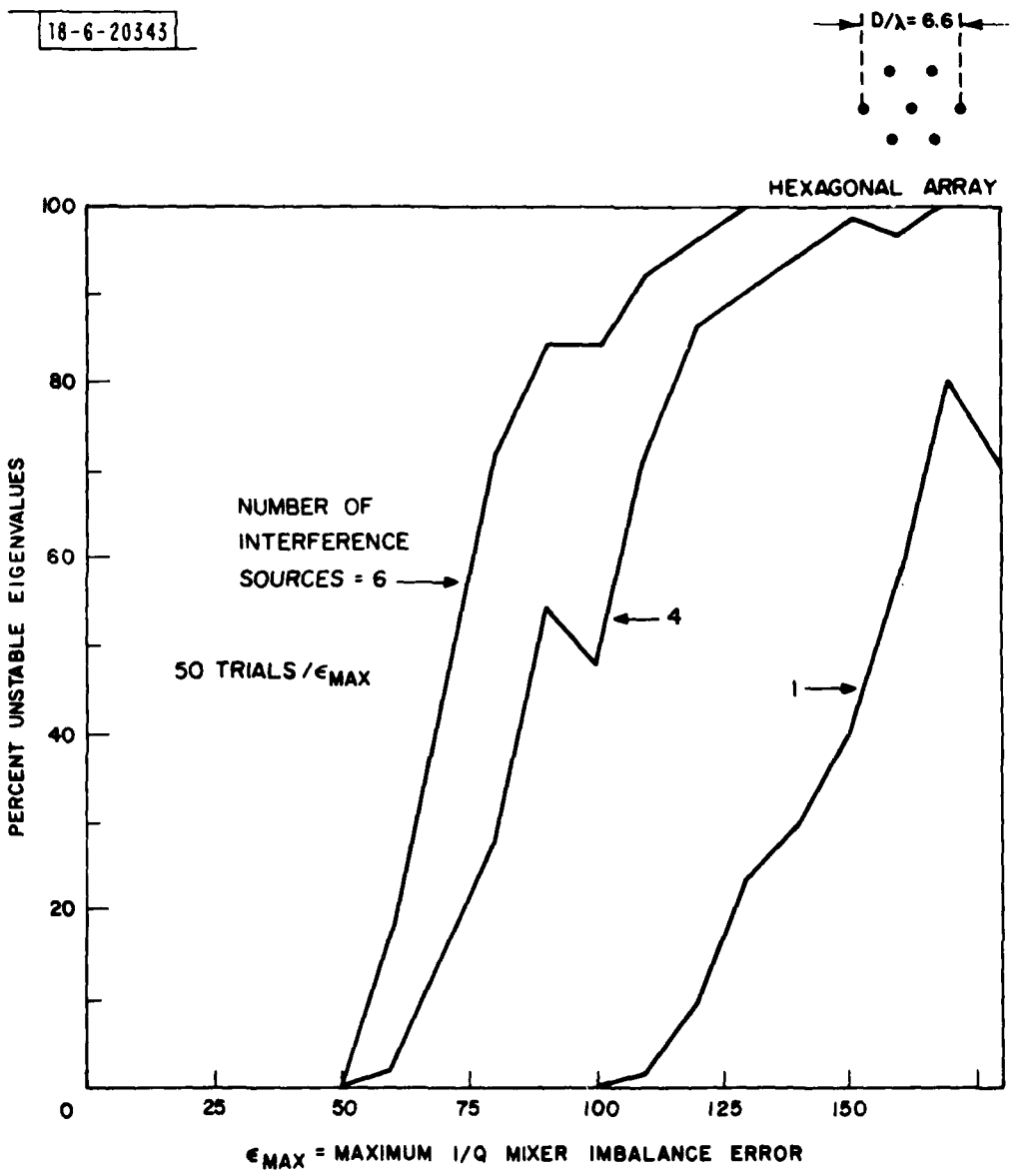

Fig. 16. Stability dependence as a function of I/Q mixer imbalance errors for 1, 4 or 6 interference sources of Table 3 incident on a 7-element hexagonal array. $D/\lambda = 6.6$, FBW = 0.

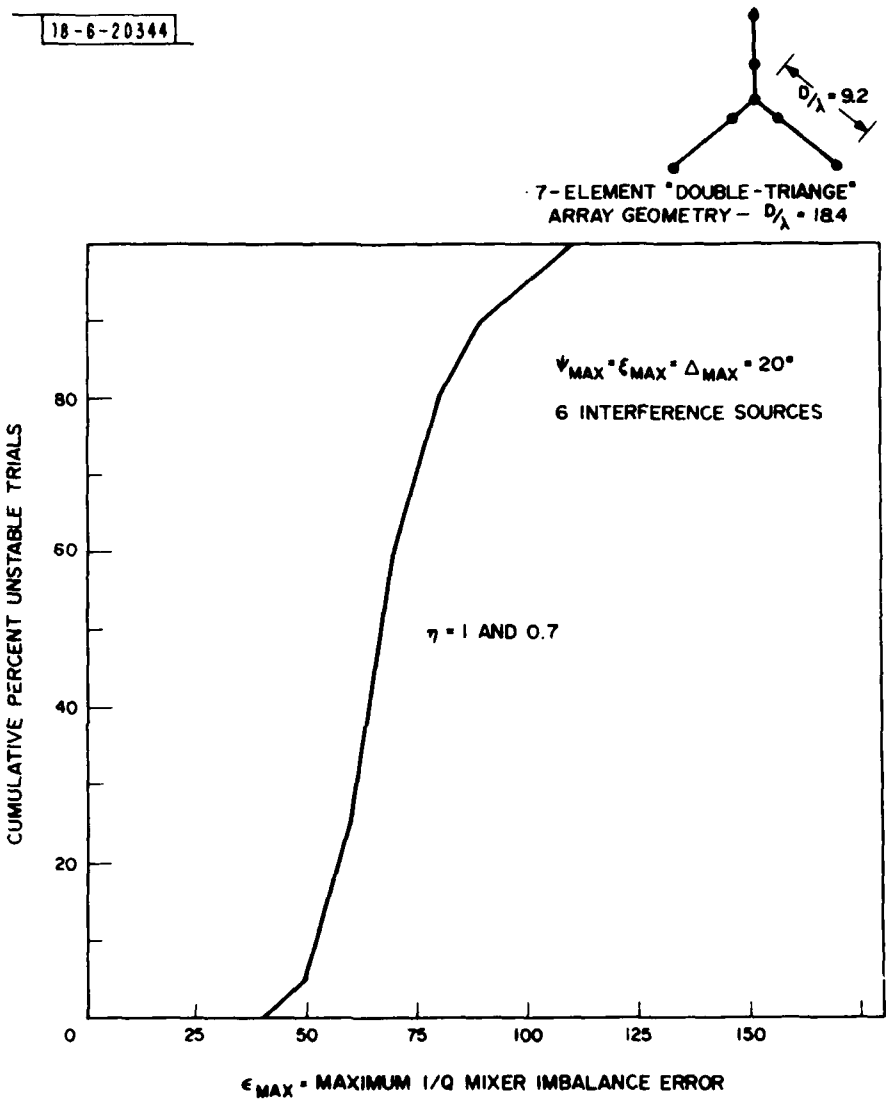

Fig. 17. Stability dependence vs. I/Q mixer imbalance errors when all component parameters ϵ_{1_k}, ϵ_{2_k}, ψ_k, ξ_k and Δ_k, k = 1, ..., 7 vary statistically using ψ_{max}, ξ_{max} and $\Delta_{max} = 20^o$. Antenna configuration used was 7-element double triangle array having $D/\lambda = 18.4$. The six interference sources of Table 1 were assumed incident on the array. FBW = 0. Results are for $\eta = 1$ and $\eta = .7$.

ε_{max}, and repeat for a new set of ψ_k, ξ_k and Δ_k. For each set of ψ_k, ξ_k and Δ_k, we store the cumulative maximum of the percent unstable values obtained vs ε_{max}. Figure 17 illustrates this cumulative maximum (i.e., the worst case result) vs ε_{max} using $\psi_{max} = \xi_{max} = \Delta_{max} = 20°$ for $\eta = 1$ and $\eta = 0.7$. The results are essentially the same for $\eta = 1.0$ and $\eta = 0.7$. Observe that the curve of Fig. 17 has shifted only slightly to the left of that for Fig. 16, for which case $\xi_{max} = \Delta_{max} = \psi_{max} = 0$. Consequently, as predicted by Fig. 14 for a single loop, errors in ζ_k, Δ_k and ψ_k are not cumulative relative to ε_{1k} and ε_{2k}. In fact, as Fig. 14 and the above simulations indicate, the loops are more tolerant to errors in ξ_k, ψ_k and Δ_k than for ε_{1k} and ε_{2k}. We conclude therefore that even loose tolerances on error parameters still allow stable loop operation, even in the worse case of N-1 sources incident on an N-element array.

E. Weight Noise

Heretofore when the time variation of the weights has been mentioned we were speaking of the statistical or ensemble average of the weights. It was pointed out in Section II, Background, that the differential equations for $\underline{w}(t)$ were derived in terms of a statistical average. In this section we consider the statistical fluctuations of $\underline{w}(t)$ around its average value. We refer to these fluctuations as weight noise. In an analog processor weight noise may arise from two sources. The first is thermal noise in the weight control circuits. Secondly, if the input signals are noisy, some of this noise is fed back to the weights, causing them to fluctuate. In digital systems, quantization and round-off errors can contribute to weight noise.

Weight noise has two observable effects. First, it increases the adapted output power of the processor over what it would be if the weights were fixed at their average value. Second, even when the nulling processor is in a steady-state, adapted condition, the continuous small weight fluctuations make it appear to be a time-varying, multi-path channel to the communications signals. Thus it will tend to smear or broaden the signal spectra. This reduces the detectability of a signal and can also cause cross-talk between signals that are separated in frequency. In this section we will quantify these two effects. We will calculate the weight noise contribution to total output power and find that it is insignificant as long as the processor dynamic range is not exceeded.

1. Circuit Noise

Circuit noise effects can be modeled as in Fig. 18(a). We will assume the input $\underline{v}(t)$ to be a noiseless process (i.e., a sinusoid) so that circuit noise is the only source of weight fluctuation. The total weight vector is the sum of a noiseless average value $\underline{w}(t)$ and a noise vector $\underline{n}(t)$ whose components are identical, but statistically independent, zero mean random processes of variance, $\overline{n^2}$. An example of such a noise source in a baseband feedback loop is the 1/f noise in the video amplifier following the correlation mixer.

Total Output Power:

Assume the processor to be in a steady-state adapted condition for which $\underline{w}(t)$ is a constant. Consider the total output power

$$P_o = E\{v_o(t)\ v_o^*(t)\} \tag{103}$$

where

$$v_o(t) = (\underline{w}^\dagger + \underline{n}^\dagger(t)) \cdot \underline{v}(t) \tag{104}$$

By substituting (104) into (103), and by using the statistical independence of the noise generators, it can easily be shown that

$$P_o = \underline{w}^\dagger \cdot \underline{\underline{R}} \cdot \underline{w} + \overline{n^2}\, P_{in} \tag{105}$$

where $\underline{\underline{R}}$ is the correlation matrix $E\{\underline{v}(t)\underline{v}(t)^\dagger\}$, $\underline{w}^\dagger \cdot \underline{\underline{R}} \cdot \underline{w}$ is the noiseless adapted output power and P_{in} is the total input power to all channels.

When testing a processor one often measures the dependence of P_{out} on P_{in} for a single interference source, usually at broadside incidence. When a narrow-band test signal is used, weight noise manifests itself as shown in Fig. 18(b) (for a hard-limited processor). When P_{in} exceeds a particular value (40 dB in this case), the weight noise dominates the output power and P_o becomes proportional to P_{in} as predicted by Eq. (105). Measurements to this effect will be presented in Section V.

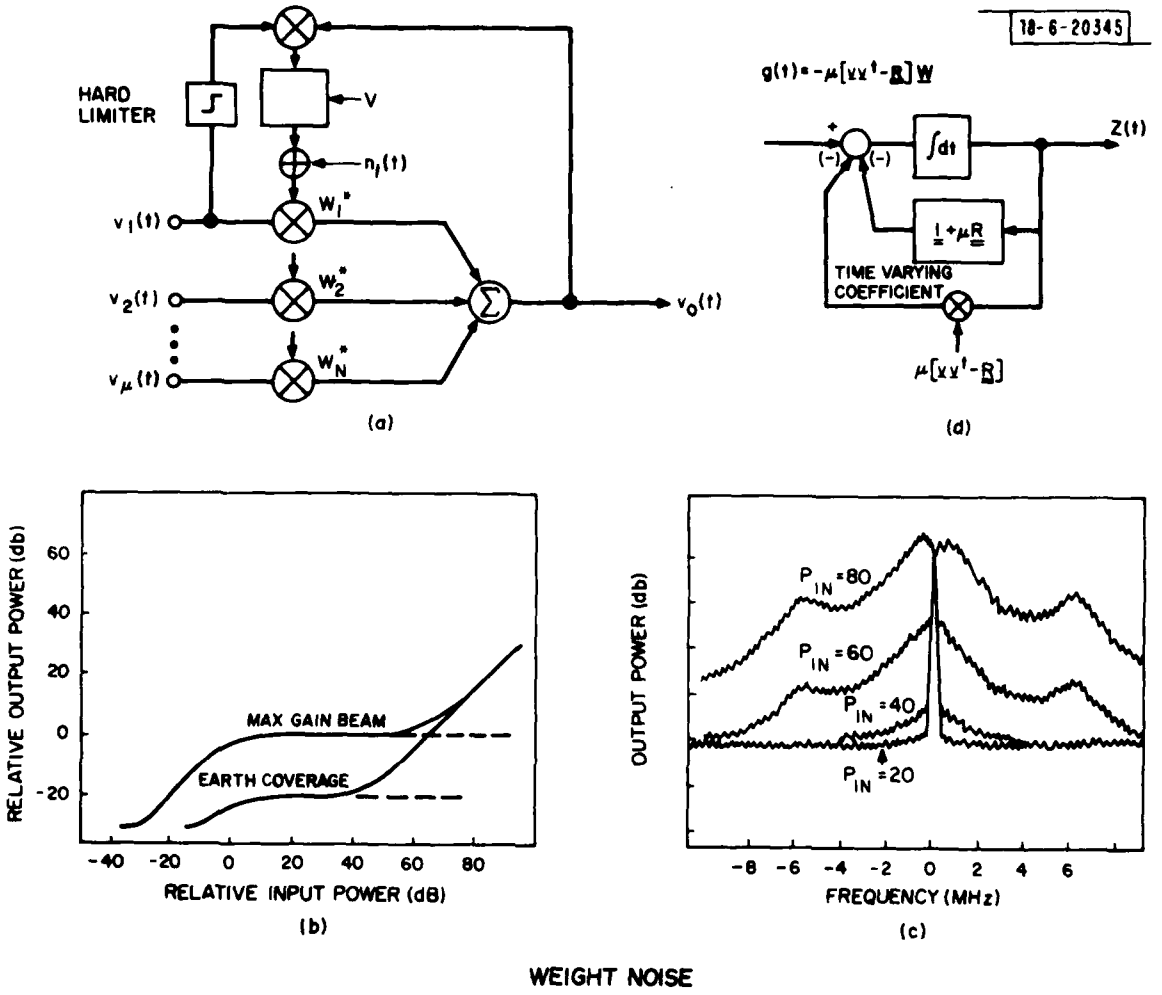

WEIGHT NOISE

Fig. 18. Effect of noise in the feedback loop circuitry on nulling system performance for a hard-limited processor. (a) Circuit noise is modelled by identical but statistically independent noise generators. (b) The effect of weight noise on the adapted P_{OUT} vs. P_{IN} characteristic of a processor with single, broadside incident source. (c) Effect of weight noise on the output spectrum for a sinusoidal input of varying power levels. (d) The equivalent linear system for weight noise arising from the interference signal.

Output Spectrum:

Weight noise modulates any signal passing through the processor and broadens its spectrum. The power spectral density of the output is

$$S_o(\omega) = \int_{-\infty}^{\infty} R_o(\tau) e^{-j\omega\tau} \, d\tau \tag{106}$$

where $R_o(\tau)$ is the output autocorrelation function,

$$R_o(\omega) = E\{v_o(t) \; v_o^*(t-\tau)\} \tag{107}$$

As in Section II, we define a correlation matrix for the channel signal vector $\underline{v}(t)$ as follows:

$$[\underline{\underline{R}}_V(\tau)] = E\{\underline{v}(t) \; \underline{v}^\dagger(t-\tau)\} \tag{108}$$

The cross-power spectral density matrix is

$$[\underline{\underline{S}}_V(\omega)] = \int \underline{\underline{R}}_V(\tau)] \; e^{-j\omega\tau} \, d\tau \tag{109}$$

With these definitions it follows from Eq. (104) that the output power spectral density is

$$S_o(\omega) = \underline{w}^\dagger \cdot \underline{\underline{S}}_V(\omega) \cdot \underline{w} + \mathrm{Tr}\{S_n^*(\omega) \circledast \underline{\underline{S}}_V(\omega)\} \tag{110}$$

where Tr is the matrix trace (sum of the diagonal elements), $S_n(\omega)$ is the weight noise spectrum and $\circledast$ denotes the convolution integral divided by 2π. For the case where the signal vector $\underline{v}(t)$ is a tone of amplitude V, $P_{in} = N|V|^2$ and we have

$$S_o(\omega) = 2\pi \{|V|^2 \; \underline{w}^\dagger \cdot \underline{w} \; \delta(\omega) + P_{in} \; S_n(\omega)\} \tag{111}$$

The first term is the line spectrum of the signal at the output ($\delta(\omega)$ is an impulse in frequency). The second is the weight noise contribution.

As an example of Eq. (111), Fig. 18(c) shows the measured output spectrum for a hard-limited processor. As P_{in} is increased, the signal component is clamped at a fixed amplitude by the adaptive processor, but the weight noise

spectrum increases in proportion to P_{in}. Of course a pure tone is not a realistic interference signal; however, this test is useful in revealing directly the circuit noise spectrum.

2. Interference Noise

We will now consider the weight noise generated by a noisy input, $\underline{v}(t)$. We will first analyze a standard Applebaum-Howells loop, i e., one without the hard limiter of Fig. 18(a). We will calculate its effect on a tone of constant amplitude, V_j, whose power is insignificant compared to the power in $\underline{v}(t)$. We will also find the weight noise contribution to total output power and show that it is insignificant as long as the processor dynamic range is not exceeded. Section 3 extends this analysis to hard limited Applebaum-Howell loops under the assumption of broadside incident interference.

Weight Noise Spectrum:

Let the total weight vector be the sum of its expected value, $\underline{w}(t)$, and a zero-mean weight noise vector $\underline{Z}(t)$. Referring to Section II, Eq. (3), the equation governing the total weight vector is

$$\tau_o(\dot{\underline{w}} + \dot{\underline{Z}}) + [\underline{\underline{I}} + \mu \underline{v}\,\underline{v}^{\dagger}] \cdot (\underline{w} + \underline{Z}) = \underline{V} \tag{112}$$

where we understand that $\underline{w}$, $\underline{Z}$ and $\underline{v}$ are functions of time. Let $\underline{v}(t)$ be a zero-mean, gaussian, band-limited process of bandwidth, BW. The basic assumption underlying the analysis of nulling processors is that τ_o and μ are chosen so that the closed-loop bandwidth, BW_C, of the processor is a small percentage of the nulling bandwidth, BW. Consequently, Z(t) is quasistatic in comparison with v(t) and can be treated as statistically independent of the instantaneous value of v(t) (although it is not independent of the past history of v(t)). With this assumption, the expectation of Eq. (112) yields the well-known equation for $\underline{w}(t)$,

$$\tau_o \dot{\underline{w}} + [\underline{\underline{I}} + \mu \underline{\underline{R}}] \cdot \underline{w} = \underline{V} \tag{113}$$

where $\underline{\underline{R}} \equiv \underline{\underline{R}}_v(o)$ in Eq. (108). Subtracting Eq. (113) from (112) yields an equation for $\underline{Z}(t)$.

$$\tau_o \dot{\underline{Z}} + [\underline{\underline{I}} + \mu \underline{\underline{R}}] \cdot \underline{Z} + \mu[\underline{v}\,\underline{v}^{\dagger} - \underline{\underline{R}}] \cdot \underline{Z} = -\mu[\underline{v}\,\underline{v}^{\dagger} - \underline{\underline{R}}] \cdot \underline{w} \tag{114}$$

This is a linear, vector differential equation with a time-varying coefficient. Figure 18(d) is the linear system representation of Eq. (114). The forcing function is

$$\underline{g}(t) = -\mu[\underline{v}\ \underline{v}^{\dagger} - \underline{\underline{R}}] \cdot \underline{w} \tag{115}$$

In Fig. 18(d) we see that the time-varying coefficient has a negligible effect compared with $\underline{g}(t)$ if $|\underline{Z}| << |\underline{w}|$. We are therefore justified in neglecting it under normal operating conditions. The differential equation for weight noise is then

$$\tau_o \dot{\underline{Z}} + [\underline{\underline{I}} + \mu\underline{\underline{R}}] \cdot \underline{Z} = \underline{g} \tag{116}$$

Now we can obtain the power spectral density of $\underline{Z}$. In multi-dimensional linear systems the relationship between power spectral densities at the inputs and outputs is

$$\underline{\underline{S}}_{out}(\omega) = \underline{\underline{H}}^{\dagger}(\omega)\ \underline{\underline{S}}_{in}(\omega)\ \underline{\underline{H}}(\omega) \tag{117}$$

where $\underline{\underline{H}}(\omega)$ is the matrix of system input-output transfer functions. From Eq. (116) we have

$$S_Z(\omega) = [(1 + j\omega\tau_o)\ \underline{\underline{I}} + \mu\underline{\underline{R}}]^{-1} \cdot \underline{\underline{S}}_g(\omega) \cdot [(1 - j\omega\tau_o)\ \underline{\underline{I}} + \mu\underline{\underline{R}}]^{-1} \tag{118}$$

Now, since $BW >> BW_C$, $\underline{\underline{S}}_g(\omega)$ is a very wide spectrum compared to the system bandwidth and we can approximate it by a constant spectral density,

$$S_g(\omega) = \frac{1}{BW} E[\underline{g}\ \underline{g}^{\dagger}]$$

From Eq. (115) we find an expression for the expectation,

$$E\{g_k\ g_\ell^*\} = \mu^2 \sum_{ij} \underline{w}_i\ \underline{w}_j^*\ \varepsilon\{v_k\ v_i^*\ v_j\ v_\ell^*\} - \mu^2\{\underline{\underline{R}} \cdot \underline{\underline{ww}}^{\dagger} \cdot \underline{\underline{R}}\}_{k\ell} \tag{119}$$

where we have used the fact that $E\{\underline{v}\ \underline{v}^{\dagger}\} = \underline{\underline{R}}$. The fourth moment in (119) can be simplified using the following identity for gaussian, complex random processes (Ref. 5, Eq. 33)

$$E\{X_1X_2^*X_3X_4^*\} = E\{X_1X_2^*\} \cdot E\{X_3X_4^*\} + E\{X_1X_4^*\} \cdot E\{X_2^*X_3\} \tag{120}$$

Using this in Eq. (119) yields

$$E\{\underline{g}\ \underline{g}^{\dagger}\} = \mu^2(\underline{w}^{\dagger} \cdot \underline{\underline{R}} \cdot \underline{w})\ \underline{\underline{R}} \tag{121}$$

$(\underline{w}^{\dagger} \cdot \underline{\underline{R}} \cdot \underline{w})$ is the adapted output power, P_o, in the absence of weight noise. From (118) we get

$$\underline{\underline{S}}_Z(\omega) = \frac{\mu^2(\underline{w}^{\dagger}\underline{\underline{R}}\underline{w})}{BW}\ [(1 + j\omega\tau_o)\ \underline{\underline{I}} + \mu\underline{\underline{R}}]^{-1}\ \underline{\underline{R}}[(1 - j\omega\tau_o)\ \underline{\underline{I}} + \mu\underline{\underline{R}}]^{-1} \tag{122}$$

which is the desired expression for the weight noise cross power spectral density. Since the off-diagonal terms of $\underline{\underline{S}}_Z(\omega)$ are non-zero, the weight noise is correlated from channel to channel unlike the case of circuit noise.

Weight Noise Interaction with the Signal:

Now let the input contain a communications signal waveform, $\underline{V}_s(t)$, buried in the interference, $\underline{v}(t)$. $\underline{V}_s(t)$ is sufficiently small so as not to affect weight adaption or weight noise. Let us find the power spectral density of the processor output, $v_o(t)$. By the same process that yielded Eq. (110), we can show that it is,

$$S_o(\omega) = \underline{w}^{\dagger} \cdot \underline{\underline{S}}_s(\omega) \cdot \underline{w} + \sum_{ij} [\underline{\underline{S}}_Z(\omega)]_{ij} \circledast [\underline{\underline{S}}_s(\omega)]_{ij} + \underline{w}^{\dagger}\ \underline{\underline{S}}_v(\omega)\ \underline{w} +$$

$$\sum_{ij} [\underline{\underline{S}}_Z(\omega)]_{ij} \circledast [\underline{\underline{S}}_v(\omega)]_{ij} \tag{123}$$

where $\underline{\underline{S}}_s(\omega)$ is the cross-spectral density of $V_s(t)$ and we have assumed $\underline{V}_s(t)$ and $\underline{v}(t)$ to be independent. The first and third terms are the signal and interference throughput respectively and the second and fourth terms represent weight noise modulation of the signal and the interference respectively. Let us examine the signal modulation effect for a sinusoidal signal. Under this assumption the third term in Eq. (123) reduces to

$$S_o'(\omega) = (\underline{V}_s^{\dagger} \cdot \underline{\underline{S}}_Z(\omega) \cdot \underline{V}_s) \tag{124}$$

It is convenient now to apply a linear transformation. From Eq. (122), we see that $\underline{\underline{S}}_Z(\omega)$ is diagonalized by the same transformation that diagonalizes $\underline{\underline{R}}$. Let $\underline{\underline{Q}}$ be a matrix whose columns are the eigenvectors of $\underline{\underline{R}}$. By definition

$$\underline{\underline{Q}}^\dagger \underline{\underline{R}} \underline{\underline{Q}} = \begin{bmatrix} s_1 & & & 0 \\ & s_2 & & \\ & & \ddots & \\ 0 & & & s_N \end{bmatrix} \tag{125}$$

where s_i is the i^{th} eigenvalue of $\underline{\underline{R}}$. Define the transformation of $\underline{\underline{S}}_Z(\omega)$ by

$$\hat{\underline{\underline{S}}}_Z(\omega) = \underline{\underline{Q}}^\dagger \underline{\underline{S}}_Z(\omega) \underline{\underline{Q}} \tag{126}$$

We have

$$[\hat{S}_Z(\omega)]_{ii} = \frac{\mu^2(\underline{w}^\dagger \underline{\underline{R}} \underline{w})}{BW} \cdot \frac{s_i}{(1 + \mu s_i)^2 (1 + \omega^2 \tau_i^2)} \tag{127}$$

where $\tau_i = \tau_o/(1 + \mu s_i)$ is the time constant associated with the i^{th} eigenvalue of $\underline{\underline{R}}$. Equation (124) becomes

$$S_o'(\omega) = \sum_{i=1}^{N} |\hat{V}_{si}|^2 \, [\underline{\underline{S}}_Z(\omega)]_{ii} \tag{128}$$

where

$$\hat{\underline{V}}_s = \underline{\underline{Q}}^\dagger \cdot \underline{V}_s$$

and

$$V_{si} = \underline{e}_i^\dagger \cdot \underline{V}_s \tag{129}$$

The final expression for the spectrum of the weight noise modulated signal is

$$S_o'(\omega) = \frac{\mu^2(\underline{w}^\dagger \underline{\underline{R}} \underline{w})}{BW} \sum_i \frac{|\hat{V}_{si}|^2 s_i}{(1 + \mu s_i)^2 (1 + \omega^2 \tau_i^2)} \tag{130}$$

Let us evaluate Eq. (130) for a single interference source having total input power, $P_{in} = s_1$. We will normalize P_{in} to the threshold power, $P_T = \mu^{-1}$. It can easily be shown that

$$(\underline{w}^{\dagger} \cdot \underline{\underline{R}} \cdot \underline{w}) = \frac{|\hat{V}_1|^2 P_{in}}{(1 + P_{in}/P_T)^2} \tag{131}$$

where $\hat{V}_1 = \underline{e}_1^{\dagger} \cdot \underline{V}$ ($\underline{V}$ is the steering vector). Equation (130) becomes

$$S_o'(\omega) = \frac{|\hat{V}_{s1}|^2 \, |\hat{V}_1|^2 \, (P_{in}/P_T)^2}{BW(1 + P_{in}/P_T)^4} \quad \frac{1}{(1 + \omega^2 \tau_1^2)} \tag{132}$$

where

$$\tau_1 = \tau_o/(1 + P_{in}/P_T)$$

From this we can see that weight noise has its maximum effect when the interference power is near threshold. In fact, the worst case for the peak spectral density $S_o'(o)$ occurs at $P_{in} = P_T$ and is

$$S_o'(o) \leq \frac{|V_s|^2}{16 \, BW} \text{ volts}^2/\text{hz} \tag{133}$$

where we have used $|\hat{V}_s| \leq |V_s|$ and $|\hat{V}_1| \leq 1$. The total power in the spectrum reaches its maximum at $P_{in} = 2P_T$ and is

$$\frac{1}{2\pi} \int_{-\infty}^{\infty} S_o'(\omega) \, d\omega \leq \frac{|V_s|^2}{4 \, BW \cdot \tau_o} \text{ volt}^2 \tag{134}$$

To a first approximation, $S_o'(\omega)$ affects the communications signals like additive gaussian noise. An important question is how much of the power of $S_o'(\omega)$ falls in the signal bandwidth. In frequency division multiplexed systems, a more important question is how much power falls into adjacent frequency slots causing cross talk between channels. Given the parameters of the communications system, these and other questions can be answered once $S_o'(\omega)$ is known.

Increase in Total Output Power Due to Weight Noise:

Let us return to Eq. (123) and consider the last two terms which are the interference noise throughput and an additional component due to weight noise modulating the interference. We will show that the latter effect causes a negligible increase in power as long as the input power is within the dynamic range of the processor. In the time domain the terms of (123) characterizing the interference output power can be written as

$$P_o = \underline{w}^\dagger \cdot \underline{\underline{R}} \cdot \underline{w} + E\{\underline{Z}^\dagger \cdot \underline{\underline{R}} \cdot Z\} \tag{135}$$

where we assume $\underline{Z}$ and $\underline{w}$ are uncorrelated. Applying the linear transformation of (125) we get

$$\varepsilon\{\underline{Z}^\dagger \cdot \underline{\underline{R}} \cdot Z\} = \sum_{i=1}^{N} E\{|\hat{Z}_i|^2\}\, s_i \tag{136}$$

We obtain $E\{|\hat{Z}_i|^2\}$ by integrating Eq. (127) over ω and dividing by 2π. With this, Eq. (136) becomes

$$P_o = \underline{w}^\dagger \cdot \underline{\underline{R}} \cdot \underline{w}\left[1 + \frac{\mu^2}{2\tau_o BW} \sum_{1=1}^{N} \frac{s_i^2}{1 + \mu s_i}\right] \tag{137}$$

The result in Eq. (137) is similar to that developed by Brennan et al.[5] for sampled data systems. The bracketed term is the contribution of weight noise to the total output power. For a single interference source we have

$$\frac{P_o}{P_T} = \frac{|\hat{V}_1|^2 (P_{in}/P_T)}{(1 + P_{in}/P_T)^2}\left[1 + \frac{1}{2\tau_o BW} \frac{(P_{in}/P_T)^2}{(1 + P_{in}/P_T)}\right] \tag{138}$$

For the weight noise to be significant the input power must satisfy

$$P_{in}/P_T \geq 2\tau_o BW \tag{139}$$

However, this violates our basic assumption that the weights are statistically independent of the input, $\underline{v}(t)$. This assumption was necessary to get Eq. (113).

It requires that the weights remain essentially constant over an interval of several times the correlation time of $\underline{v}(t)$, which in turn implies

$$\frac{\tau_o}{\mu s_{max}} \gg \left(\frac{1}{BW}\right) \tag{140}$$

because $\tau_o/\mu s_{max}$ is the minimum time constant in the processor transfer function (Eq. 122). Using $s_{max} \approx P_{in}$, we have as the condition for validy of this analysis

$$\frac{P_{in}}{P_T} \ll \tau_o \cdot BW \tag{141}$$

which contradicts (139). (In fact, a common definition of the processor dynamic range is $P_{in}/P_T \leq (1/5)\ BW \cdot \tau_o$.) We conclude, therefore, that we can never observe the effect of $\underline{Z}(t)$ on the total power output if the processor is operating within its dynamic range.

3. Hard-Limited Processors

This analysis can be extended only in a limited way to the hard-limited Applebaum-Howells loop (Fig. 18(a)). This type of processor is described by Gabriel (Ref. 2). The reason for hard limiting is to decrease the dynamic range requirements on the correlation mixer and subsequent circuits. As mentioned in Section V of this report and in Ref. 7, hard limiters do have a harmful effect on system performance in that they make it difficult for a processor to detect and null the smaller of two signals of widely different power levels. Because hard limiting is used so often in practice, weight noise effects in hard-limited processors is of interest. Therefore the necessary modifications to the preceding analysis are pointed out.

In a hard-limited system the correlation mixer output is described by

$$X_k(t) = \frac{v_k(t)\ v_o^*(t)}{|v_k(t)|} \tag{142}$$

Consequently the basic differential equation is

$$\tau_o(\dot{\underline{w}} + \dot{\underline{Z}}) + [\underline{\underline{I}} + \mu h \underline{\underline{M}}](\underline{w} + \underline{Z}) = \underline{V}$$

where $\underline{\underline{M}}$ is given by

$$[\underline{\underline{M}}]_{ij} = \frac{v_i v_j^*}{|v_i|} \tag{143}$$

This can be compared with Eq. (112) for the standard system. Brennan and Reed calculated the mean value of $\underline{\underline{M}}$ for a gaussian input (Ref. 6) and found it to be

$$E\{\underline{\underline{M}}\} = \sqrt{\frac{\pi}{4}} \cdot \frac{1}{\sqrt{\bar{v}^2}} \underline{\underline{R}} \tag{144}$$

where $\bar{v}^2$ is the input power per channel and $\underline{\underline{R}}$ is the channel signal correlation matrix $E\{\underline{v}\ \underline{v}^\dagger\}$. (This result is valid only for array antennas with equal gain elements because the power is assumed to be equal in all channels.) With this result, the analysis proceeds as before. The equation for weight noise is

$$\tau_o \dot{\underline{Z}} + \left[\underline{\underline{I}} + \frac{\mu h}{\sqrt{\bar{v}^2}} \underline{\underline{R}}\right] \cdot Z = \underline{g} \tag{145}$$

The equivalent expression to Eq. (119) is

$$[E\{\underline{g}\ \underline{g}^\dagger\}]_{k\ell} = \mu^2 h^2 \sum_{ij} \underline{w}_i \underline{w}_j^* E\left\{\frac{v_k v_i^* v_j v_\ell^*}{|v_k|\,|v_\ell|}\right\} - \mu^2 h^2 [\underline{\underline{\bar{M}}} \cdot \underline{\underline{W}}\ \underline{\underline{W}}^\dagger \cdot \underline{\underline{\bar{M}}}]_{k\ell} \tag{146}$$

The expectation cannot be simplfied in general. However, if we restrict $\underline{v}(t)$ to broadside incidence (i.e., all channel signals are equal), the expectation reduces to $E\{|v|^2\}$. Equation (146) reduces to

$$E\{g\ g^\dagger\} = \frac{\mu^2 h^2}{\bar{v}^2} \left(1 - \frac{\pi}{4}\right) (\underline{w}^\dagger \cdot \underline{\underline{R}} \cdot \underline{w})\ \underline{\underline{R}} \tag{147}$$

which is very similar to Eq. (121) for the standard system except that it is restricted to the case of broadside incidence. Proceeding as before the weight noise spectrum (equivalent to Eq. (127)) becomes

$$[S_Z(\omega)]_{11} = \frac{\mu^2 h^2 N(1 - \pi/4)}{BW} \frac{1}{(1 + \mu h\sqrt{Ns_1})^2 (1 + \omega^2\tau_1^2)} \tag{148}$$

where

$$\tau_1 = \tau_o/(1 + \mu h\sqrt{Ns_1}) \quad .$$

(For broadside incidence the only significant eigenvalue is $s_1 = P_{in}$.) The expression for $(\underline{w}^\dagger \cdot \underline{\underline{R}} \cdot \underline{w})$ in a hard-limited system under these conditions is

$$(\underline{w}^\dagger \cdot \underline{\underline{R}} \cdot \underline{w}) = \frac{|\hat{V}_1|^2 P_{in}}{(1 + \sqrt{P_{in}/P_T})^2} \tag{149}$$

which is comparable to (131). We have defined the threshold for a hard-limited system to be

$$P_T = (\mu^2 h^2 N)^{-1} \quad . \tag{150}$$

The weight noise modulation of a tone signal yields the output spectrum

$$S_o'(\omega) = \frac{|\hat{V}_{s1}|^2 |\hat{V}_1|^2 (P_{in}/P_T)}{BW(1 + \sqrt{P_{in}/P_T})^4} \frac{1}{(1 + \omega^2\tau_1^2)} \tag{151}$$

This can be compared to (132) for the standard system. The maximum value of the peak of the spectrum again occurs at $P_{in} = P_T$ and is

$$S_o'(o) \leq \frac{(1 - \pi/4) |V_s|^2}{16\ BW} \text{ volts}^2/\text{hz} \tag{152}$$

which is very near the result for the standard system. The total spectrum power reaches a maximum at $P_{in} = 4\ P_T$ and is

$$\frac{1}{2\pi} \int S_o'(\omega)\ d\omega \leq \frac{2(1 - \pi/4) |V_s|^2}{27\ \tau_o \cdot BW} \text{ volts}^2 \tag{153}$$

which is about 6 dB less than for the standard system. This is because of the narrower bandwidth of a hard-limited system for the same filter time constant, τ_o.

The equivalent to Eq. (139) for total output power is

$$\frac{P_o}{P_T} = \frac{|\hat{V}_1|^2 (P_{in}/P_T)}{(1 + \sqrt{P_{in}/P_T})^2} \left[1 + \frac{(1 - \pi/4)}{2\tau_o \cdot BW} \cdot \frac{(P_{in}/P_T)}{(1 + \sqrt{P_{in}/P_T})}\right] \tag{154}$$

The weight noise contribution is therefore insignificant until P_{in} exceeds

$$\frac{P_{in}}{P_T} \geq (2\tau_o \cdot BW)^2 \tag{155}$$

which is far above the dynamic range capability of the processor.

V. EVALUATION OF SYSTEM PERFORMANCE

In the previous sections we developed quantitative estimates of the effects of various component errors on system performance -- namely achievable cancellation and loop stability. In this Section we show how the effects of these various component errors reveal themselves in measurements made on a real system, and conversely, how one can tailor the system measurements to evaluate the errors inherent in the processor or antenna. We address this subject from the viewpoint of component effects on cancellation. Component effects on loop stability are either obvious (e.g., unstable loops) or directly measurable by observing the transient behavior of the loops during adaption.

An experimental adaptive nulling processor was constructed and evaluated in order to discover the limits on performance imposed by component errors in the hardware. A detailed description of the processor is given in Ref. 9. Here we limit our discussion to the measurement techniques employed for evaluating the processor cancellation performance. The weight circuits were initially the PIN-diode design of Fig. 9. Following that a set of weights based on transconductance multipliers was installed and evaluated.

The following technique was used to evaluate the individual weight circuits before they were installed in the processor. A digital feedback loop was implemented using an HP 8505 network analyzer and an HP 9825 desktop computer. A CW tone at band center is applied to the input of a single weight and the digital feedback loop was activated. Closing the loop causes the weight to "turn off." At this point the weighted path exactly cancels the feedthrough weighted contribution of the output path (see Fig. 19). The weight I and Q control voltages are then frozen, and the input is swept in frequency across the band. The resultant plot of output power vs frequency for two of the weight circuits is shown in Fig. 19. It is clear that for wideband systems, the feedthrough can contribute significantly to the total output power across the band. These weights operated at an IF frequency of 120 MHz.

Figure 19 illustrates the effect of weight feedthrough for a single channel. In a processor using N parallel channels, it was shown in Section IV-C that the cancellation deteriorates by a factor of N^2 (assuming equal feedthrough levels). Measured data illustrating this are presented in Fig. 20. Here, one channel of the weight sub-system is fixed as a reference input, and the number of cancelling channels is varied from 2 to 8 using a switch network designed into the test system. Broadband noise of fixed bandwidth is applied to the input of each weight through an N-way divider. The resulting measured output spectra for various numbers of cancellation channels is illustrated by the N^2 dependence. For the same measurement, the N^2 effect is illustrated in a different manner in Fig. 21. Here the measured increase in total output power is plotted as the number of cancelling channels and is increased compared to the theoretical N^2 behavior. The measurements indicate that three of the weight circuits have 7.5 dB more feedthrough than the other four.

The above results are for the PIN-diode weight design of Fig. 9. In this circuit the feedthrough is dominated by the isolation and time delay of the quadrature hybrid. The second weight design we evaluated uses the principle of transconductance multipliers and is illustrated in Fig. 22. To assess the

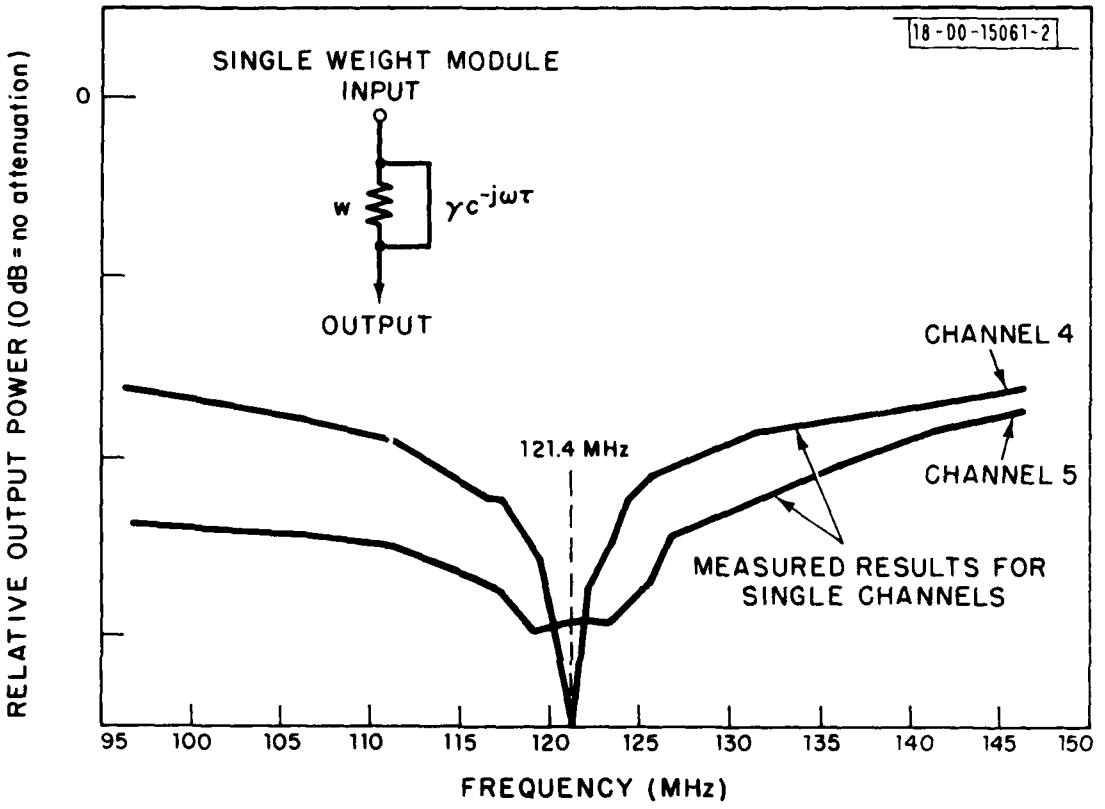

Fig. 19. Weight feedthrough effects on cancellation over the nulling band using a simple weight. Results for two different channels (4 and 5) are plotted.

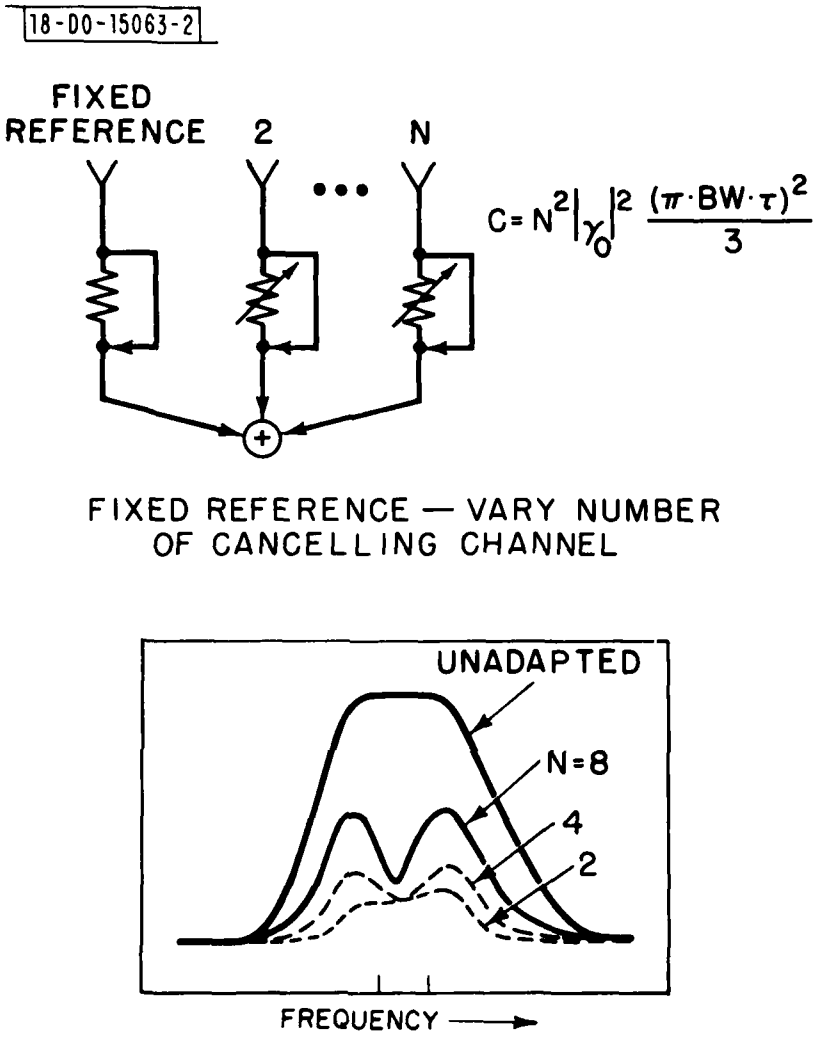

Fig. 20. Effects of weight feedthrough on cancellation as the number of cancelling channels is increased from two to eight.

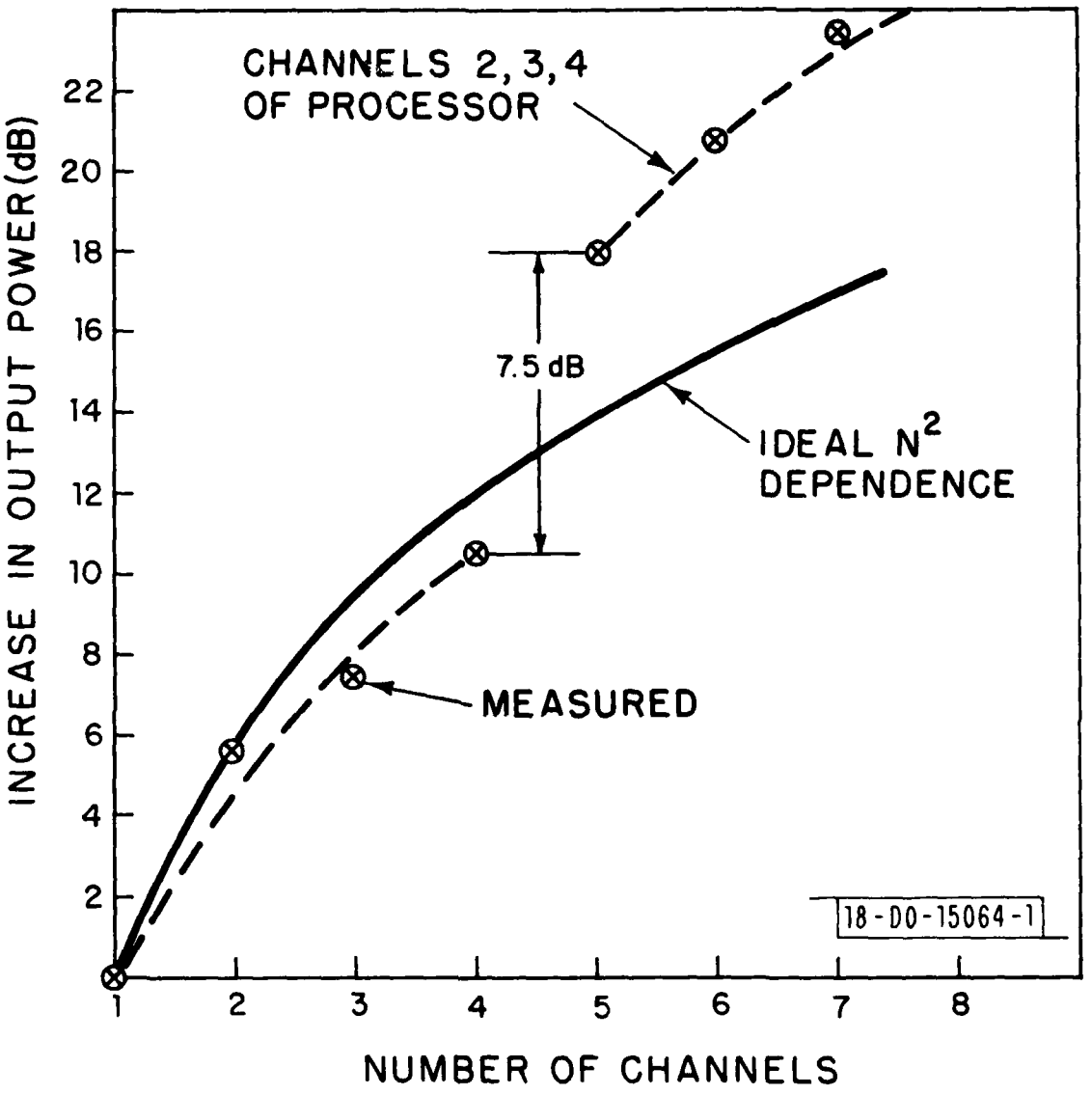

Fig. 21. Measured increase in total output power due to weight feedthrough as a function of the number of cancelling channels.

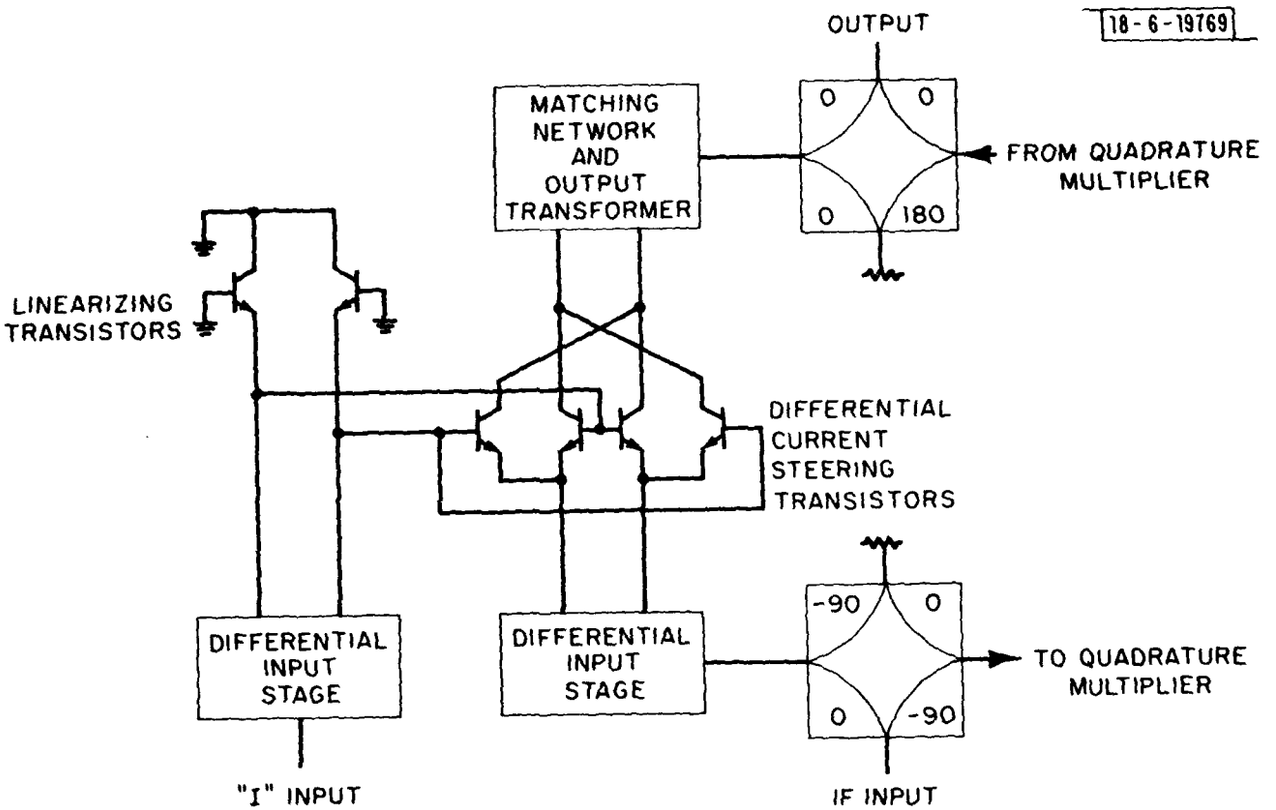

Fig. 22. Alternate I/Q weight design using the principle of transconductance multipliers. Center frequency = 121.4 MHz.

improvement over the PIN-diode weights, we use the eigenvalue estimate of the achievable cancellation given by Eq. (24). With fixed I and Q control voltages the amplitude and phase response of each channel is measured separately as a function of frequency with a network analyzer. The correlation matrix, $\underline{\underline{R}}$, is computed from the data parametrically as a function of bandwidth, BW. The eigenvalues of $\underline{\underline{R}}$ are then computed and plotted as functions of BW. The result of processing the data in this way is illustrated in Fig. 23 for both the transconductance multiplier weights and for the PIN-diode weights. Recalling from Eq. (24) that $C \propto s_2/s_1$, we anticipate a 15 dB improvement in wideband cancellation performance with the transconductance weights. This performance improvement was indeed realized when the weights were installed in the processor.

The previous discussion has indicated several techniques useful for the evaluation of the effects of weight feedthrough. We have shown that feedthrough results in an N^2 degradation in broadband output power relative to a single channel even if the weight feedthrough paths are identical in their frequency response (i.e., they track perfectly).

We now consider the effects of channel tracking errors which arise from the fact that the frequency transfer functions of each channel differ slightly because of component differences. When considering the effect of channel tracking errors, we emphasize that it is the <u>total</u> channel response from input to output which must track. A valuable technique for separating the effects of different components on the overall tracking performance of a channel is to assemble and evaluate the processor sequentially, beginning with the N-way combiner, proceeding to the weights, then the IF sections, and finally the RF front ends, until the total processor is assembled. At each stage of assembly, channel tracking measurements with data reduction similar to that discussed above are made to determine which stages dominate the cancellation performance.

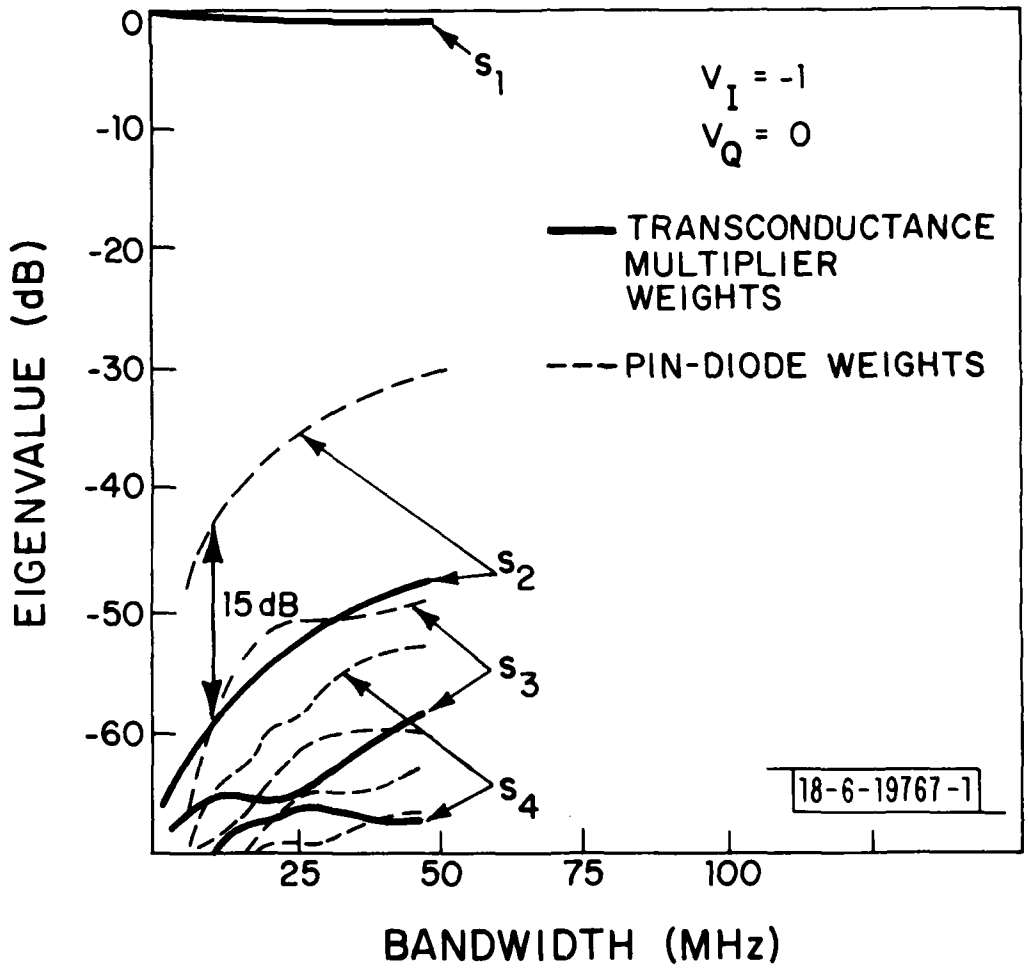

Fig. 23. Eigenvalues of the 7-weight channels vs. bandwidth (MHz) for both the pin-diode weight design of Fig. 9 and the transconductance multiplier weight design of Fig. 22. Frequency response of each channel obtained using a fixed control voltage $V_I = -1$, $V_Q = 0$.

When this process is complete it will be found in general that one or two channels are measurably worse than the others. Figure 24 illustrates the effect of an anomalously bad channel on the eigenvalues of the processed channel tracking data. For an earth-coverage quiescent radiation pattern and a planar array of earth coverage elements, only a single channel will be "on" in the unadapted mode. The corresponding beam steering vector is $\underline{V}^{\dagger} = [0, \ldots 0,1,0 \ldots]$ where the 1 appears in the reference (or "on") channel. Choosing a dominant error channel as the reference degrades the performance significantly. In fact, if one measures the cancellation as a function of reference channel, there will be one channel which yields the best cancellation. This channel should then be designated as the reference.

Figure 25 illustrates the effect for the transconductance multiplier weight circuits of the processor. It shows the measured, broadband cancellation as a function of reference channel. There are 7 channels in all. Note that a significant improvement in cancellation can be achieved by selecting the reference channel. For comparison, Fig. 25 also shows the computed cancellation as determined from the eigenvalues of the measured tracking data from the swept frequency measurement discussed previously. The discrepancy between the two curves indicates that tracking errors in these particular weights are a function of weight setting. The swept frequency tracking data were obtained with fixed I and Q control drive voltages to each weight (in their minimum attenuation state), whereas the actual cancellation was measured with the weights at their adapted, steady-state values. Figure 25 applies to the weight circuits alone.

Figure 26 shows the equivalent data with the remaining stages of each channel added. These are the IF amplifiers, band-limiting filters and finally the RF preamplifiers and mixers. The measured and computed results (again, computed from the measured tracking data) are now more closely in agreement confirming that the transconductance multiplier weights are not the dominant components in limiting the achievable cancellation. Of the remaining IF and RF components, there was in fact no dominant component. Each RF and IF subsection contributed in roughly equal measure to the cancellation degradation. The existence of an "optimum" reference channel is also evident from Fig. 26.

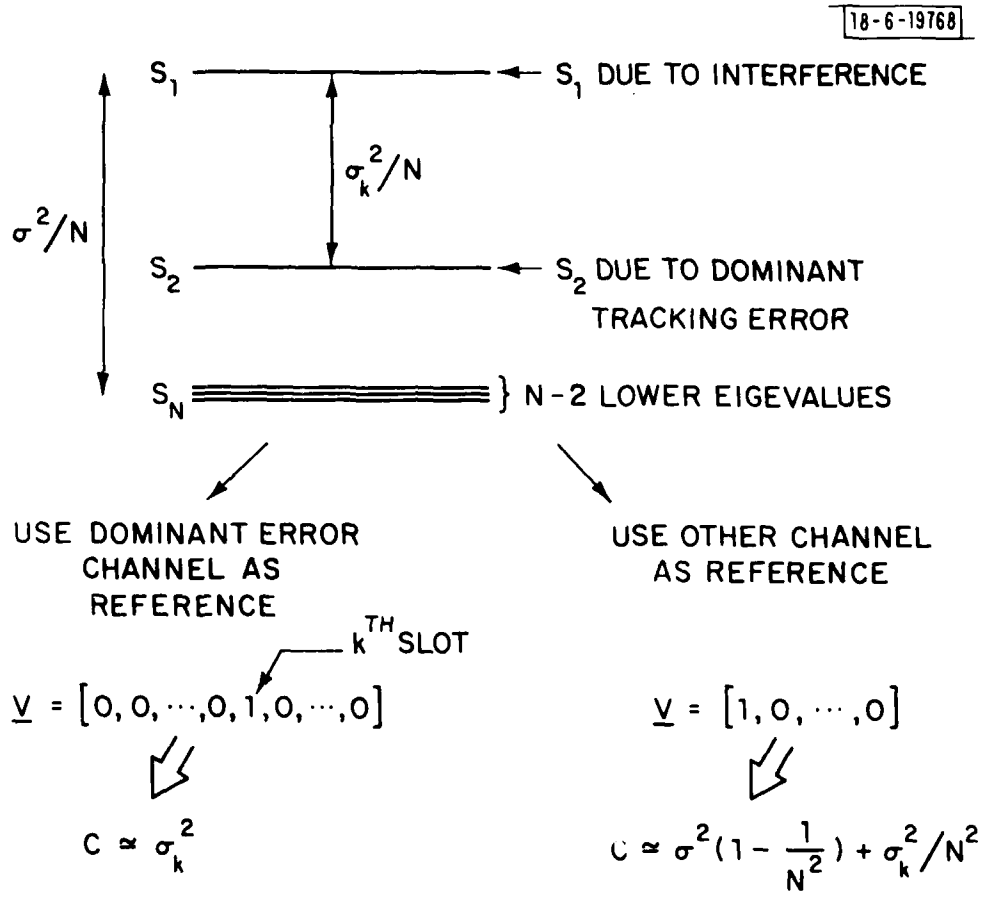

Fig. 24. Effect of an anomalously bad channel on the cancellation performance of the processor when the bad channel is used as a reference channel.

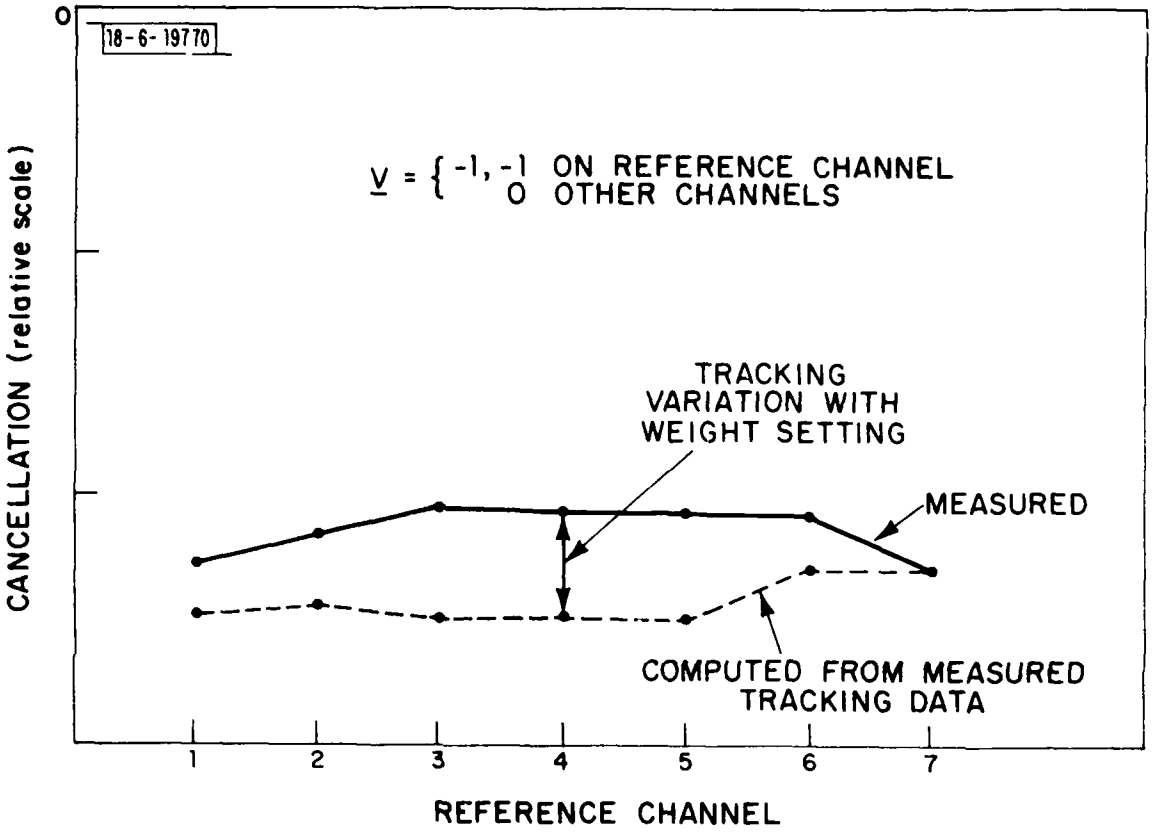

Fig. 25. Measured cancellation vs. channel used as reference for transconductance multiplier weights, compared to the computed cancellation using the measured frequency response for each channel with control voltage = (-1, -1).

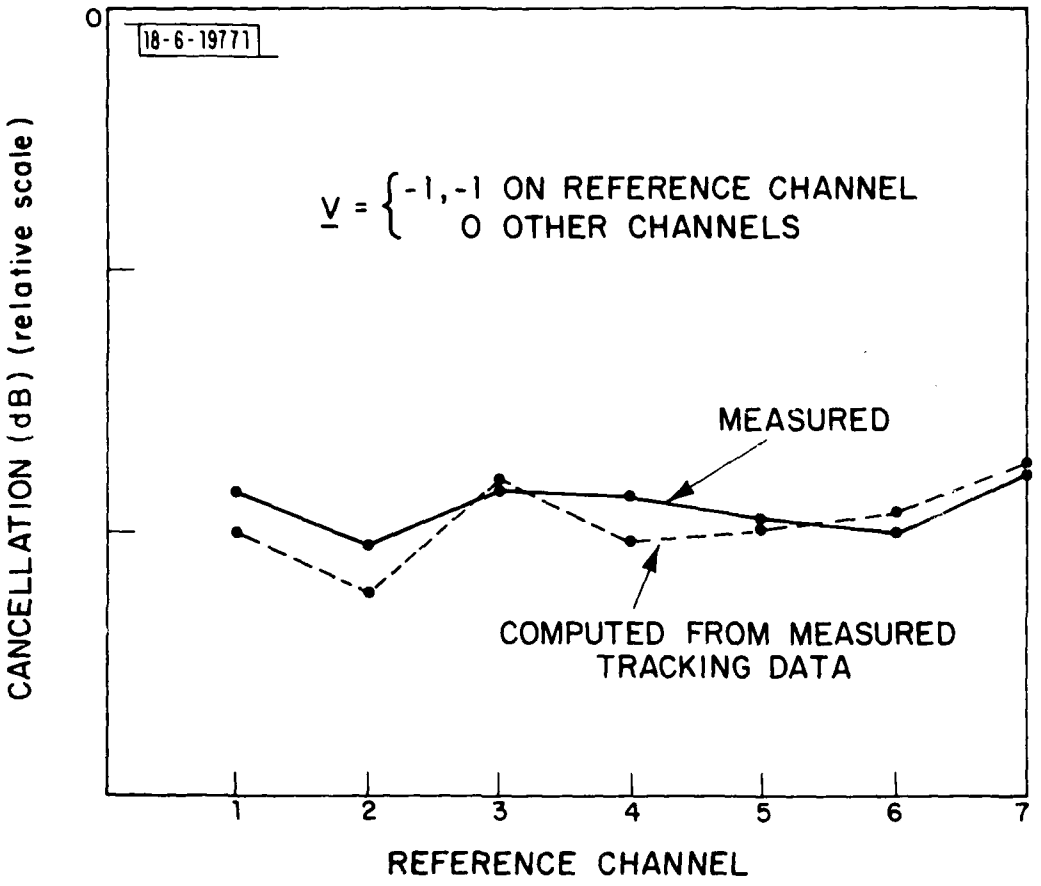

Fig. 26. Measured cancellation vs. channel used as reference with the remaining stages (IF through UHF) of the processor added.

The previous results have illustrated the use of channel tracking measurements for determining component effects on achievable cancellation. Still another presentation exists which yields the effects of specific component errors on performance, and this technique will now be considered. This useful technique can be explained with reference to the output power vs input power characteristic of a nulling processor* (Fig. 27). Consider first an ideal system employing a hard limiter in each feedback channel operating first in the quiescent (without nulling), then in the adapted (with nulling) mode. Assume that a test signal of variable bandwidth and power is applied to the processor through an N-way splitter. This simulates broadside incident of a single source. In the quiescent mode, as P_{in} to a given channel increases, P_{out} increases in a linear relationship to P_{in}. In the adapted mode, a threshold level, P_t, exists where the nulling processor just "senses" the input power level. At this threshold, 6 dB of cancellation results. As P_{in} increases further, P_{out} ideally remains fixed at a constant level as a consequence of the hard-limiting action in the feedback loop. The achieved cancellation is very nearly equal to the difference between the quiescent and adapted levels. In an ideal system, therefore, cancellation increases without limit as P_{in} increases. For a real system, however, only some maximum cancellation is achievable. As one increases P_{in} above threshold in a real processor, the output power remains constant only over a limited range of P_{in}. At some value of P_{in}, the output power begins to increase and becomes proportional to P_{in}. By repeating this measurement as each section of the processor is added, the result of the measurement then yields directly the error effect that is dominating the performance degradation. By tailoring the input appropriately, this effect can usually be identified. Representative results are illustrated on the Figure, not necessarily in order of importance.

---

*The characteristic curve in Fig. 27 is applicable to processors with hard limiters in the feedback loops (Ref. 7).

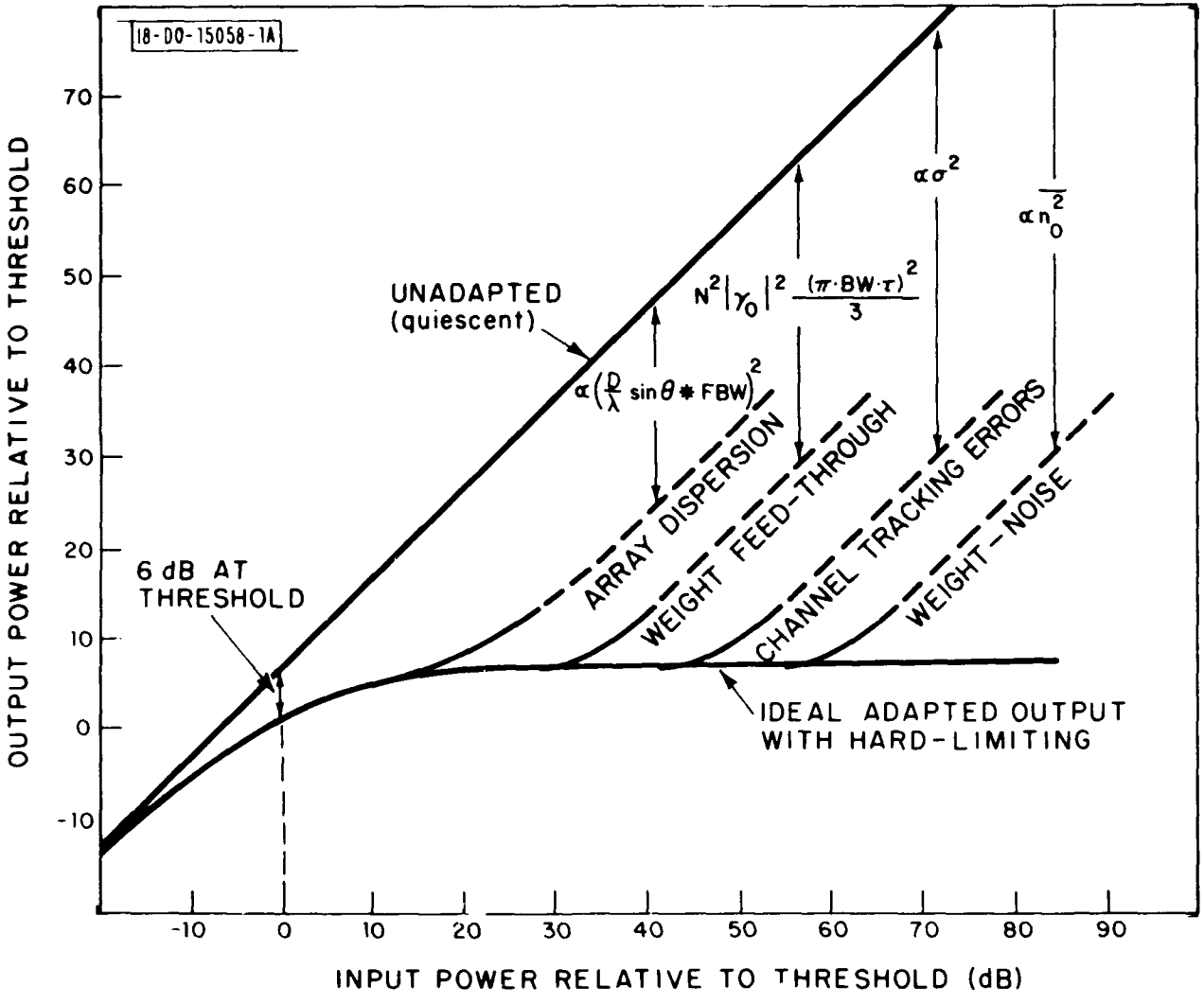

Fig. 27. Effects of various components on achievable cancellation for an Applebaum-Howell type adaptive loop.

AD-A081 711 MASSACHUSETTS INST OF TECH LEXINGTON LINCOLN LAB F/G 9/5
FACTORS AFFECTING THE PERFORMANCE OF ADAPTIVE ANTENNA SYSTEMS A--ETC(U)
AUG 79 J T MAYHAN, F W FLOYD F19628-78-C-0002
UNCLASSIFIED TN-1979-14 ESD-TR-79-197 NL

2 OF 2

END
DATE FILMED
4-80
DTIC

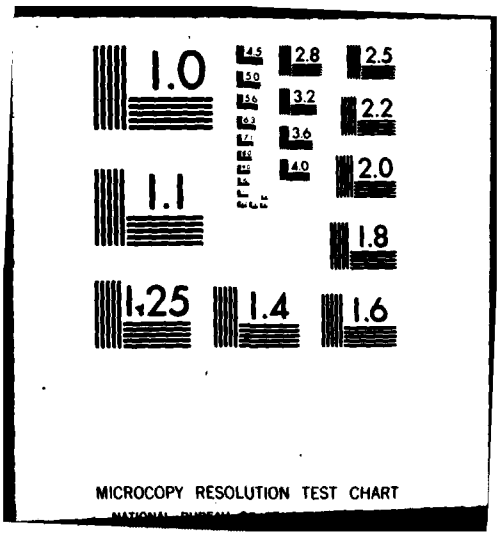
1.0
1.1
1.25
1.4
1.6
1.8
2.0
2.2
2.5
2.8
3.2
3.6
4.0
4.5
5.0
5.6
6.3
7.1
8.0
9.0
MICROCOPY RESOLUTION TEST CHART

Figure 28 is an example of this technique as applied to the demonstration processor using the PIN-diode weight circuits. Several cases of interest are presented. First consider the earth coverage mode, where a single channel is used as reference. When the test input is a tone, then the achievable cancellation is limited by the weight noise arising from the baseband circuitry (Section IV-E-1). When a wideband test signal is applied to the processor simulating broadside incidence on the array, the achievable cancellation is limited either by channel tracking errors or weight feedthrough. Both effects yield the same trends when P_{out} is plotted vs P_{in}. Therefore this technique alone cannot distinguish between the two. The fact that it was weight feedthrough from the PIN-diode weights that dominated these results was determined by the N^2 dependence discussed previously. Another interesting fact is that when the steering vector changes from earth coverage to a maximum gain beam mode, the quiescent output power increases accordingly, because the array gain increases. However (as discussed in Section III-3), the adapted output in the feedthrough dominated region is independent of the steering vector. This results in greater cancellation for one steering vector than for another. This is an example of the ambiguity inherent in using cancellation level as a means of specifying system performance.

Figure 29 illustrates similar results for a case where the test signal was time delayed to each channel in a way to simulate an 8° angle-of-arrival on a specified array geometry to emphasize the effect of array dispersion. Comparison of the measurement with computer simulation of the array bandwidth characteristics yields results which confirm that array dispersion is the dominant factor in this case.

The previous discussion has centered on evaluating the effects of component errors (i.e., deviations from ideal behavior) on performance. We now consider the effect of hard-limiting in the feedback loop. While not an error source strictly speaking, hard limiters can have a harmful effect on performance and for that reason are mentioned briefly here. For a single interference source, it is relatively simple to show that hard-limiting reduces the

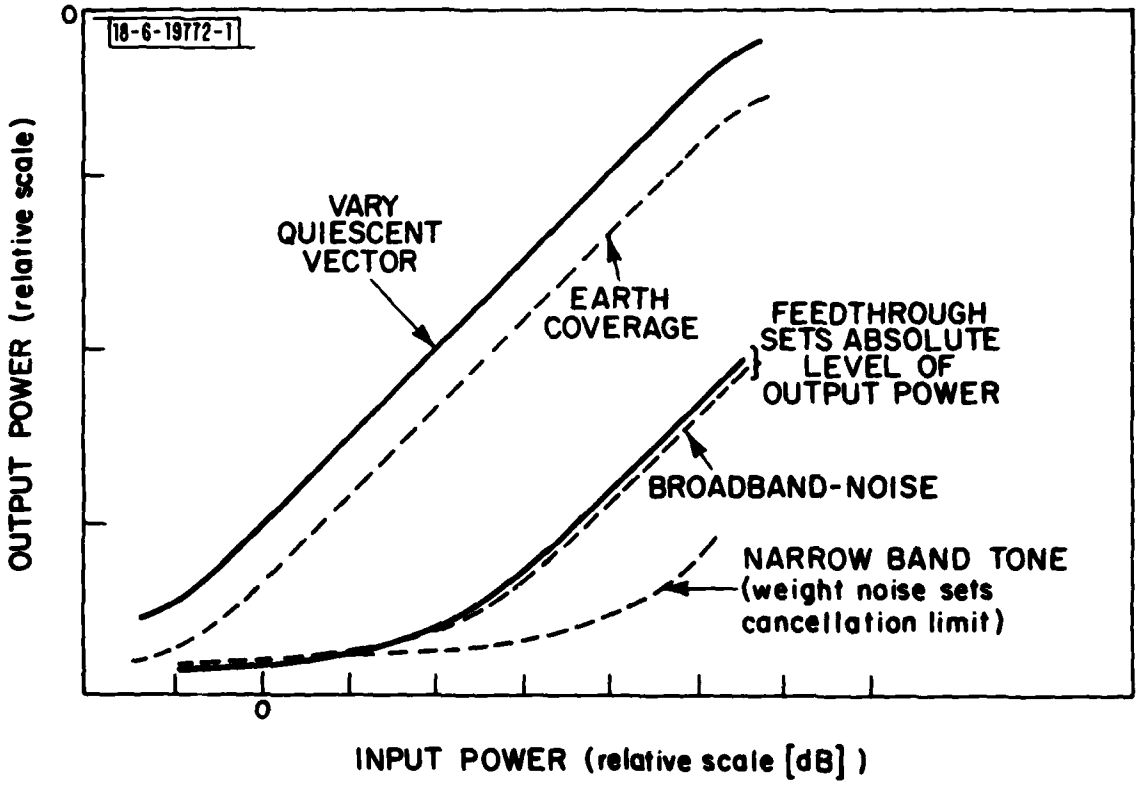

Fig. 28. Measured cancellation trends – output power vs. input power for selected inputs and beam-steering parameters.

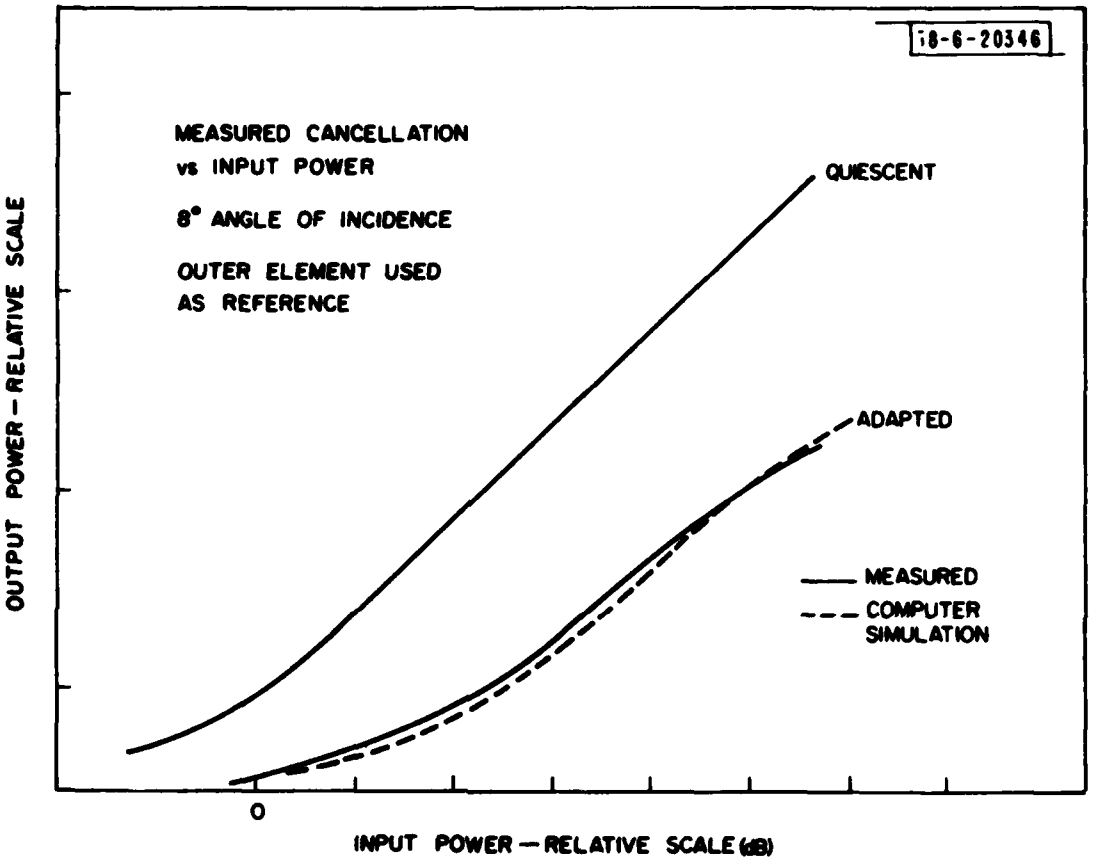

Fig. 29. Measured cancellation trends – output power vs. input power for input simulating an 8° angle of incidence using the 7-element double triangle configuration in the insert of Fig. 17.

circuit dynamic range requirements in the feedback loops. For example, if the processor is designed to operate over a 40 dB dynamic range of input power, the correlator mixer and subsequent circuits must operate over an 80 dB range of power if no hard limiter is employed. With hard limiting, the dynamic range requirement on the correlator is reduced to 40 dB. However, if there are two interference sources which are significantly spread in power level, they give rise to two widely spaced eigenvalues in the signal correlation matrix. It can be shown that[7] the effect of the hard-limiter is to suppress the smaller eigenvalue (see Table 1), so that it is essentially not sensed by the processor. The degree to which this happens depends on the degree to which the larger eigenvalue is above threshold. For this measurement, the eigenvalue s_1 (controlled by an incident source at a given angle of arrival having power P_1) is fixed relative to threshold. The second eigenvalue s_2 (controlled by a second source eminating from a different angle of arrival having power P_2) is varied, and the output power is measured as s_2 is varied. The results are plotted in Fig. 30 for a system having a specific dynamic range. The region over which the small eigenvalue is not sensed is determined by s_1/P_t, the ratio of the larger eigenvalue relative to threshold. By examining the measured results, it becomes clear that the system cancellation taking into account <u>both</u> sources is limited to $\sim \sqrt{s_1/P_t}$. Hence, if s_1/P_t is the desired cancellation level, then the dynamic range required of the baseband circuitry is s_1/P_t whether or not a hard-limiter is used. A small eigenvalue might arise from a second incident source of low power level (as simulated above), or it may result from a single <u>wideband source</u> incident on a dispersive antenna. In this second case the hard-limiter essentially prohibits the processor from compensating for array dispersion by using up more than one degree of freedom to form a broadband null. In summary, a hard-limiter does not reduce the circuit dynamic range requirements when two sources of widely differing power levels are present, and requires a broadband antenna geometry when deep cancellation of a single source is desired. We conclude that processors which must null multiple sources over a wide dynamic range of power should not use hard limiters in the feedback loops.

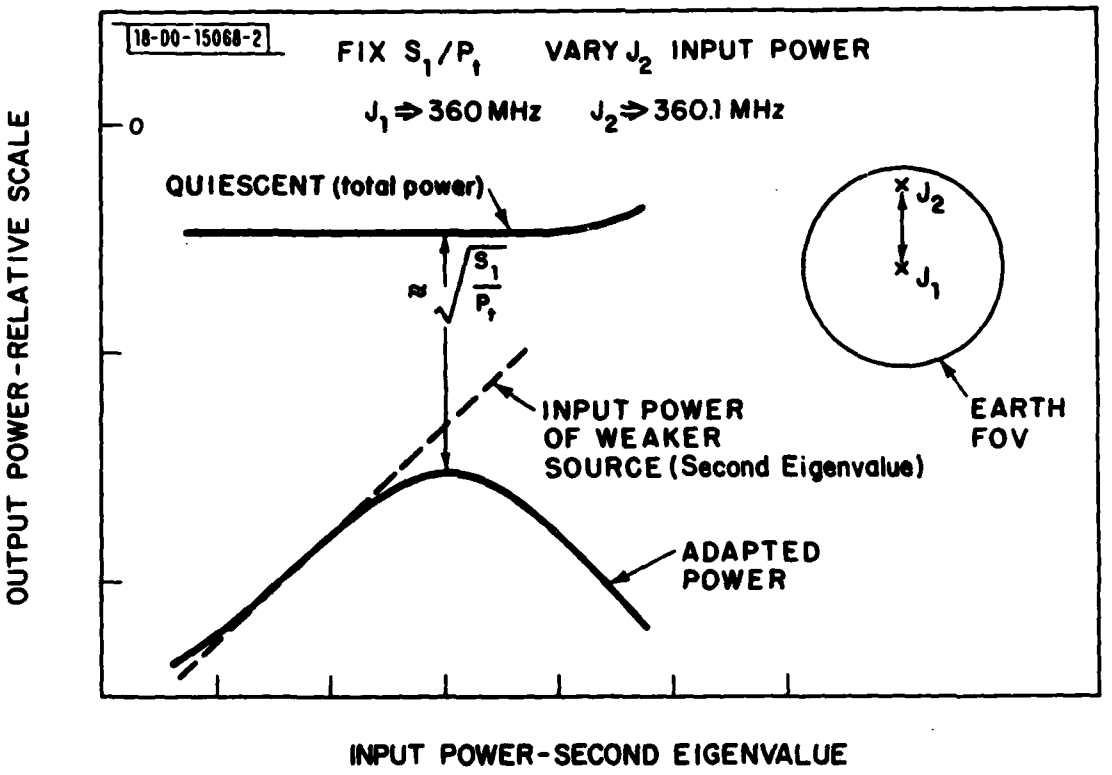

Fig. 30. Measured hard-limiter suppression of the second eigenvalue generated by a weaker interference source.

ACKNOWLEDGEMENTS

It is a pleasure to acknowledge the help and support of numerous colleagues who have contributed their time in discussing the ideas presented in this technical note. Numerous discussions with A. J. Simmons, L. J. Ricardi, W. C. Cummings, B. M. Potts, and D. A. Siegel are greatly appreciated. The programming support of L. Niro was invaluable in providing simulation data for cross-checking with the measured results and estimates of Table 1. Discussions with H. S. Babbitt were instrumental in leading up to the stability diagram of Fig. 14. Special thanks are also due to D. A. Brown, who helped perform the measurements on the demonstration processor.

REFERENCES

1. J. T. Mayhan, "Bandwidth Limitations on Achievable Cancellation for Adaptive Nulling Systems," Technical Note 1978-1, Lincoln Laboratory, M.I.T. (17 February 1978), DDC AD-A054160.

2. W. F. Gabriel, "Adaptive Arrays – An Introduction," Proc. IEEE, 64, 239 (1976).

3. W. B. Davenport, Jr. and W. L. Root, Random Signals and Noise (McGraw-Hill, New York, 1958), p. 60.

4. J. T. Mayhan, "Adaptive Nulling with Multiple-Beam Antennas," Appendix A, Technical Note 1976-18, Lincoln Laboratory, M.I.T. (30 September 1976), DDC AD-A034652/8.

5. L. E. Brennan, E. L. Pugh and I. S. Reed, "Control Loop Noise in Adaptive Array Antennas," IEEE Trans. Aerosp. and Electron. Syst., AES-7, 254 (1971).

6. L. E. Brennan and I. S. Reed, "Effect of Envelope Limiting in Adaptive Array Control Loops," IEEE Trans. Aerosp. and Electron. Syst., AES-7, 698 (1971).

7. J. T. Mayhan and F. W. Floyd, "Some Effects of Hard Limiting in Adaptive Antenna Systems," Technical Note 1979-15, Lincoln Laboratory, M.I.T. (in preparation).

8. A. R. Dion and L. J. Ricardi, "A Variable-Coverage Satellite Antenna-System," Proc. IEEE, 59, 252 (1971).

9. D. Siegel et al., "Feedback Nulling Demonstration System Hardware," Technical Note 1979-12, Lincoln Laboratory, M.I.T. (in preparation).

APPENDIX

In this Appendix we estimate the eigenvalue ratio s_2/s_1 for a phased array antenna employing N elements each having element gain G_e. Let a wavefront be incident on the array from angles Θ, Φ. The wavefront is normalized to unity amplitude. The correlation matrix as defined at the antenna output ports is given by (for broadband noise incidence)

$$\underline{\underline{R}} \equiv \langle G_e \, e^{-j\omega(T_k - T_q)} \rangle \tag{A1}$$

where $\langle \cdot \rangle$ denotes the frequency average

$$\langle \cdot \rangle \equiv \frac{1}{BW} \int_{\omega_o - BW/2}^{\omega_o + BW/2} (\cdot) \, d\omega \tag{A2}$$

and T_k is the time delay for the wavefront to reach the $k^{\underline{th}}$ element relative to an arbitrary reference position on the array:

$$T_k = \frac{D}{2c} \sin\theta \left[x_k \cos\phi + y_k \sin\phi \right] \tag{A3}$$

and the x_k, y_k are the element position normalized to $\frac{D}{2}$ $(x_k^2 + y_k^2 \leq 1)$. The eigenvalue s_1 is simply given by NG_e, since s_1 corresponds to applying a set of weights which points a maximum beam toward the interferfence source having maximum array gain NG_e. In order to estimate s_2, we expand $\underline{\underline{R}}$ in the form

$$\underline{\underline{R}} = \underline{\underline{R}}_0 + \Delta\underline{\underline{R}} \tag{A4}$$

where $\underline{\underline{R}}_0$ is the correlation matrix assuming zero bandwidth, and $\Delta\underline{\underline{R}}$ represents the perturbation to $\underline{\underline{R}}_0$ due to non-zero bandwidth effects. Clearly, then, from Eq. (A1),

$$\underline{\underline{R}}_{0_{k,q}} = G_e \, e^{-j\omega_0(T_k - T_q)} \tag{A5}$$

To obtain $\Delta\underline{\underline{R}}$, we expand $\underline{\underline{R}}$ in the form

$$\underline{\underline{R}}_{k,q} = G_e \langle e^{-j\omega_o(T_k-T_q)} \, e^{-j\Delta\omega(T_k-T_q)} \rangle \approx$$

$$G_e \, e^{-j\omega_o(T_k-T_q)} - j \, G_e \langle \Delta\omega \rangle (T_k-T_q) \, e^{-j\omega_o(T_k-T_q)}$$

$$- G_e \langle \frac{\Delta\omega^2}{2} \rangle (T_k-T_q)^2 \, e^{-j\omega_o(T_k-T_q)}$$

The term involving $\Delta\omega$ averages to zero, so that from (A6) we obtain

$$\Delta\underline{\underline{R}} = - G_e \frac{(\omega_o FBW)^2}{24} (T_k-T_q)^2 \, e^{-j\omega_o(T_k-T_q)} \tag{A7}$$

The eigenvalue s_2 can then be estimated according to:

$$s_2 = \max_{\underline{e}} \frac{\underline{e}^\dagger \cdot \underline{\underline{R}} \cdot \underline{e}}{\underline{e}^\dagger \cdot \underline{e}} \tag{A8}$$

where only vectors $\underline{e}$ such that $\underline{e}^\dagger \cdot \underline{e}_1 = 0$ are used in the maximization. Since $\underline{e}^\dagger \cdot \underline{\underline{R}}_o = 0$, ($\underline{e}_1$ is the first eigenvector of $\underline{\underline{R}}_o$ and $\underline{\underline{R}}$), then

$$s_2 = \max_{\underline{e}} G_e \frac{(\omega_o FBW)^2}{24} \sum_k \sum_q (e_k^* \, e^{-j\omega_o T_k}) \, (e_q \, e^{+j\omega_o T_q}) \, (T_k-T_q)^2 \tag{A9}$$

We note from (A9) the special case $T_k = T_q$ (broadside incidence) where $s_2 = 0$. Furthermore, since

$$\sum_k e_k^* \, e^{-j\omega_o T_k} = 0 \tag{A10}$$

(i.e., $\underline{e}^\dagger \cdot \underline{\underline{R}}_0 \cdot \underline{e} = 0$), the factor $(T_k-T_q)^2$ in (A9) essentially looks like a correlated tracking error between channels which increases as $(D/\lambda \cdot \sin\theta)^2$. Furthermore, Eq. (A10) is <u>independent of D/λ</u>, as e_k^* simply negates the D/λ phase term $e^{-j\omega_o T_k}$ so that the sum in (A10) adds to zero. Thus the only term inside the sum in (A9) which depends on D/λ is the factor $(T_k-T_q)^2$. Noting Eq. (A3), we can factor D/λ sinθ from inside the sum to rewrite (A9) in the form:

$$s_2 = \frac{NG_e}{24} (D/\lambda \cdot \sin\theta \cdot FBW)^2 \underset{\underline{e}}{\text{Max}} \left\{ \frac{1}{N} \sum_k \sum_q (e_k^* e^{-j\omega_o T_k}) (e_q e^{+j\omega_o T_q}) \right.$$

$$\left. \cdot \left[\left(\frac{x_k - x_q}{c} \right) \cos\Phi + \left(\frac{y_k - y_q}{c} \right) \sin\Phi \right]^2 \right\} \qquad \text{(A11)}$$

The term inside the maximization bracket is independent of $D/\lambda \sin\theta$, FBW and only weakly dependent on N. Thus we conclude

$$s_2 = K'(NG_e) (D/\lambda \sin\theta \, FBW)^2$$

Employing Eq. (24) of the text results in

$$C = K \frac{s_2}{s_1} = KK'(D/\lambda \sin\theta \, FBW)^2 \qquad \text{(A13)}$$

which is the desired result.

UNCLASSIFIED

SECURITY CLASSIFICATION OF THIS PAGE *(When Data Entered)*

(19) REPORT DOCUMENTATION PAGE		READ INSTRUCTIONS BEFORE COMPLETING FORM
1. REPORT NUMBER (18) ESD-TR-79-197	2. GOVT ACCESSION NO.	3. RECIPIENT'S CATALOG NUMBER
4. TITLE *(and Subtitle)* (6) Factors Affecting the Performance of Adaptive Antenna Systems and Some Evaluation Techniques		5. TYPE OF REPORT & PERIOD COVERED (9) Technical Note (14) TN- 6. PERFORMING ORG. REPORT NUMBER Technical Note 1979-14
7. AUTHOR(s) (10) Joseph T. Mayhan and Franklin W. Floyd		8. CONTRACT OR GRANT NUMBER(s) (15) F19628-78-C-0002
9. PERFORMING ORGANIZATION NAME AND ADDRESS Lincoln Laboratory, M.I.T. P.O. Box 73 Lexington, MA 02173		10. PROGRAM ELEMENT, PROJECT, TASK AREA & WORK UNIT NUMBERS (16) Program Element No. 63431F Project No. 2029
11. CONTROLLING OFFICE NAME AND ADDRESS Air Force Systems Command, USAF Andrews AFB Washington, DC 20331		12. REPORT DATE (11) 9 August 1979 13. NUMBER OF PAGES 108
14. MONITORING AGENCY NAME & ADDRESS *(if different from Controlling Office)* Electronic Systems Division Hanscom AFB Bedford, MA 01731 (12) 107		15. SECURITY CLASS. *(of this report)* Unclassified 15a. DECLASSIFICATION DOWNGRADING SCHEDULE

16. DISTRIBUTION STATEMENT *(of this Report)*

Approved for public release; distribution unlimited.

17. DISTRIBUTION STATEMENT *(of the abstract entered in Block 20, if different from Report)*

18. SUPPLEMENTARY NOTES

None

19. KEY WORDS *(Continue on reverse side if necessary and identify by block number)*

adaptive antenna system	phased array
adaptive processor	nulling
multiple beam antenna	radiation pattern characteristics

20. ABSTRACT *(Continue on reverse side if necessary and identify by block number)*

The basic performance of an adaptive antenna system is influenced somewhat independently by two sub-systems: the antenna and the adaptive processor. Choice of the antenna type (multiple beam antenna or phased array) and the design of the adaptive processor (which is used to control the weighting at each antenna feed port) depends strongly on the specific requirement of a particular system. To date, much has been published on the ideal performance characteristics of adaptive nulling antenna systems. However, little has been published on the effects of hardware component imperfections on system performance. To characterize these effects is the purpose of this note. We present methods for categorizing, analyzing and measuring the effects of a few of the key components which are common to the majority of adaptive systems implemented to date. Some examples we will discuss are those effects due to antenna type, antenna tolerance errors, channel tracking errors, weighting circuits, hard-limiters, correlators and base-band components. We analyze these from the viewpoint of the degree of cancellation achievable by the adaptive processor and also their impact on loop dynamics (where appropriate). In order to illustrate the various effects, measured performance results obtained using an experimental Applebaum-Howell type adaptive processor will be presented.

DD FORM 1 JAN 73 1473 EDITION OF 1 NOV 65 IS OBSOLETE

UNCLASSIFIED

SECURITY CLASSIFICATION OF THIS PAGE *(When Data Entered)*

207650